2017-10-01

An Investigation into Isogeometric Blended Shells

David Scott Willoughby
Brigham Young University

An Investigation into Isogeometric Blended Shells

David Scott Willoughby II

A thesis submitted to the faculty of
Brigham Young University
in partial fulfillment of the requirements for the degree of

Master of Science

Michael A. Scott, Chair
David W. Jensen
Richard J. Balling
Thomas W. Sederberg

Department of Civil and Environmental Engineering

Brigham Young University

ABSTRACT

An Investigation into Isogeometric Blended Shells

David Scott Willoughby II
Department of Civil and Environmental Engineering, BYU
Master of Science

Improvements to isogeometric blended shells are introduced which blend traditional Reissner-Mindlin shells, and Kirchhoff-Love shells, with an exact interpolation of the shell director increment. A gradient extraction operator is introduced which allows derivatives of basis functions to be exactly expressed as a linear combination of the basis functions themselves. Several benchmarks are investigated and the new blended shell is compared with different shell elements in ABAQUS and NASTRAN. In addition, the effect of different quadrature schemes is included in the comparisons. The new isogeometric blended shell performs comparably in some benchmarks, and even outperforms commercial shell finite elements in some benchmarks. Future improvements to the formulation are discussed.

Keywords: IGA, Kirchhoff-Love shells, Reissner-Mindlin shells, blended shells

ACKNOWLEDGMENTS

I would like to thank Dr. Mike Scott for all of his help and support during my graduate program at BYU. He has provided valuable guidance and it has been an honor and a privilege to be able to work with him. I would also like to express gratitude to my fellow researcher Zhihui Zou for all of his help in this work.

I appreciate each member of my graduate committee for the time that they have invested in me. Dr. David Jensen has become a good friend and mentor of mine. I have always been impressed with the way that Dr. Tom Sederberg has been able to demystify complex subjects. Dr. Rick Balling has authored several engineering textbooks that are probably the most valuable pieces of my young engineering library. I recognize how privileged I have been to associate with all of these professors.

In addition, I would like to thank my family. Thank you to my wife, Paige, who has been a constant source of help and encouragement.

TABLE OF CONTENTS

LIST OF TABLES

LIST OF FIGURES

CHAPTER 1. INTRODUCTION

1.1 Isogeometric Analysis

Engineering design can be thought of as the process of delineating and drawing out a plan for a structure that will meet the desired needs. Engineering analysis is then the determination of displacements or stresses of a certain design under prescribed loads. Before computers, design engineers worked at drawing boards and designs were drawn with pencils on vellum and Mylar. The design drawings were passed to stress analysts and the interaction between designer and analyst was simple and direct [6]. Although design and analysis are generally distinct tasks, there clearly exists an interconnectedness between the two. An analysis can not be done without a design, and a design may be altered in accordance with analysis results. Although design and analysis are inseparably connected, these two industries have evolved separately. Over the past six decades, two major branches of computational engineering have emerged: Computer Aided Design [CAD] and Finite Element Analysis [FEA], both multi-billion dollar industries. Because they have evolved separately, CAD and FEA do not interface efficiently. The current engineering process of design and analysis is as follows:

1. A geometric design is made using a CAD program.

2. The geometry of the design is decomposed into simpler, more manageable pieces and a finite element mesh is created, approximating curved geometry.

3. A finite element analysis is run using an FEA program.

4. If the designer is satisfied with the analysis, then this is the end. He/she may want to change the design because of the results of step 3. If this is the case, then the designer must return to step 1.

This process is very time consuming and, therefore, very costly. The conversion from the CAD geometry to the FEA mesh, the bridge between CAD and FEA, is the most time-consuming part of the engineering design-analysis process. It is estimated that 80% of analysis time is spent converting CAD geometry to an approximate FEA mesh [6]. There are many other disadvantages of having to convert the CAD geometry to the FEA mesh. For example, any curved surface will usually be approximated by linear or parabolic segments (as pointed out in step 2 above). This can cause major problems in shell structures that are very sensitive to geometric imperfections. In addition, FEA meshes that use linear or parabolic interpolating functions lack the inter-element smoothness required by some kinematic descriptions. Isogeometric Analysis (IGA), as proposed by Hughes et al. originally in 2005 [7], is intended to be a technology that unites or integrates the two into one system, thus eliminating the need to approximate the geometry: the original design geometry is used in the analysis. This is done by using Non-Uniform Rational B-Splines (NURBS), commonly used to represent curves, surfaces, and volumes in commercial CAD programs, as a basis for analysis. IGA has application to many fields such as fluid flow, fracture mechanics, elasticity, and even modeling in the biomedical field. Because there is no need to approximate the geometry, engineering design and analysis becomes much less costly.

One area that IGA has unlocked has been thin-shelled structures based on the Kirchhoff-Love kinematic description. This shell description is not able to be modeled in traditional FEA programs because these shells require inter-element smoothness that traditional FEA basis functions lack. These shell elements have several advantages. For example, the kinematic description only contains 3 degrees of freedom (DOF) per node, as opposed to traditional 6 DOF FEA elements. This decrease in DOFs can lead to great increases in speed in the analysis of thin-walled structures. Another major advantage to Kirchhoff-Love shells is that they do not have shear locking because classical Kirchhoff-Love shells do not have shear strains. This feature of not capturing shear strains creates an obvious disadvantage: Kirchhoff-Love shells can't capture shear deformation, which could lead to misleading results in thick shells. Another disadvantage of these shells is that it is hard to enforce clamped boundary conditions because they have no rotational DOFs. In this work these shells will be referred to as KL3.

A hierarchic family of Kirchhoff-Love shells was proposed in [8]. This family of shells has its base in the classical Kirchhoff-Love shell as described above with three displacement DOFs

of the shell midsurface. It creates a hierarchic director rotation vector that is used to capture the rotations of the director due to shear deformation. This improves the classical Kirchhoff-Love shell by allowing shear deformation without shear locking. Boundary conditions are still difficult to enforce, however. These shells will be referred to as KL5.

Traditional FEA for the most part uses shell elements that are based on the Reissner-Mindlin shell kinematic description. This kinematic description does not require smoothness. Traditional shell finite elements have six DOFs, three displacement and three global rotations, as previously mentioned. The advantages are that they do not require C^1smoothness, they can capture transverse shear deformation, and they facilitate the imposition of clamped or symmetry boundary conditions because of their 3 global rotational DOFs. The main disadvantage of these shells is that they are susceptible to shear-locking. These shells will be referred to as RM6.

There is an equivalent shell element which we will refer to as RM5, that has three displacement DOFs of the shell midsurface and two rotational DOFs about local axes that lie tangent to the shell. An advantage of this kinematic description is that these shells have one less DOF than RM6 shells. One disadvantage to these shells is that imposition of symmetry boundary conditions is difficult because you can only constrain rotation about local axes, when usually we would like to constrain rotation about the global coordinate axes. In addition, although only C^0 basis functions are required, these shells do require smooth geometry.

Because each shell kinematic description has advantages and disadvantages, it is useful to be able to blend the different shell kinematic descriptions. For example, it is useful to have the nodes on the boundary be RM6 in order to facilitate the imposition of boundary conditions, nodes in thin smooth areas be KL3 to reduce the number of DOFs, and nodes in thicker areas be KL5 in order to reduce the number of DOFs, avoid shear locking, and still be able to capture transverse shear deformation. An isogeometric blended shell was presented in [9] which blended RM6/RM5 shells and KL3 shells. The present work introduces KL5 shells into the blending.

An extensive suite of benchmarks is presented that not only tests the performance of the proposed isogeometric blended shell, but also compares the results to the isogeometric blended shell presented in [9] and to commercial shell finite elements from ABAQUS and NASTRAN. The proposed isogeometric blended shell outperforms the isogeometric blended shell presented in

[9]. It also performs comparably to commercial finite elements, and in some cases outperforms them. It is the first such comparison of isogeometric shell elements to commercial finite elements.

CHAPTER 2. B-SPLINE AND NURBS FUNDAMENTALS

As we will use non-uniform rational B-splines (NURBS) as a basis for our analysis, a brief treatment on the subject is necessary. A B-spline, short for basis-spline, is a piecewise function of Bezier curves connected with C^{p-1} continuity in the general case, where p is equal to the polynomial degree of the B-spline basis functions. This continuity is extremely important in order to be able to use shell formulations based on Kirchhoff-Love thin shell theory.

2.1 Univariate B-spline Basis Functions

2.1.1 Knot Vectors

B-spline basis functions are defined with a knot vector and a polynomial order. A knot vector is a set of non-decreasing parametric coordinates, denoted $\Xi = \{s_1, s_2, \ldots, s_{n+p+1}\}$ where s_i is the i^{th} knot in the knot vector, n is the number of B-spline basis functions and p is the polynomial order. A knot vector contains p end condition knots at each end, that provide no meaningful information. Knots that are not end condition knots are called interior knots, and the differences in neighboring interior knots are called knot spans. Each knot span corresponds to one Bezier curve in the B-spline, and one element in IGA. A uniform knot vector is a knot vector where all of the knots are equally spaced. A non-uniform knot vector does not necessarily have equally spaced knots. This is what the non-uniform in NURBS comes from.

2.1.2 B-spline Basis Functions

B-spline basis functions can be evaluated using the Cox-de Boor recursion formula where higher order basis functions are defined recursively in terms of lower order basis functions, starting

with the piecewise constant function:

$$N_A^0(s) = \begin{cases} 1, & \text{if} \quad s_A \leq s < s_{A+1} \\ 0, & \text{otherwise} \end{cases} \tag{2.1}$$

$$\tag{2.2}$$

Basis functions of first order and higher are then defined as:

$$N_A^p(s) = \frac{s - s_A}{s_{A+p} - s_A} N_A^{p-1}(s) + \frac{s_{A+p+1} - s}{s_{A+p+1} - s_{A+1}} N_{A+1}^{p-1}(s). \tag{2.3}$$

B-spline basis functions have many desirable properties. For example, they form a partition of unity, and are therefore coordinate system independent, are linearly independent, interpolate the end control points, obey the convex hull property, and obey the variation diminishing property.

2.1.3 B-spline Basis Function Derivatives

Derivatives of B-spline basis functions of degree p are able to be represented in terms of degree $p-1$ B-spline basis functions, because of their recursive definition. The derivative of the A^{th} basis function of degree p can be represented as:

$$\frac{d}{ds} N_A^p(s) = \frac{p}{s_{i+p} - s_i} N_A^{p-1}(s) - \frac{p}{s_{i+p+1} - s_{i+1}} N_{A+1}^{p-1}(s) \tag{2.4}$$

Higher order derivatives, which will be necessary for Kirchhoff-Love shells, can be expressed as

$$\frac{d^k}{d^k s} N_A^p(s) = \frac{p}{s_{i+p} - s_i} \left(\frac{d^{k-1}}{d^{k-1} s} N_A^{p-1}(s) \right) - \frac{p}{s_{i+p+1} - s_{i+1}} \left(\frac{d^{k-1}}{d^{k-1} s} N_{A+1}^{p-1}(s) \right) \tag{2.5}$$

It will later be shown that derivatives of B-spline basis functions of degree p can be expressed as a linear combination of the degree p basis functions themselves.

2.2 B-spline Curves

A B-spline curve is constructed by assigning a vector valued coefficient $\mathbf{P_A}$ to each B-spline basis function, $N_A(s)$. The vector valued coefficients are called control points. Each basis function, therefore, acts as a weighting function of its control point. Thus, a B-spline curve of degree p is defined as:

$$\mathbf{C}(s) = \sum_A \mathbf{P_A} N_A^p(s) \tag{2.6}$$

The vector-valued control points have d components where d is the dimension of the space that they are in. The piecewise linear interpolation of sequential control points is called the control polygon.

2.2.1 h-Refinement: Knot Insertion

One way to enrich the basis functions is knot insertion. Knots may be inserted into the original knot vector while preserving the exact same geometry and parametrization of the curve. This may sound counter-intuitive because we know that the parametric continuity of a B-spline curve depends on the knot multiplicity. By carefully choosing the new control points, however, the original geometric continuity and parametrization at every point on the curve can be maintained. Let the original knot vector be $\Xi = \{s_1, s_2, \ldots, s_{n+p+1}\}$. We can add m knots to obtain a new knot vector $\bar{\Xi} = \{\bar{s}_1, \bar{s}_2, \ldots, \bar{s}_{n+m+p+1} = s_{n+p+1}\}$. The new basis functions can be evaluated as was done previously and the new corresponding control points can be calculated as:

$$\bar{\beta} = \mathbf{T}^p \beta \tag{2.7}$$

where β is the vector of the original control points, $\bar{\beta}$ is the vector of updated control points after inserting the knots, and $\mathbf{T}^p$ is a second order tensor that maps between the original control points

and the updated control points. $\mathbf{T}^p$ is defined recursively as:

$$T_{ij}^0 = \begin{cases} 1, & \text{if} \quad \bar{s}_i \in [\, s_j, s_{j+1}) \\ 0, & \text{otherwise} \end{cases} \tag{2.8}$$

(2.9)

and

$$T_{ij}^{q+1} = \frac{\bar{s}_{i+q} - s_j}{s_{j+q} - s_j} T_{ij}^q + \frac{s_{j+q+1} - \bar{s}_{i+q}}{s_{j+q+1} - s_{j+1}} T_{ij+1}^q \quad \text{for } q = 0, 1, 2, \ldots, p-1 \tag{2.10}$$

Because each knot interval corresponds to an element in IGA, knot insertion can function as a mechanism to refine the mesh, analogous to *h*-refinement in traditional FEA, provided that knots are inserted in between current knot values. The case of inserting a knot that increases the multiplicity of an already existing knot will be discussed in Section 2.2.3.

2.2.2 *p*-Refinement: Degree Elevation

Degree elevation is another method to enrich the basis functions while keeping the original geometry and parametrization of the B-spline curve. Degree elevation is done by inserting knots until all original knot values have a multiplicity of $p-1$ (see Bézier Extraction section). The new B-spline control points are the same as the control points for each corresponding Bézier curve. Then the polynomial order is increased on each individual Bézier curve segment. Finally, extra knots from the process are removed in order to obtain the degree elevated B-spline control points.

2.2.3 *k*-Refinement: Smoothness Reduction

One final way to enrich the basis functions is to increase the multiplicity of existing knots. The process is the same as inserting a new unique knot. By increasing the multiplicity of existing knots the smoothness of the basis functions can be reduced. This also reduces the support of the basis functions. There is no analagous refinement method in traditional FEA. One example of

when smoothness reduction would be useful is in the case of a point load. You could insert knots around the point load, thus isolating the basis functions in that area.

2.3 B-spline Surfaces

Shells, as analyzed in FEA and IGA, will be treated as a two-dimensional surface in $\mathbb{R}^3$. A B-spline surface is the tensor product of two univariate B-spline curves. Thus a B-spline surface can be represented as

$$\mathbf{S}(s,t) = \sum_{A}^{n}\sum_{B}^{m} N_A^p(s) M_B^q(t) \mathbf{P}_{A,B} \tag{2.11}$$

where $\mathbf{P}_{A,B}$ are the control net of control points, $N_A^p(s)$ are the n number of degree p basis functions corresponding to a knot vector $\Xi = \{s_1, s_2, \ldots, s_{n+p+1}\}$, and $M_B^q(t)$ are the m number of degree q basis functions corresponding to a knot vector $\eta = \{t_1, t_2, \ldots, t_{m+q+1}\}$.

2.4 NURBS

B-spline curves as described thus far are very powerful and able to capture many interesting geometries. They are incapable, however, of representing conic sections (circles, ellipses, etc.) exactly. We can greatly expand the geometries we can model by introducing a scalar weight that pairs with each basis function and control point pair. By doing so we are able to change our basis functions from piecewise polynomial functions to piecewise rational functions. NURBS basis functions are defined as

$$R_A^p(s) = \frac{w_A N_A^p(s)}{\sum_{A=1}^{n} w_A N_A^p(s)} \tag{2.12}$$

where $N_A^p(s)$ are the n number of non-rational B-spline basis functions and w_A are the weights that correspond to each basis function. Notice that if all the weights are equal to one then the denominator of Equation (2.12) is equal to one because of the partition of unity, and the NURBS basis functions degenerate into B-spline basis functions.

The weight for each control point/basis function determines how much influence that control point basis function pair has on the curve. Although negative weights are possible, the present

work will only consider positive weights. As the weight of a control point approaches positive infinity the curve approaches that control point. As the weight of a control point approaches zero, that control point loses any influence on the curve.

The B-spline refinement techniques discussed previously can be performed on a NURBS curve by converting the control points to homogeneous coordinates, performing the refinement, and then converting back to spatial coordinates. Homogeneous coordinates are the spatial coordinates multiplied by the weight, and storing the weight as an additional coordinate. For example, control points with coordinates (x_A, y_A, z_A) and weights w_A would have homogenous coordinates $(x_A * w_A, y_A * w_A, z_A * w_A, w_A)$. Then the refinement technique could be applied as would be done on a non-rational B-spline curve, and then the weights would be divided out at the end.

A NURBS surface is the tensor product of two univariate NURBS curves, analogous to what is done for non-rational B-splines.

2.5 NURBS as a Basis for FEA

In the previous sections NURBS have been explained as a representation of geometry. Isogeometric analysis uses NURBS, not only to represent geometry, but also as basis functions to approximate a solution space. In traditional FEA this is called an isoparametric element; an element that uses the same basis functions to interpolate the known geometry and the unknown displacement field. The difference between an isoparametric element in traditional FEA and isogeometric analysis is that in isogeometric analysis basis functions are used that are able to exactly represent the geometry. Thus it is not necessary to make any geometric approximations.

2.5.1 The Finite Element Method

The finite element method is a numerical method to obtain an approximate solution to boundary value problems for partial differential equations. The governing partial differential equations for the problem in their original form are called the strong form of the boundary value problem. This strong form is then converted to an equivalent integral expression called the weak form. This is done so that the approximate solution will not to have to satisfy the governing differential equations everywhere, but rather it will only have to satisfy them in an integral or average sense.

Our approximate solution will also have to strictly satisfy the displacement and traction boundary conditions.

The geometric domain upon which the problem is to be solved is decomposed into smaller sub-domains, or elements. This process is called discretization. As the elements get smaller and smaller the approximate solution that only satisfies the PDE's in an average sense will approach the actual solution that satisfies the PDE's everywhere.

The solution is computed on each element as the linear combination of a chosen basis that minimizes the error. The approximation of the weak form as a linear combination of the chosen basis is called the Galerkin form. In traditional FEA Lagrangian interpolating polynomials are normally used as the chosen basis. The theory of isogeometric analysis is to use the same basis functions that CAD programs use to describe the geometry (usually NURBS). By doing so the geometry can be exactly represented, eliminating any geometric approximations. There are numerous other advantages to using NURBS basis functions as a basis for the solution. The most obvious advantage is that it streamlines the engineering design-analysis process, eliminating the costly step of geometry decomposition/approximation. There are also mathematical advantages to using NURBS as a basis for analysis. For example NURBS basis functions are, in general, C^{p-1} continuous on the element boundaries. Many classes of analysis problems require a certain degree of continuity that is very difficult to achieve using traditional piecewise-linear basis functions.

2.5.2 The Bézier Extraction Operator

One minor complication in using NURBS as a basis for analysis is that in general NURBS basis functions span multiple elements, making it difficult to apply local element routines like integration of the basis over an element. The solution is to extract the Bernstein basis functions from the NURBS basis functions and corresponding control points. By doing so, all isogeometric local element routines can be integrated seamlessly into an existing FEA framework. This process is called Bézier extraction. This is done by performing knot insertion, as previously described, until each knot has a multiplicity of p, which results in basis functions that are C^0 at the element boundaries. Thus Bézier basis functions and control points can be extracted from a NURBS geometry, and element routines can be performed on the Bézier basis functions.

2.5.3 The Gradient Extraction Operator

The evaluation of the increment of director, $\Delta\mathbf{d}$, for different shell formulations requires that certain quantities be lifted to control points. The lifting is achieved through a simple application of Bézier projection [10] on the element level. We compute an element gradient extraction operator $\mathbf{G}^e = [G^\alpha_{BA}]$ such that the gradients of the local B-spline basis functions are represented as a linear combination of the B-spline basis functions themselves on the level of elements as

$$N_{B,\alpha} = \sum_A G^\alpha_{BA} N_A. \tag{2.13}$$

where A and B here are the basis function index. As an example, the gradients of B-spline basis functions of degree 2 are calculated this way and depicted in Figure 2.1. The third gradient extraction operator is given in Equation (2.14).

$$\mathbf{G}^e = \begin{bmatrix} -9 & -3 & 3 \\ 12 & 0 & -12 \\ -3 & 3 & 9 \end{bmatrix} \tag{2.14}$$

Since the B-spline basis are one order higher than their derivatives, the latter can be exactly represented by the original B-spline basis. In other words, Bézier projection results in exact derivatives of the basis in this case. Using the gradient extraction operator, the gradient of any field, ψ, with respect to the parametric coordinates can be lifted to the control points as

$$\psi_{,\alpha} = \sum_B N_{B,\alpha}\psi_B \tag{2.15}$$

$$= \sum_B \sum_A G^\alpha_{BA} N_A \psi_B \tag{2.16}$$

$$= \sum_A N_A \psi^\alpha_A \tag{2.17}$$

where

$$\psi^\alpha_A = \sum_B G^\alpha_{BA}\psi_B. \tag{2.18}$$

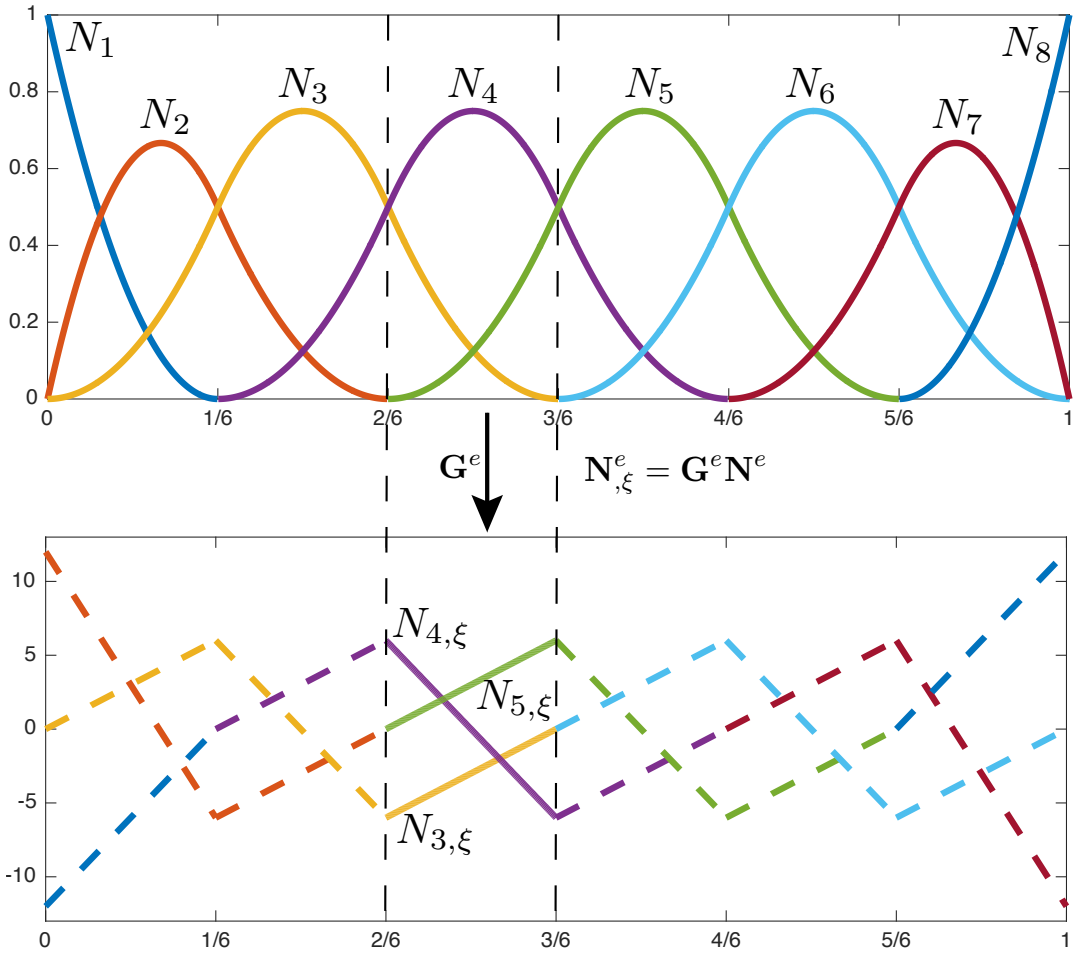

Figure 2.1: Gradient extraction operator on element $e = 3$ (top: B-spline basis, $p = 2$. bottom: derivatives of B-spline basis).

is the control values of the gradient field. Thus, the extraction operator, which only needs to be calculated once during the whole analysis process, offers an unified framework to calculate all gradient fields exactly for polynomial geometry. This will improve the computational accuracy, especially for geometrically nonlinear problems. Meanwhile, as can be seen later, it also facilitates the construction of blended shell formulations for various shell kinematics by lifting the gradient field to the control points. Other shell or beam kinematics can easily be included within this framework.

CHAPTER 3. SHELL GEOMETRY AND KINEMATICS

In this section, we will discuss four different shell kinematic descriptions. The geometry and notation explained in this section will apply to all four shells. They will also have the same mid-surface displacement, $\bar{\mathbf{u}}$. The subsequent sections will discuss the variation of the current shell director, $\mathbf{d}$, for each particular shell.

As shown in Figure 3.1, a shell in the reference configuration is described by a reference midsurface $\bar{\mathbf{X}}$ and an inextensible director vector field $\mathbf{D}$,

$$\mathbf{X}(s^1, s^2, s^3) = \bar{\mathbf{X}}(s^1, s^2) + s^3 \frac{h}{2} \mathbf{D}(s^1, s^2) \tag{3.1}$$

where h is the shell thickness, and s^3 is the thickness coordinate ranging from -1 to 1. The director $\mathbf{D}$ is chosen to be the unit normal to the reference surface

$$\mathbf{D} = \frac{\bar{\mathbf{X}}_{,1} \times \bar{\mathbf{X}}_{,2}}{|\bar{\mathbf{X}}_{,1} \times \bar{\mathbf{X}}_{,2}|} \tag{3.2}$$

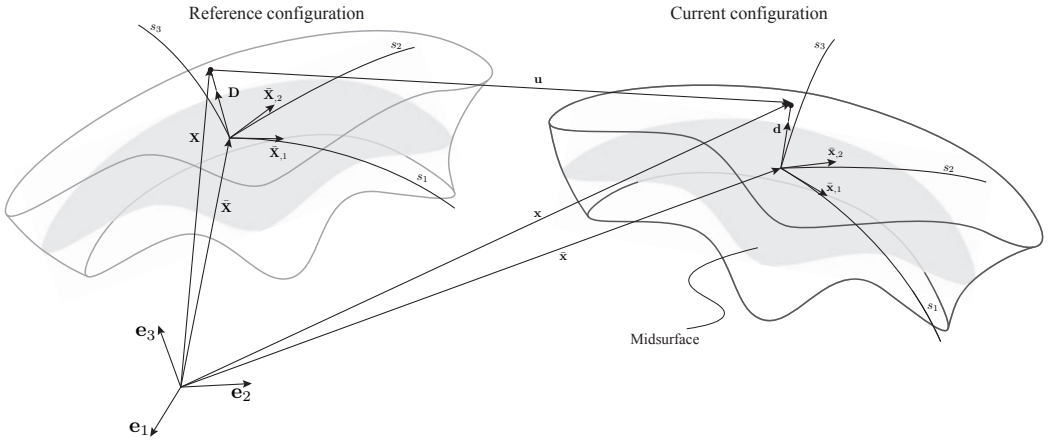

Figure 3.1: Reference and current configuration of the shell

where $(\cdot)_{,\alpha}$ denotes $\partial(\cdot)/\partial s^{\alpha}$. Similarly, the current configuration $\mathbf{x}$ can be written as

$$\mathbf{x}(s^1, s^2, s^3) = \bar{\mathbf{x}}(s^1, s^2) + s^3 \frac{h}{2} \mathbf{d}\left(s^1, s^2\right) \tag{3.3}$$

where $\bar{\mathbf{x}}$ is the midsurface in the current configuration and $\mathbf{d}$ is the current director vector. The displacement of the shell is written as

$$\mathbf{u} = \mathbf{x} - \mathbf{X} \tag{3.4}$$

$$= \bar{\mathbf{u}} + s^3 \frac{h}{2} [\mathbf{d} - \mathbf{D}] \tag{3.5}$$

$$= \bar{\mathbf{u}} + s^3 \Delta\mathbf{d} \tag{3.6}$$

where $\bar{\mathbf{u}}$ is the displacement of the reference surface and $\Delta\mathbf{d}$ is the increment of the director. Using standard techniques [11] we can construct an orthonormal lamina basis, $\{\mathbf{e}_i^{\ell}\}_{i=1}^{3}$, with coordinates $(\theta^1, \theta^2, \theta^3)$ at any point on the midsurface. Note that $\mathbf{e}_3^{\ell}$ is normal to the surface. The lamina basis is used to enforce the zero normal stress condition common to shell models. The transformation from global to lamina coordinates is

$$\mathbf{q} = [q_{ij}] = [\mathbf{e}_1^{\ell} \quad \mathbf{e}_2^{\ell} \quad \mathbf{e}_3^{\ell}]^T \tag{3.7}$$

and the gradient of lamina coordinates with respect to parametric coordinates is

$$\frac{\partial \theta^i}{\partial s^j} = \mathbf{e}_i^{\ell} \cdot \frac{\partial \mathbf{x}}{\partial s^j}. \tag{3.8}$$

The displacement in lamina coordinates is $\mathbf{u}^{\ell} = \mathbf{q}\mathbf{u}$ and the displacement gradient in lamina coordinates is

$$\frac{\partial \mathbf{u}^{\ell}}{\partial \theta^j} = \mathbf{q} \frac{\partial \mathbf{u}}{\partial s^k} \frac{\partial s^k}{\partial \theta^j} \tag{3.9}$$

where

$$\frac{\partial \mathbf{u}}{\partial s^k}\frac{\partial s^k}{\partial \theta^j} = \frac{\partial \mathbf{u}}{\partial s^k}J^{-1}_{kj} \tag{3.10}$$

$$= \sum_\alpha \frac{\partial \mathbf{u}}{\partial s^\alpha}J^{-1}_{\alpha j} + \frac{\partial \mathbf{u}}{\partial s^3}J^{-1}_{3j} \tag{3.11}$$

$$= \sum_\alpha \frac{\partial \bar{\mathbf{u}}}{\partial s^\alpha}J^{-1}_{\alpha j} + s^3\sum_\alpha \frac{\partial \Delta\mathbf{d}}{\partial s^\alpha}J^{-1}_{\alpha j} + \Delta\mathbf{d}J^{-1}_{3j} \tag{3.12}$$

$$= \sum_\alpha \bar{\mathbf{u}}_{,\alpha}J^{-1}_{\alpha j} + s^3\sum_\alpha \Delta\mathbf{d}_{,\alpha}J^{-1}_{\alpha j} + \Delta\mathbf{d}J^{-1}_{3j}. \tag{3.13}$$

3.1 Reissner-Mindlin Shells, RM6 and RM5

3.1.1 RM6 Shell Director

The most predominant shell theory used in traditional FEA programs is Reissner-Mindlin shell theory or "thick-shell" theory. This is because the Reissner-Mindlin shell formulation only requires C^0 continuous basis functions. Standard linear piecewise "hat" functions typically used in FEA are able to satisfy that requirement. In contrast, Kirchhoff-Love shells require C^1 smoothness between elements, a requirement that these "hat" functions are not able to satisfy. This is the reason that Reissner-Mindlin shells are so ubiquitous in FEA.

The basic concept of this shell theory is that each node has three global translational DOFs and three global rotational DOFs. The shell director, which begins normal to the shell midsurface in the reference configuration, is not required to remain normal in the current or deformed configuration. Reissner-Mindlin shells are able to capture transverse shear deformation because of this feature. The current shell director can be expressed as the reference shell director rotated about three global axes.

$$\mathbf{d}^{RM6} = \mathbf{R}(\omega)\mathbf{D} \tag{3.14}$$

The rotation can be expressed as an infinite series,

$$\mathbf{R}(\omega) = exp(\hat{\omega}) = \sum_{n\geq 0}\frac{\hat{\omega}^n}{n!} \tag{3.15}$$

where

$$\hat{\boldsymbol{\omega}} = skew(\boldsymbol{\omega}) \tag{3.16}$$

3.1.2 Increment of RM6 Shell Director, $\Delta\mathbf{d}^{RM6}$

We can interpolate the variation of the current shell director as

$$\Delta\mathbf{d}^{RM6} = \sum_{A\in RM6} \frac{h}{2} N_A \Delta\mathbf{d}_A^{RM6} \tag{3.17}$$

$$= \sum_{A\in RM6} \frac{h}{2} N_A \,\mathrm{skew}(\mathbf{d}_A)^T \boldsymbol{\omega}_A \tag{3.18}$$

$$= \sum_{A\in RM6} \mathbf{H}_A \boldsymbol{\omega}_A \tag{3.19}$$

where $\boldsymbol{\omega}_A = [\omega_{A1} \quad \omega_{A2} \quad \omega_{A3}]^{\mathrm{T}}$. Note that only C^0 basis functions are required by this theory. Since three *global* rotations are used this kinematic description can be used in the presence of kinks and intersections with other structural members.

3.1.3 Increment of RM5 Shell Director, $\Delta\mathbf{d}^{RM5}$

A standard Reissner-Mindlin shear deformable shell theory with two local rotations can be formulated as

$$\Delta\mathbf{d}^{RM5} = \sum_{A\in RM5} \frac{h}{2} N_A \Delta\mathbf{d}_A^{RM5} \tag{3.20}$$

$$= \sum_{A\in RM5} \frac{h}{2} N_A \,\mathrm{skew}(\mathbf{d}_A)^T \begin{bmatrix} \mathbf{e}_{A1}^f & \mathbf{e}_{A2}^f \end{bmatrix} \boldsymbol{\beta}_A \tag{3.21}$$

$$= \sum_{A\in RM5} \mathbf{G}_A \boldsymbol{\beta}_A \tag{3.22}$$

where

$$\text{skew}(\mathbf{d}_A)^{\mathrm{T}} = \begin{bmatrix} 0 & d_{A3} & -d_{A2} \\ -d_{A3} & 0 & d_{A1} \\ d_{A2} & -d_{A1} & 0 \end{bmatrix} \tag{3.23}$$

and $\boldsymbol{\beta}_A = [\beta_{A1} \quad \beta_{A2}]^T$ are the local rotations. Note that $\left\{\mathbf{e}_{Ai}^f\right\}$ is the fiber basis constructed at node A that lie tangent to the shell using standard techniques [11]. Note that smooth geometry but only C^0 basis functions are required by this theory.

3.2 Kirchhoff-Love Shell, KL3

Kirchhoff-Love shell theory has rarely been used in the field of FEA because the formulation requires C^1 smoothness, something not easily achieved using standard FEA basis functions. KL3 shells have 3 global displacement DOFs. The KL3 formulation is free from shear locking because it doesn't take into account transverse shear deformation. For KL3 "thin-shell" theory the current director vector $\mathbf{d}$ is set to the unit normal vector with respect to the current reference surface. In other words,

$$\mathbf{d} = \frac{\mathbf{p}}{||\mathbf{p}||} \tag{3.24}$$

where

$$\mathbf{p} = \mathbf{x}_{,1} \times \mathbf{x}_{,2}. \tag{3.25}$$

3.2.1 Increment of KL3 Shell Director, $\Delta\mathbf{d}^{KL3}$

In the linear setting $\Delta\mathbf{d} = \delta d = d_{,\alpha}$. By differentiating Equation (3.24) we obtain,

$$\mathbf{d}_{,\alpha} = \left(\frac{(\mathbf{p}_{,\alpha} \otimes \mathbf{p}) - (\mathbf{p} \otimes \mathbf{p}_{,\alpha})}{\mathbf{p} \cdot \mathbf{p}} \right) \mathbf{d}. \tag{3.26}$$

where $\otimes$ denotes the tensor product and

$$\mathbf{p}_{,\alpha} = \mathbf{x}_{,1\alpha} \times \mathbf{x}_{,2} + \mathbf{x}_{,1} \times \mathbf{x}_{,2\alpha} \tag{3.27}$$

Then, the linearized increment $\Delta\mathbf{d}^{KL3}$ can be written as

$$\Delta\mathbf{d}^{KL3} = \frac{h}{2}\frac{1}{||\mathbf{p}||}\left(\mathbf{I} - \mathbf{d}\otimes\mathbf{d}\right)\left(\bar{\mathbf{u}}_{,1} \times \mathbf{x}_{,2} + \mathbf{x}_{,1} \times \bar{\mathbf{u}}_{,2}\right) \tag{3.28}$$

Standard approximate interpolation of the increment of director

Since the blended shell kinematics is formulated based on the degenerated shell, a standard approach in FEA to interpolate the increment of director is used in [12] as

$$\Delta\mathbf{d}^{KL3} \approx \frac{h}{2}\sum_{A\in KL3} N_A \Delta\mathbf{d}_A^{KL3} \tag{3.29}$$

where

$$\Delta\mathbf{d}_A^{KL3} = \frac{1}{||\mathbf{p}_A||}\left(\mathbf{I} - \mathbf{d}_A\otimes\mathbf{d}_A\right)\left(\left(\bar{\mathbf{u}}_A^1 \times \mathbf{x}_A^2\right) + \left(\mathbf{x}_A^1 \times \bar{\mathbf{u}}_A^2\right)\right) \tag{3.30}$$

$$\tag{3.31}$$

where $\mathbf{p}_A$, $\mathbf{d}_A$, $\bar{\mathbf{u}}_A^\alpha$ and $\mathbf{x}_A^\alpha$ are the nodal values of $\mathbf{p}$, $\mathbf{d}$, $\bar{\mathbf{u}}_{,\alpha}$ and $\mathbf{x}_{,\alpha}$, respectively.

Proposed exact interpolation of the increment of director

The proposed approach does not interpolate the whole $\Delta\mathbf{d}^{KL3}$, but only the unknown variable $\bar{\mathbf{u}}$. Thus, we can make full use of exact geometry benefits IGA offered. This leads to very accurate shell formulations for highly curved geometry regardless of mesh density. Keeping the

exact geometry quantities, Equation (3.28) can be interpolated as

$$\begin{aligned}\Delta\mathbf{d}^{KL3} &= \frac{h}{2}\frac{1}{||\mathbf{p}||}(\mathbf{I}-\mathbf{d}\otimes\mathbf{d})\left(\sum_{A\in KL3}N_A\left(\sum_{B\in S}G^1_{BA}\bar{\mathbf{u}}_B\right)\times\mathbf{x}_{,2}\right.\\ &\qquad\left.+\,\mathbf{x}_{,1}\times\sum_{A\in KL3}N_A\left(\sum_{B\in S}G^2_{BA}\bar{\mathbf{u}}_B\right)\right) \qquad (3.32)\\ &= \frac{h}{2}\frac{1}{||\mathbf{p}||}(\mathbf{I}-\mathbf{d}\otimes\mathbf{d})\sum_{A\in KL3}N_A\sum_{B\in S}\left(G^2_{BA}\,\mathrm{skew}(\mathbf{x}_{,1})\right.\\ &\qquad\left.-\,G^1_{BA}\,\mathrm{skew}(\mathbf{x}_{,2})\right)\bar{\mathbf{u}}_B \qquad (3.33)\\ &= \sum_{B\in S}\mathbf{E}^{KL3}_B\bar{\mathbf{u}}_B \qquad (3.34)\end{aligned}$$

where the abbreviation

$$\mathbf{E}^{KL3}_B = \frac{h}{2}\frac{1}{||\mathbf{p}||}(\mathbf{I}-\mathbf{d}\otimes\mathbf{d})\sum_{A\in KL3}N_A(G^2_{BA}\,\mathrm{skew}(\mathbf{x}_{,1})-G^1_{BA}\,\mathrm{skew}(\mathbf{x}_{,2})) \qquad (3.35)$$

and the superscript on $\mathbf{E}$ denotes the node set which is used in the underlying sum. In this case the node set is $KL3$.

We demonstrate the benefits of exact increment of the director on solution accuracy in Section 6.1.5. Compared with the approximate interpolation of the increment of director, the proposed approach needs more computational cost. But as mentioned before, since we have lifted all gradient fields to the control points by using the gradient extraction operator, the exact geometric quantities, such as, $\mathbf{d}$ and $\mathbf{x}_{,\alpha}$, can be calcualted with minimal compuational efforts. Thus, for a predefined error bound, the proposed approach still yields considerable savings in computational cost, and also makes the blended shell more robust regardless of the mesh density.

3.3 Hierarchic Kirchhoff-Love Shell, KL5

This work uses a hierarchic Kirchhoff-Love shell based on that presented by Echter et. al in [8]. The KL5 shell has the same three global displacement DOF as KL3 shells. KL5 shells have a hierarchic difference vector that is added to the KL3 director. This hierarchic difference vector, $\mathbf{w}$, contains two parameters that capture only shear deformation. The KL5 shell director can then

be expressed as,

$$\mathbf{d}^{KL5} = \mathbf{d}^{KL3} + \mathbf{w} \tag{3.36}$$

where

$$\mathbf{w} = w_1 \mathbf{x}_{,1} + w_2 \mathbf{x}_{,2} \tag{3.37}$$

Note that $\mathbf{w}$ is a function of the in-plane parametric coordinates only, and does not vary through the thickness of the shell.

3.3.1 Increment of KL5 Shell Director, $\Delta\mathbf{d}^{KL5}$

In the linear setting, the variation of the director can be expressed as

$$\Delta\mathbf{d}^{KL5} = \Delta\mathbf{d}^{KL3} + \Delta\mathbf{w} \tag{3.38}$$

where

$$\begin{aligned}
\Delta\mathbf{w} &= \frac{h}{2}\left(w_{1,1}\mathbf{x}_{,1} + w_{2,2}\mathbf{x}_{,2}\right) && (3.39)\\
&= \frac{h}{2}\sum_{A\in KL5} N_A \sum_{B\in KL5}\left(G^1_{BA} w_{B1}\mathbf{x}_{,1} + G^2_{BA} w_{B2}\mathbf{x}_{,2}\right) && (3.40)\\
&= \frac{h}{2}\sum_{B\in KL5}\left(\sum_{A\in KL5} N_A \begin{bmatrix} G^1_{BA}\mathbf{x}_{,1} & G^2_{BA}\mathbf{x}_{,2}\end{bmatrix}\right)\mathbf{w}_B && (3.41)\\
&= \sum_{B\in KL5}\mathbf{F}_B\mathbf{w}_B. && (3.42)
\end{aligned}$$

Therefore

$$\begin{aligned}
\Delta\mathbf{d}^{KL5} &= \sum_{C\in S}\mathbf{E}^{KL5}_C\bar{\mathbf{u}}_C + \sum_{B\in KL5}\mathbf{F}_B\mathbf{w}_B && (3.43)\\
&= \sum_{C\in S}\left(\mathbf{E}^{KL5}_C\bar{\mathbf{u}}_C + \left(\sum_{B\in KL5}\mathbf{F}_B\delta_{BC}\right)\mathbf{w}_C\right). && (3.44)
\end{aligned}$$

Note that $\Delta\mathbf{w}$ in Equation (3.39) is constructed via derivatives of the primitives of shear angles instead of the shear angles themselves. This yields improved shear stress quality due to the equal order interpolation. Also, approximations similar to those described in Section 3.2.1 can also be employed in the definition of $\Delta\mathbf{d}^{KL5}$.

4.1 Final Blending

Recall that

$$\mathbf{u} = \bar{\mathbf{u}} + s^3 \left(\Delta \mathbf{d}^{KL3} + \Delta \mathbf{d}^{KL5} + \Delta \mathbf{d}^{RM5} + \Delta \mathbf{d}^{RM6} \right). \tag{4.1}$$

Plugging in the definitions of each kinematic description yields

$$\begin{aligned} \mathbf{u} = & \sum_{A \in S} N_A \bar{\mathbf{u}}_A + \sum_{A \in S} s^3 \mathbf{E}_A^{KL3} \bar{\mathbf{u}}_A \\ & + \sum_{A \in S} s^3 \left(\mathbf{E}_A^{KL5} \bar{\mathbf{u}}_A + \left(\sum_{B \in KL5} \mathbf{F}_B \delta_{BA} \right) \mathbf{w}_A \right) \\ & + \sum_{A \in S} \left(\sum_{C \in RM5} s^3 \mathbf{G}_C \delta_{CA} \right) \boldsymbol{\beta}_A + \sum_{A \in S} \left(\sum_{D \in RM6} s^3 \mathbf{H}_D \delta_{DA} \right) \boldsymbol{\omega}_A \end{aligned} \tag{4.2}$$

which can be further simplified to

$$\begin{aligned} \mathbf{u} = & \sum_{A \in S} \left(N_A + s^3 \left(\mathbf{E}_A^{KL3} + \mathbf{E}_A^{KL5} \right) \right) \bar{\mathbf{u}}_A \\ & + \sum_{A \in S} s^3 \left(\sum_{B \in KL5} \mathbf{F}_B \delta_{BA} \right) \mathbf{w}_A + \sum_{A \in S} s^3 \left(\sum_{C \in RM5} \mathbf{G}_C \delta_{CA} \right) \boldsymbol{\beta}_A \\ & + \sum_{A \in S} s^3 \left(\sum_{D \in RM6} \mathbf{H}_D \delta_{DA} \right) \boldsymbol{\omega}_A. \end{aligned} \tag{4.3}$$

CHAPTER 5. THE PRINCIPAL OF VIRTUAL WORK

In this paper, we restrict the geometrically exact blended shell formulation to linear elastic problems. The starting point is the principle of virtual work in the spatial configuration,

$$\delta\Pi(\boldsymbol{u}) = \int_{\Omega} \boldsymbol{\sigma}(\boldsymbol{u}) : \delta\boldsymbol{\varepsilon}\, \mathrm{d}\Omega - \int_{\Gamma} \boldsymbol{t} \cdot \delta\boldsymbol{u}\, \mathrm{d}\Gamma - \int_{\Omega} \boldsymbol{b} \cdot \delta\boldsymbol{u}\, \mathrm{d}\Omega = 0 \tag{5.1}$$

where Ω is the current configuration, Γ is the boundary of the current configuration, $\boldsymbol{\sigma}$ is the Cauchy stress, $\boldsymbol{\varepsilon}$ is the small strain tensor, $\boldsymbol{t}$ is the traction, and $\boldsymbol{b}$ is the body force.

5.0.1 Reduced Constitutive Equation

The linear elastic constitutive equations of three-dimensional elasticity are written in the lamina coordinate system. In the lamina coordinate system, the zero normal-stress assumption, $\sigma_{33}^{\ell} = 0$, is enforced by solving for the strain component ε_{33}^{ℓ} in terms of the other strain components. This resulting reduced constitutive equation is written as

$$\tilde{\boldsymbol{\sigma}}^{\ell} = \tilde{\mathbf{D}}^{\ell} \tilde{\boldsymbol{\varepsilon}}^{\ell} \tag{5.2}$$

where

$$\tilde{\boldsymbol{\sigma}}^{\ell} = \begin{Bmatrix} \tilde{\sigma}_{11}^{\ell} \\ \tilde{\sigma}_{22}^{\ell} \\ \tilde{\sigma}_{12}^{\ell} \\ \tilde{\sigma}_{23}^{\ell} \\ \tilde{\sigma}_{31}^{\ell} \end{Bmatrix}, \tag{5.3}$$

$$\tilde{\boldsymbol{\varepsilon}}^{\ell} = \begin{Bmatrix} \tilde{\varepsilon}^{\ell}_{11} \\ \tilde{\varepsilon}^{\ell}_{22} \\ 2\tilde{\varepsilon}^{\ell}_{12} \\ 2\tilde{\varepsilon}^{\ell}_{23} \\ 2\tilde{\varepsilon}^{\ell}_{31} \end{Bmatrix} = \begin{Bmatrix} \frac{\partial u^{\ell}_1}{\partial \theta^{\ell}_1} \\ \frac{\partial u^{\ell}_2}{\partial \theta^{\ell}_2} \\ \frac{\partial u^{\ell}_1}{\partial \theta^{\ell}_2} + \frac{\partial u^{\ell}_2}{\partial \theta^{\ell}_1} \\ \frac{\partial u^{\ell}_2}{\partial \theta^{\ell}_3} + \frac{\partial u^{\ell}_3}{\partial \theta^{\ell}_2} \\ \frac{\partial u^{\ell}_3}{\partial \theta^{\ell}_1} + \frac{\partial u^{\ell}_1}{\partial \theta^{\ell}_3} \end{Bmatrix}, \tag{5.4}$$

and

$$\tilde{\mathbf{D}}^{\ell} = \frac{E}{1-\nu^2} \begin{bmatrix} 1 & \nu & 0 & 0 & 0 \\ \nu & 1 & 0 & 0 & 0 \\ 0 & 0 & \frac{1-\nu}{2} & 0 & 0 \\ 0 & 0 & 0 & \kappa\frac{1-\nu}{2} & 0 \\ 0 & 0 & 0 & 0 & \kappa\frac{1-\nu}{2} \end{bmatrix} \tag{5.5}$$

where E is the Young's modulus, ν is the Poisson's ratio, and κ is a shear correction factor, which is used to improve the shear deformation approximation and commonly taken to be $\frac{5}{6}$ [13]

5.0.2 Strain-Displacement Matrix

Substituting (4.1) into the definition of strain (5.4) and rewriting the result in terms of the nodal strain-displacement matrix $\mathbf{B}_A$ yields

$$\tilde{\boldsymbol{\varepsilon}}^{\ell} = \sum_A \boldsymbol{B}_A \begin{Bmatrix} \bar{\mathbf{u}}_A \\ \boldsymbol{\varphi}_A \end{Bmatrix} \tag{5.6}$$

where $\bar{\mathbf{u}}_A$ is the vector of nodal displacements and $\boldsymbol{\varphi}_A$ is the vector of nodal rotations. The interpretation of the nodal rotations depends on the associated nodal director.

5.0.3 Discretization of the Weak Form

The weak form (5.1) can be written in matrix form as

$$\mathbf{K}\mathbf{u} = \mathbf{f} \tag{5.7}$$

where $\mathbf{K}$ is the stiffness matrix and $\mathbf{f}$ is the external force vector. $\mathbf{K}$ and $\mathbf{f}$ are assembled from element stiffness matrices $\mathbf{K}^e$ and external force vectors $\mathbf{f}^e$ where e denotes an element index. The entries of $\mathbf{K}^e = [K^e_{AB}]$ and $\mathbf{f}^e = \{f^e_A\}$ are calculated as

$$\mathbf{K}^e_{AB} = \int_{\Omega^e} \mathbf{B}_A^{\mathrm{T}} \tilde{\mathbf{D}} \mathbf{B}_B d\Omega \tag{5.8}$$

$$f^e_A = \int_{\Omega^e} N_A \bar{\mathbf{b}} d\Omega + \int_{\Gamma^e} N_A \bar{\mathbf{t}} d\Gamma \tag{5.9}$$

where $\bar{\mathbf{b}}$ and $\bar{\mathbf{t}}$ are the equivalent body force and boundary traction vectors, respectively.

CHAPTER 6. NUMERICAL RESULTS

6.1 Numerical Results

We present an extensive suite of benchmark problems to assess the accuracy and robustness of the blended shell formulation. We exercise the different kinematic descriptions in the blending in both the thick and thin shell regimes. In all cases, we leverage RM5 and RM6 nodes for the imposition of boundary conditions. Interior nodes are set to KL3, KL5, RM5, or RM6 to demonstrate the behavior of the blending. We denote an example where boundary nodes are set to RM6 and interior nodes are set to KL3 by RM6/KL3. Other blendings follow the same notational pattern. By increasing smoothness and employing different quadrature schemes we explore the behavior of shear and membrane locking for thick and very thin shells. We denote a Gauss quadrature scheme with $p+1$ points in each direction over an element by QP1, a reduced Gauss quadrature scheme with p points in each direction over an element by QP0, and the non-uniform, reduced Gauss quadrature scheme described in [14–16] by QNU. The quadrature points for these three schemes are illustrated with an exemplary NURBS patch in Figure 6.1. Note that QNU is essentially a one-point quadrature scheme *for all orders* away from the shell boundaries so it is the most *efficient* quadrature scheme of the three.

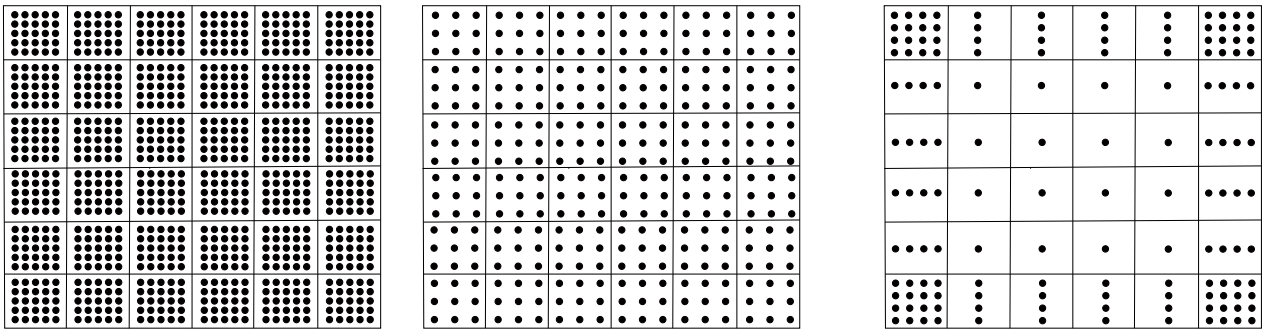

(a) Full integration (QP1). (b) Reduced integration (QP0). (c) Non-uniform integration (QNU).

Figure 6.1: Different integration rules for a NURBS patch, $p = 4$.

Where appropriate, we benchmark our shell formulation against the workhorse shell elements in both Nastran and Abaqus. To the best of the authors knowledge this is the first extensive head-to-head comparison between IGA shell elements and standard FEA shell elements. The benchmarks we solve are:

- In-plane bending of a straight cantilever beam (Section 6.1.1).
- Out-of-plane bending of a straight cantilever beam (Section 6.1.2).
- Simply supported rectangular plate subject to a distributed load (Section 6.1.3)
- Clamped rectangular plate subject to a distributed load (Section 6.1.4).
- Cylindrical shell subject to an end load acting in the radial direction (Section 6.1.5).
- The Scordelis-Lo roof problem (Section 6.1.6).
- The pinched cylinder problem (Section 6.1.7).
- The hemispherical shell with a hole (Section 6.1.8).
- The pinched sphere problem (Section 6.1.9).

The commercial element types used in our study are shown in Table 6.2. For each element type we list the number of nodes per element, the number of degrees-of-freedom per node, and the quadrature scheme (full, reduced, or either). For Abaqus shell elements S4 and S4R a Reissner-Mindlin description is used for thick shells which transitions to a discrete Kirchhoff shell theory as the shell thickness decreases. For Abaqus shell elements S4R5 and S8R5 a discrete Kirchhoff shell theory is employed. All the Nastran shell elements employ a Reissner-Mindlin shell theory where several approaches to drilling stiffness can be selected by the user. For the beam and plate problems we study the convergence behavior for both thick and thin shells and demonstrate the ability of an element to capture the effects of thickness changes robustly. When plots of comparisons are made the plots in the left column will be comparisons against Abaqus shell elements while the plots in the right column will be comparisons against Nastran elements.

Table 6.1: Commercial FEA shell elements (Abaqus [1, 2] and Nastran [3, 4]) used in this study.

Element Types		# Nodes	# Dofs/Node	Quadrature
Abaqus	S4	4	6	Full
	S4R	4	6	Reduced
Nastran	QUAD4	4	6	Either
	QUADR	4	6	Either

We make most comparisons on a per degree-of-freedom basis or for a fixed number of degrees-of-freedom with decreasing thickness. Although higher-order shell elements are traditionally more expensive to assemble than low-order shell elements this picture is changing dramatically with the introduction of new quadrature and assembly schemes optimized for higher-order smooth basis functions [17]. We present most comparisons in graphical form but include all computed values in the form of tables in Appendix A for the reader interested in conducting additional benchmarking.

6.1.1 In-Plane Bending of a Straight Cantilever Beam

The straight cantilever beam exercises the principal element deformation modes such as constant and linearly varying strains and curvatures [18]. In this case, we subject the beam to in-plane bending as shown in Figure 6.2. The beam has a length of $L = 6$, width $b = 0.2$, and thickness, $t = 0.1$. It is fixed on the left end and subject to a traction $q_z = 5.0$ on the right end. The material has Young's modulus, $E = 1e^7$, and Poisson's ratio, $\nu = 0.3$. The maximum downward displacement at the free end is monitored. The exact Bernoulli beam theory solution is $u_{exact} = 0.1080$.

The results of the test for B-spline basis functions of degree $p = 2$ and maximal smoothness are shown in Figure 6.3 while the results for $p = 3$ are shown in Figure 6.4. Notice that, even for QP1, increasing smoothness alleviates locking. For a fixed degree p reduced quadrature QNU effectively alleviates locking and enjoys efficiency advantages over the other quadrature schemes QP1 and QP0. Surprisingly, the Abaqus shell elements perform very poorly for this benchmark. The IGA and Nastran results are virtually indistinguishable. Tabulated results for this problem can be found in Appendix A.1.

Table 6.2: Benchmark Parameters.

Benchmark	Geometry	Material Properties	Loading
In-Plane Bending of Cantilever Beam	$L = 6$ $b = 0.2$ $t = 0.1$	$E = 1.0e7$ $\nu = 0.3$	$q_z = 5.0$
Out-of-Plane Bending of Cantilever Beam	$L = 6$ $b = 0.2$ $t = 0.1$	$E = 1.0e7$ $\nu = 0.3$	$q_z = 5.0$
Simply Supported Plate/Clamped Plate	$L = 10$ t varies	$E = 1.0e3$ $\nu = 0.3$	$q_z = 1.0t^3$
Cylindrical Shell	$R = 10$ $b = 1$ t varies	$E = 1.0e3$ $\nu = 0$	$q_x = 0.1t^3$
Scordelis-Lo Roof	$R = 300$ $L = 600$ $t = 3.0$ 80° arc	$E = 3.0e6$ $\nu = 0.3$ $\rho = 5.3971e-4$ $g = 386$	gravity loading
Pinched Cylinder	$R = 3.0$ $L = 6.0$ $t = 0.03$	$E = 3.0e10$ $\nu = 0.3$	$P = 1.0$
Hemispherical Shell with Hole	$R = 10.0$ 18° hole $t = 0.04$	$E = 6.825e7$ $\nu = 0.3$	$P = 2.0$
Pinched Sphere	$R = 20.0$ $t = 0.04$	$E = 1.0e^7$ $\nu = 0.3$	$P = 10.0$

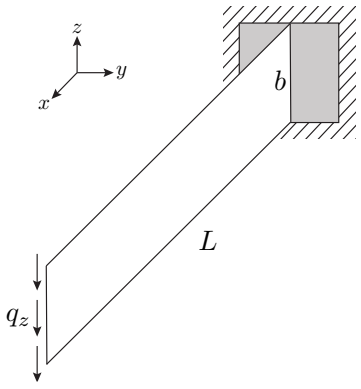

Figure 6.2: Schematic for the in-plane bending of a straight cantilever beam.

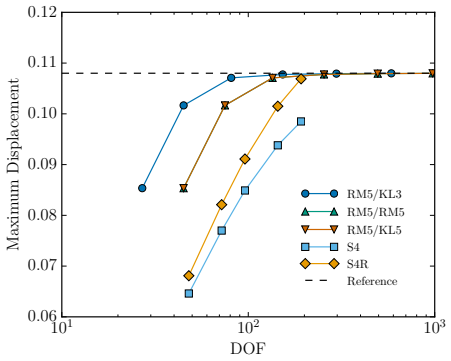

(a) $p = 2$, QP1 quadrature.

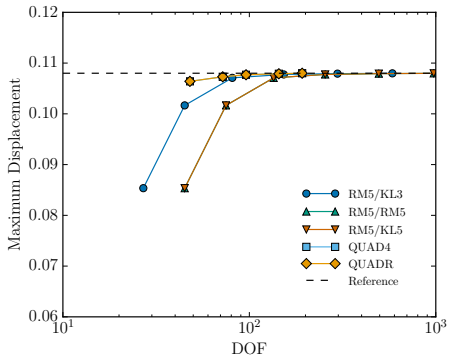

(b) $p = 2$, QP1 quadrature.

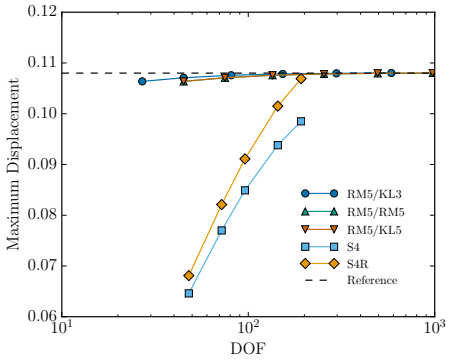

(c) $p = 2$, QP0 quadrature.

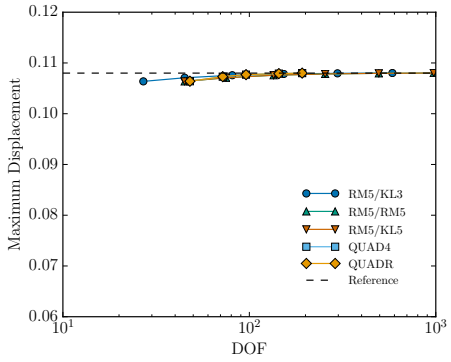

(d) $p = 2$, QP0 quadrature.

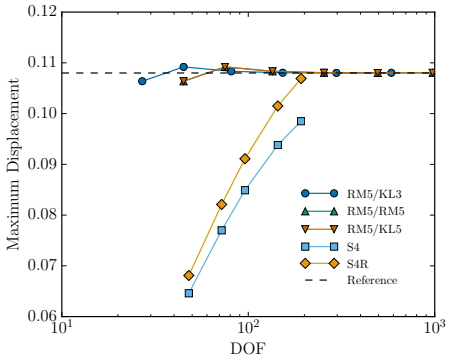

(e) $p = 2$, QNU quadrature.

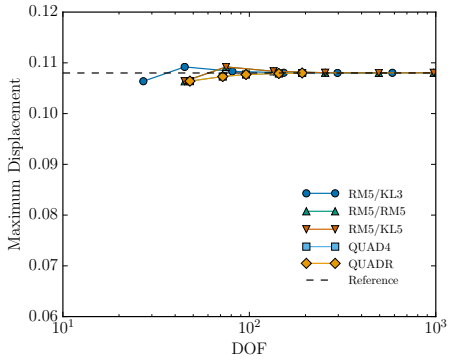

(f) $p = 2$, QNU quadrature.

Figure 6.3: Maximum deflection for in-plane bending of a cantilever beam, $p = 2$.

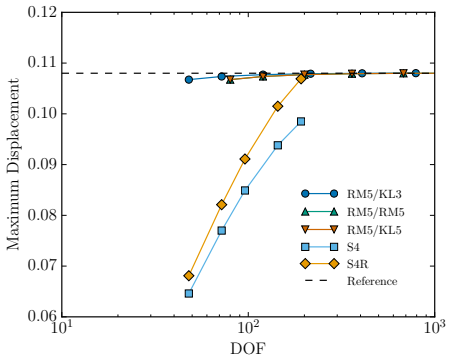

(a) $p = 3$, QP1 quadrature.

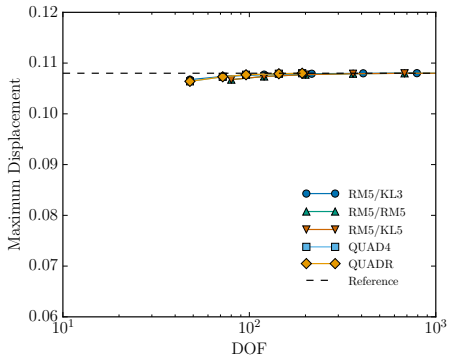

(b) $p = 3$, QP1 quadrature.

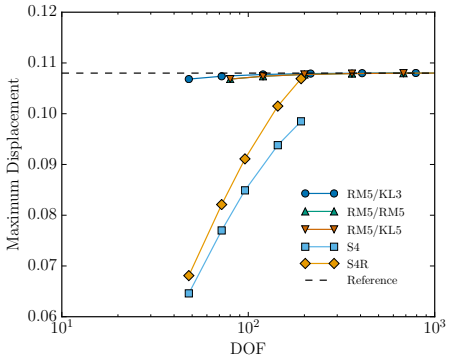

(c) $p = 3$, QP0 quadrature.

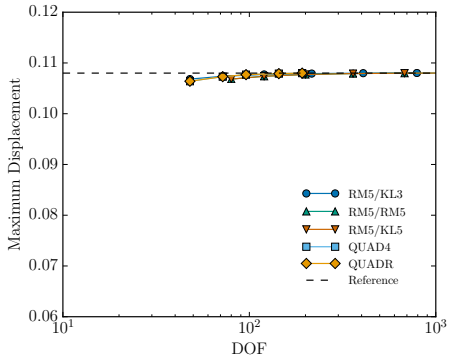

(d) $p = 3$, QP0 quadrature.

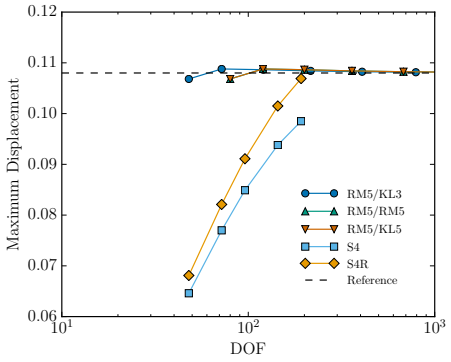

(e) $p = 3$, QNU quadrature.

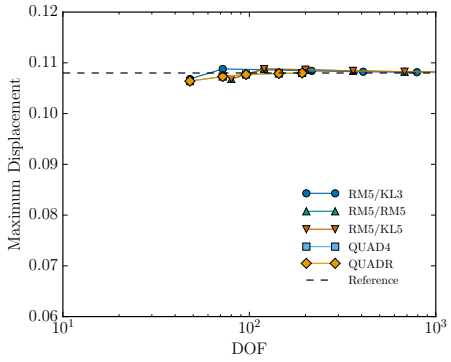

(f) $p = 3$, QNU quadrature.

Figure 6.4: Maximum deflection for in-plane bending of a cantilever beam, $p = 3$.

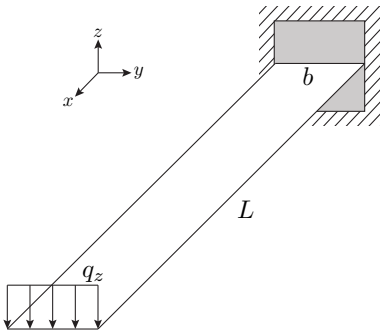

Figure 6.5: Schematic for the out-of-plane bending of a straight cantilever beam.

6.1.2 Out-of-Plane Bending of a Straight Cantilever Beam

In this case we subject a straight cantilever beam to to out-of-plane bending as shown in Figure 6.5. The beam has a length of $L = 6$, width $b = 0.2$, and thickness $t = 0.1$. It is fixed on the left end and subject to a traction $q_z = 5.0$ on the right end. The material has Young's modulus, $E = 1e^7$, and Poisson's ratio, $\nu = 0.3$. The maximum downward displacement at the free end is monitored. The exact Bernoulli beam theory solution is $u_{exact} = 0.4321$.

The results of the test for B-spline basis functions of degree $p = 2$ and maximal smoothness are shown in Figure 6.6 while the results for $p = 3$ are shown in Figure 6.7. Notice that RM5/KL3 approaches the exact solution faster than any of the other element types for all quadrature rules and degrees. It is also interesting to note that RM5/RM5 and RM5/KL6 perform identically in the in-plane bending problem because of the absence of transverse shear locking. They perform differently, however, in the out-of-plane bending problem where shear locking is present. This is due to the formulation of KL5 being shear locking free. As can be seen from Figure 6.3 to 6.7, IGA shell elements perform well in both in-plane and out-of-plane bending, more so than Abaqus or Nastran elements. This generality is very desirable in structural elements. Tabulated results for this problem can be found in Appendix A.2.

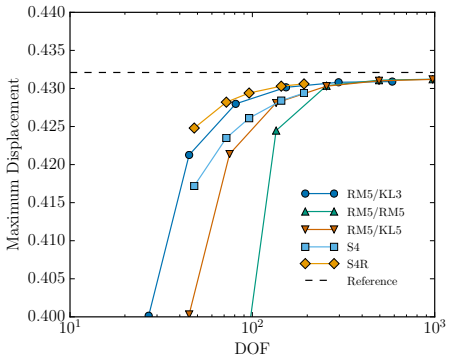

(a) $p = 2$, QP1 quadrature.

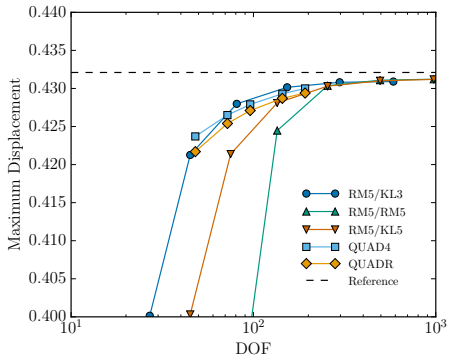

(b) $p = 2$, QP1 quadrature.

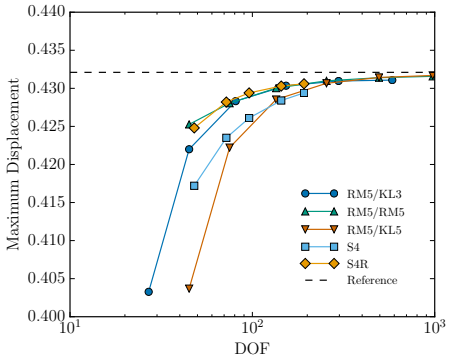

(c) $p = 2$, QP0 quadrature.

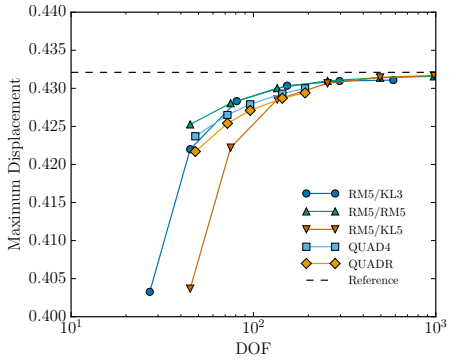

(d) $p = 2$, QP0 quadrature.

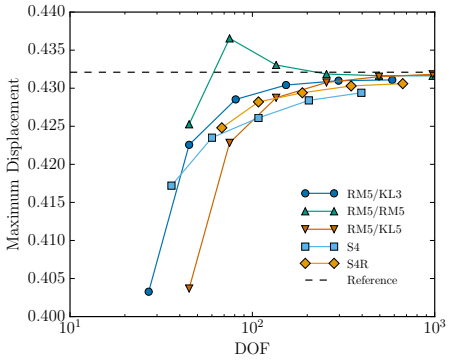

(e) $p = 2$, QNU quadrature.

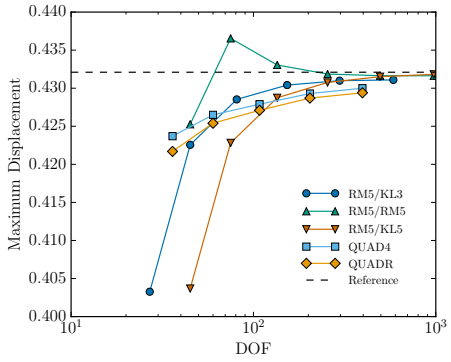

(f) $p = 2$, QNU quadrature.

Figure 6.6: Maximum deflection for out-of-plane bending of a cantilever beam, $p = 2$.

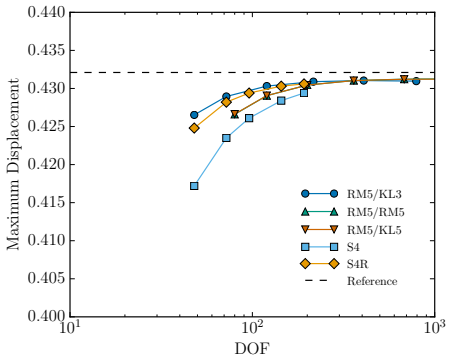

(a) $p = 3$, QP1 quadrature.

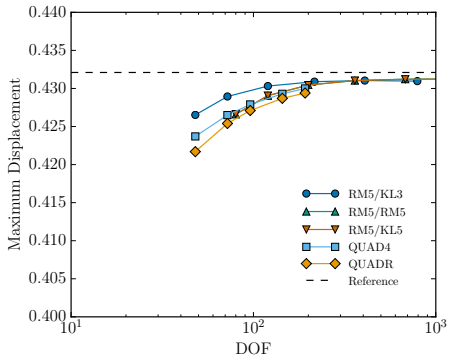

(b) $p = 3$, QP1 quadrature.

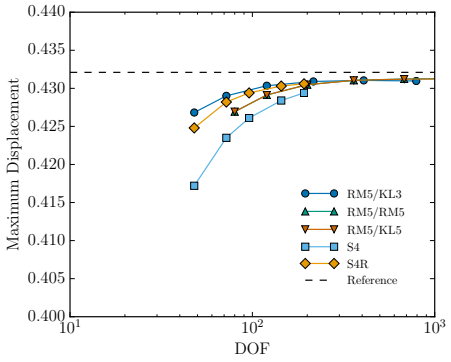

(c) $p = 3$, QP0 quadrature.

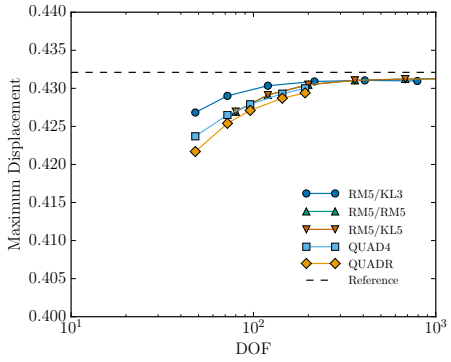

(d) $p = 3$, QP0 quadrature.

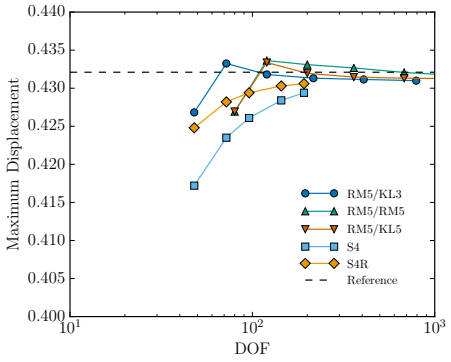

(e) $p = 3$, QNU quadrature.

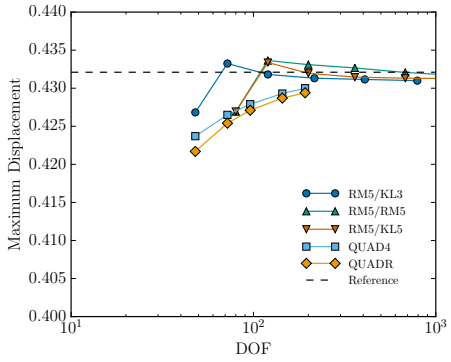

(f) $p = 3$, QNU quadrature.

Figure 6.7: Maximum deflection for out-of-plane bending of a cantilever beam, $p = 3$.

6.1.3 Simply Supported Square Plate

In this section, we investigate the representation of shear stress for RM5/KL5 and RM5/RM5 through a simply supported square plate under uniform transverse loading. This simple problem is chosen due to the absence of membrane stress, which allows us to study the shear stress independently. The schematic of this problem is shown in Figure 6.8, with length $L = 10$, Young's modulus $E = 1000$, and Poisson's ratio $\nu = 0.3$. Two cases of slenderness, $\frac{L}{t} = 100$ and 10000, are investigated. The load is set to be $q_z = t^3$. The geometry is discretized with 10 B-spline elements in both x nand y directions.

The contour plots of transverse shear stress q_{xz} for $p = 2$ and $\frac{L}{t} = 100$ are shown in Figure 6.9. As can be seen, significant oscillations occur for the standard RM5/RM5 elements for all three quadrature rules, among which the reduced quadrature rule and the non-uniform show worse transverse shear stress representation due to the inaccurate integration. The oscillations occur along the boundaries for RM5/KL3 with all quadrature rules, since the RM5 kinematics is assigned along the boundaries. They are dramatically reduced in the interior, however, and even disappeared with the full quadrature rule.

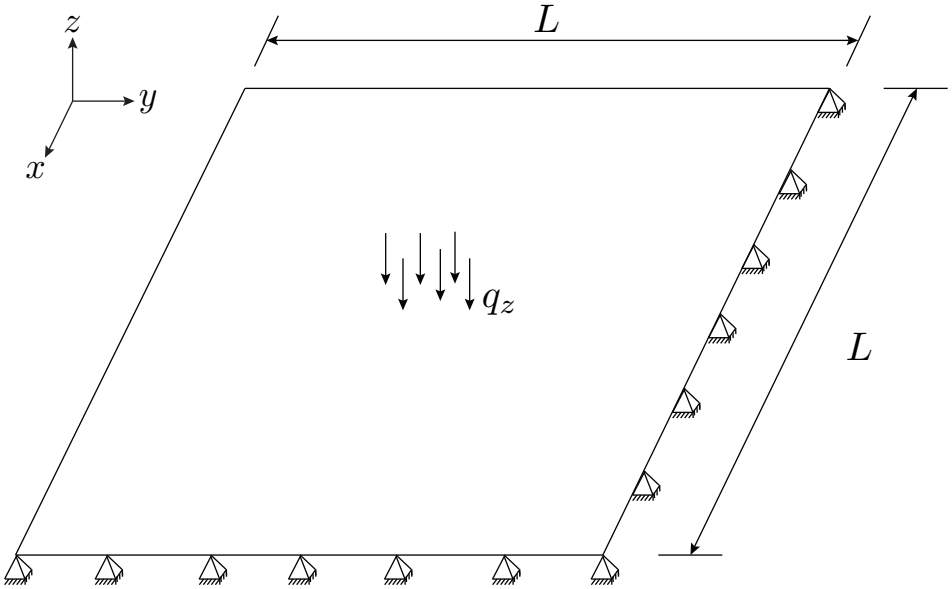

Figure 6.8: Schematic for the simply supported plate.

The superiority of RM5/KL3 in representing the transverse shear results from that the rotation, $\Delta\mathbf{w}$, is defined in terms of the derivatives of shear angles as shown in Equation (3.40). Thus, the imbalance of function spaces in approximating $\Delta\mathbf{d}^{KL3}$ and $\Delta\mathbf{w}$ is now removed. Similar phenomena is observed in the very thin shell with slenderness $\frac{L}{t} = 10000$, even though the shear shear itself is relatively small in this case. As shown in Figure 6.11 and 6.12, for $p = 3$, the oscillations decrease significantly for RM5/RM5 due to the fact that higher order basis increase the approximation ability. However, the superiority of RM5/KL5 to RM5/RM5 in representing the shear stress is still apparent.

6.1.4 Clamped Square Plate Subject to a Uniformly Distributed Load

We analyze the clamped square plate subject to a uniform distributed load as shown in Figure 6.13. The square plate has length $L = 10$, Young's modulus $E = 1000$, and Poisson's ratio $\nu = 0.3$. The thickness t is varied to give a slenderness ratio $\frac{L}{t}$. The distributed load is set to $q = t^3$. The maximum displacement at the center of the plate is monitored. The exact solution is $u_{max} = 0.138173$. The plate is modeled with both quadratic and cubic B-splines of maximal smoothness. In all cases, the boundary nodes are set to RM5 simplifying the imposition of clamped boundary conditions. The internal nodes are set to either KL3, KL5, or RM5.

Figure 6.14 shows the behavior of the blended shell for increasing slenderness. Note the shear locking free behavior for RM5/KL3 and RM5/KL5 for increasing slenderness. Setting boundary nodes to RM5 does not appear to disrupt the shear locking free behavior of KL3 and KL5 and simplifies the imposition of clampled boundary conditions. The shear locking in RM5/RM5 is alleviated by both reduced quadrature (QNU) and increasing polynomial degree. Figures 6.15 and 6.16 compare the blended shell to commercial shell elements in Abaqus and Nastran (see Table 6.2) for a slenderness ratio $\frac{L}{t} = 1000$. In all cases, the blended shell is competitive with the FEA shell elements. Note that for higher degrees and smoothness the IGA accuracy deteriorates slightly. This is because the maximal smoothness basis functions have difficulty capturing the sharp boundary layers created by the clamped boundary conditions. Locally reducing smoothness will alleviate this discrepancy but is not pursued in this work. Note that additional data for this problem is tabulated in Appendix A.3.

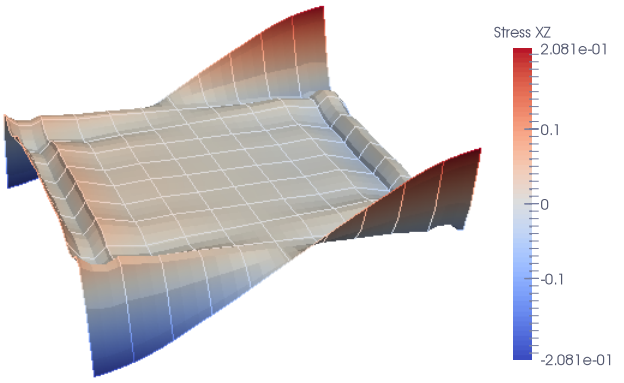

(a) $RM5/KL5$, QP1 quadrature.

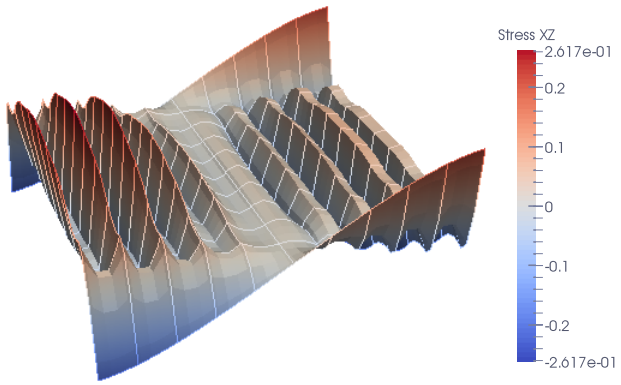

(b) $RM5/RM5$, QP1 quadrature.

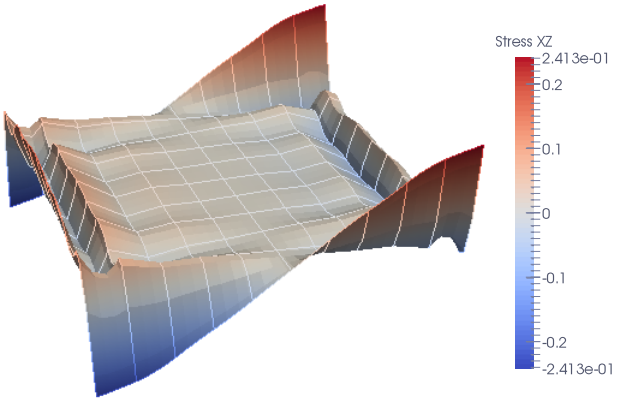

(c) $RM5/KL5$, QP0 quadrature.

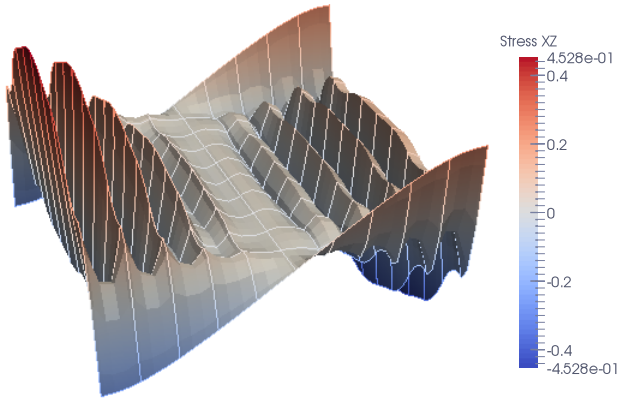

(d) $RM5/RM5$, QP0 quadrature.

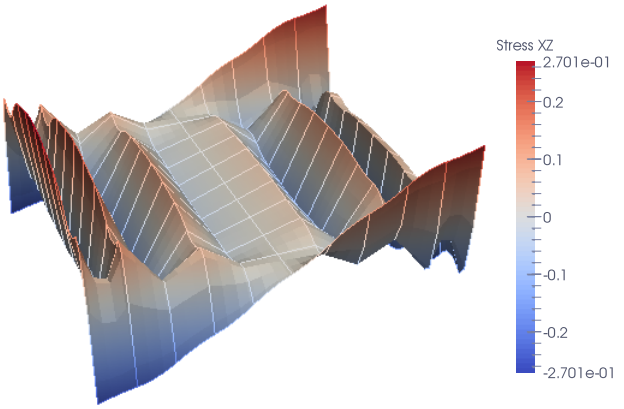

(e) $RM5/KL5$, QNU quadrature.

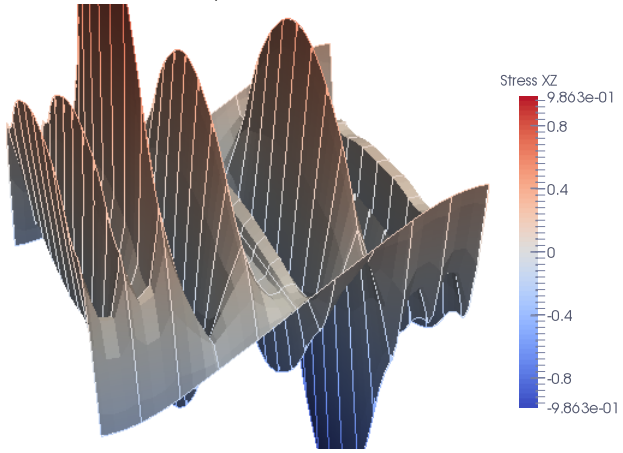

(f) $RM5/RM5$, QNU quadrature.

Figure 6.9: Shear stress, q_{xz}, for simply supported plate with $p = 2$ and $L/t = 100$.

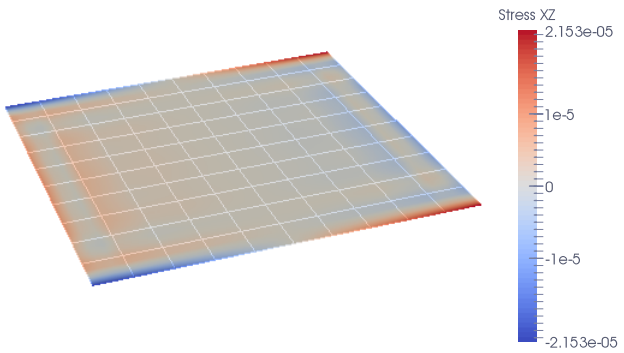

(a) $RM5/KL5$, QP1 quadrature.

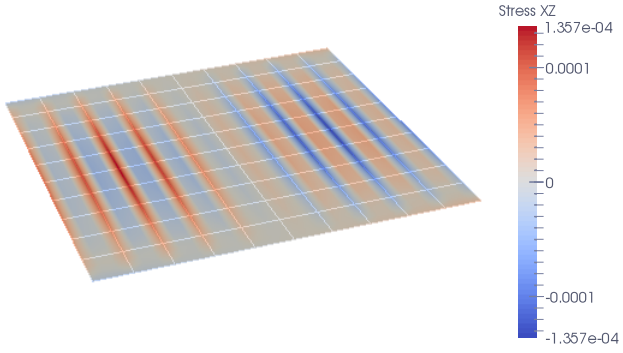

(b) $RM5/RM5$, QP1 quadrature.

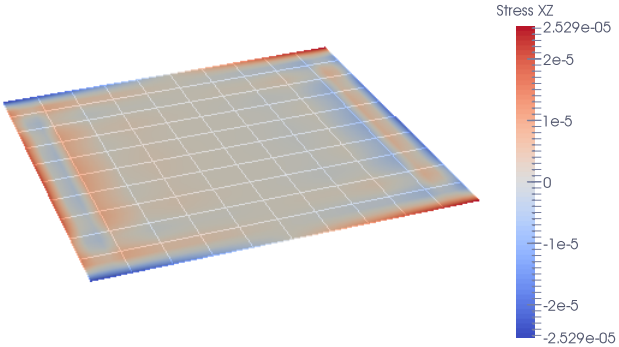

(c) $RM5/KL5$, QP0 quadrature.

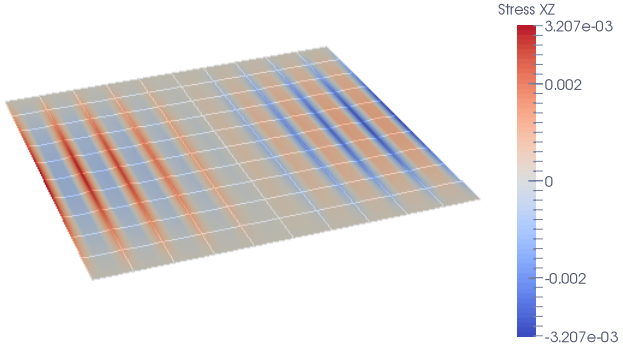

(d) $RM5/RM5$, QP0 quadrature.

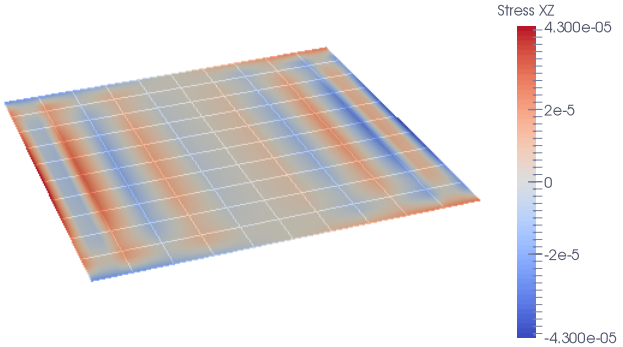

(e) $RM5/KL5$, QNU quadrature.

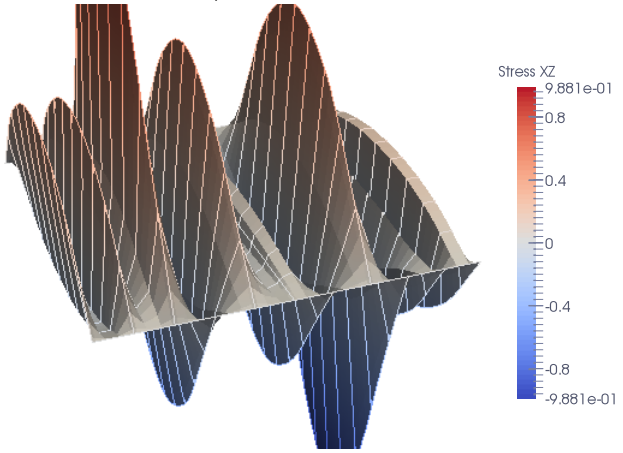

(f) $RM5/RM5$, QNU quadrature.

Figure 6.10: Shear stress, q_{xz}, for simply supported plate with $p = 2$ and $L/t = 10000$.

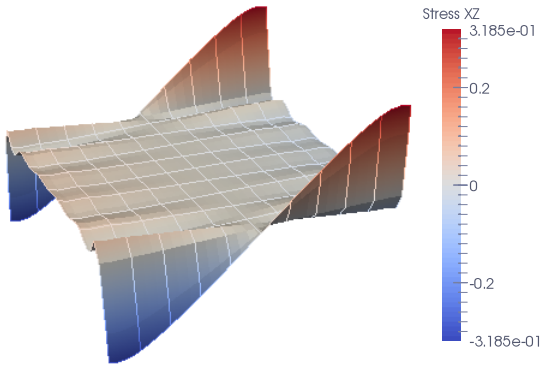

(a) $RM5/KL5$, QP1 quadrature.

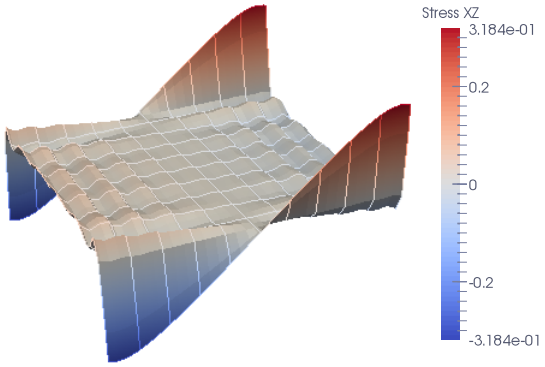

(b) $RM5/RM5$, QP1 quadrature.

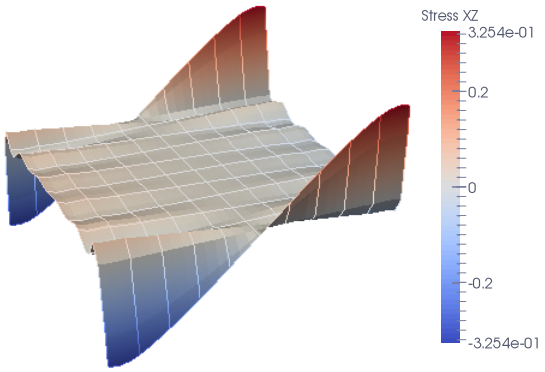

(c) $RM5/KL5$, QP0 quadrature.

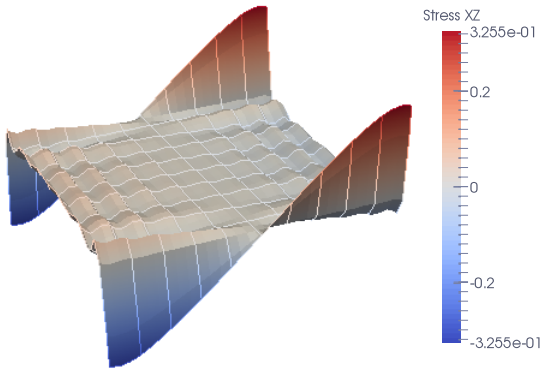

(d) $RM5/RM5$, QP0 quadrature.

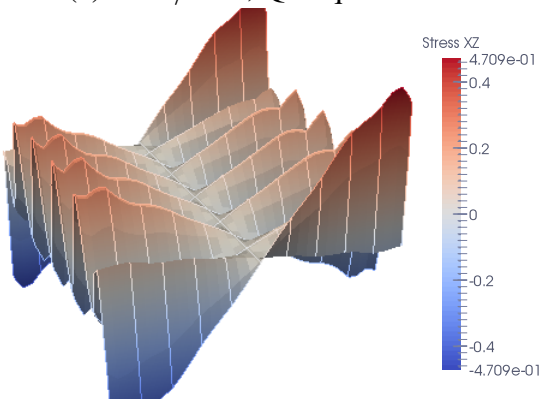

(e) $RM5/KL5$, QNU quadrature.

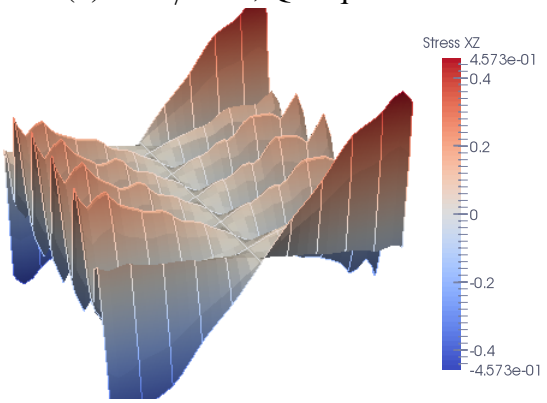

(f) $RM5/RM5$, QNU quadrature.

Figure 6.11: Shear stress, q_{xz}, for simply supported plate with $p = 3$ and $L/t = 100$.

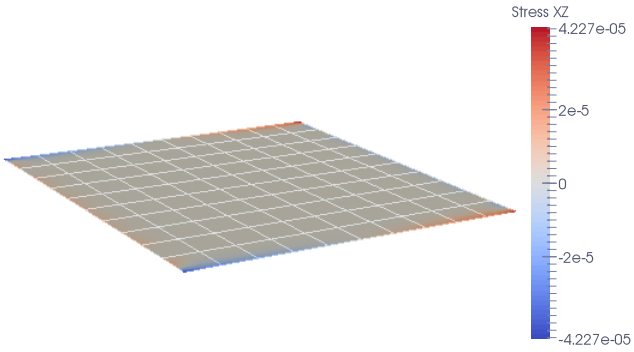

(a) $RM5/KL5$, QP1 quadrature.

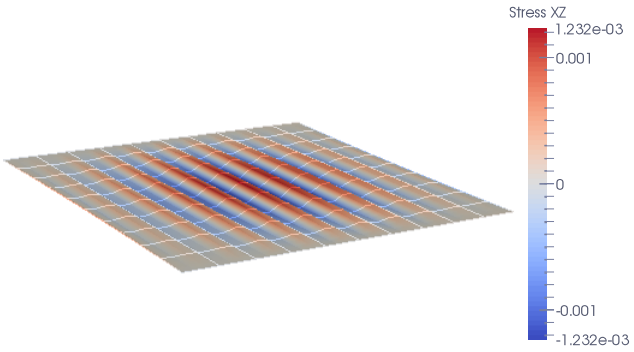

(b) $RM5/RM5$, QP1 quadrature.

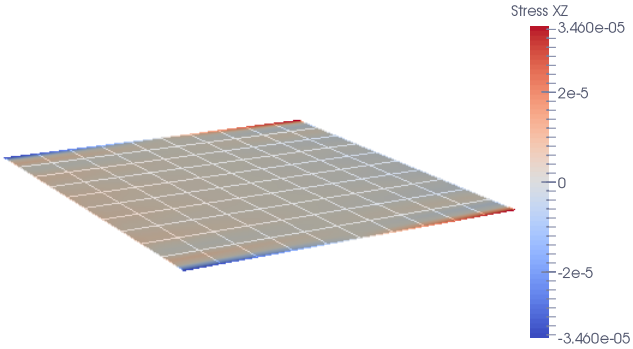

(c) $RM5/KL5$, QP0 quadrature.

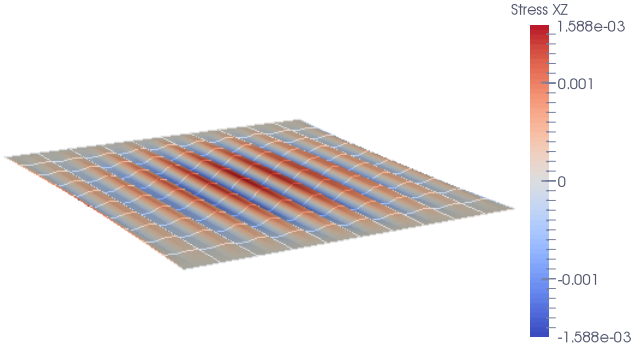

(d) $RM5/RM5$, QP0 quadrature.

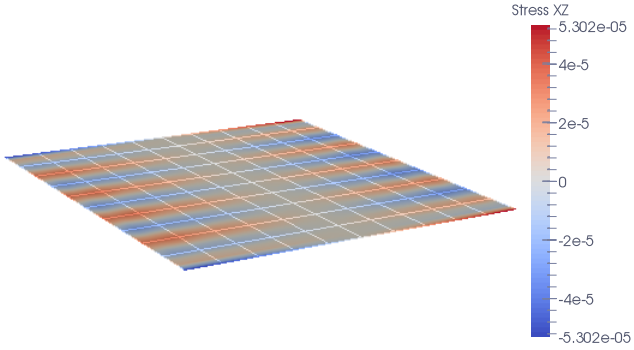

(e) $RM5/KL5$, QNU quadrature.

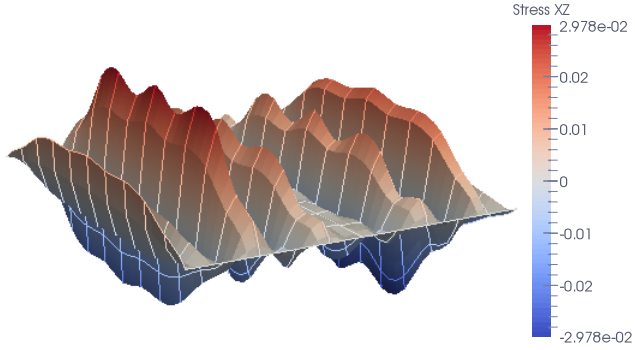

(f) $RM5/RM5$, QNU quadrature.

Figure 6.12: Shear stress, q_{xz}, for simply supported plate with $p = 3$ and $L/t = 10000$.

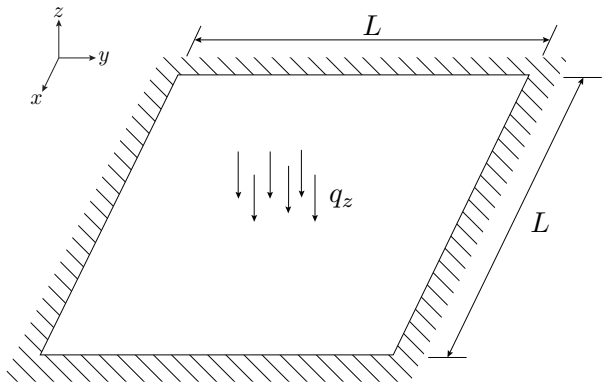

Figure 6.13: Schematic for a clamped square plate subject to a uniform distributed load.

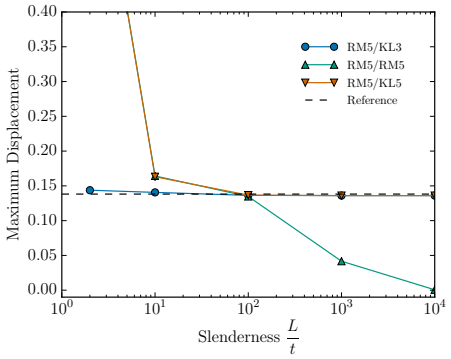

(a) $p = 2$, QP1 quadrature.

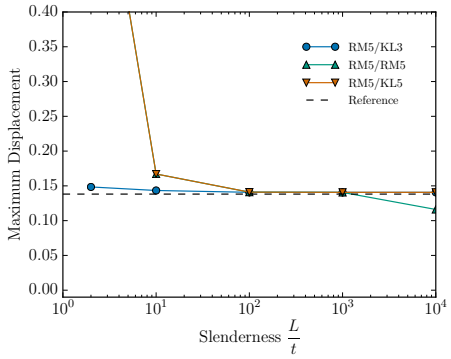

(b) $p = 3$, QP1 quadrature.

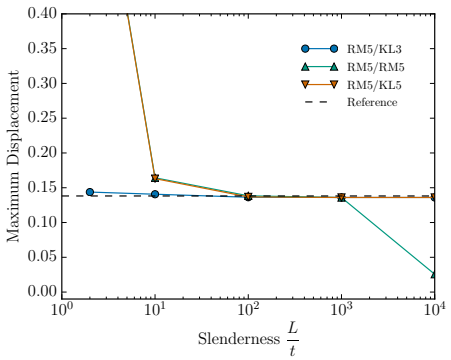

(c) $p = 2$, QP0 quadrature.

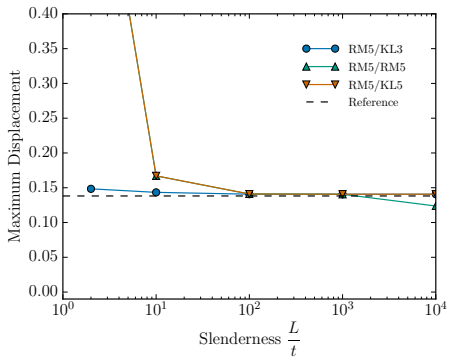

(d) $p = 3$, QP0 quadrature.

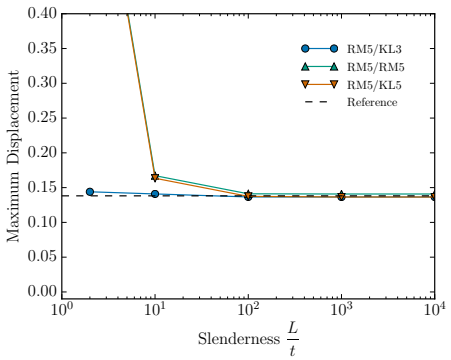

(e) $p = 2$, QNU quadrature.

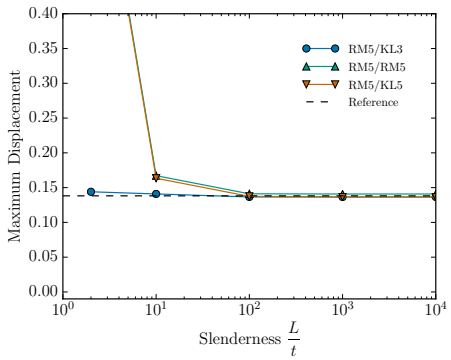

(f) $p = 3$, QNU quadrature.

Figure 6.14: Maximum deflection for a square clamped plate with 16×16 elements, subject to a uniform distributed load for different quadrature rules QP1, QP2, QNU and polynomial degrees $p = 2, 3$.

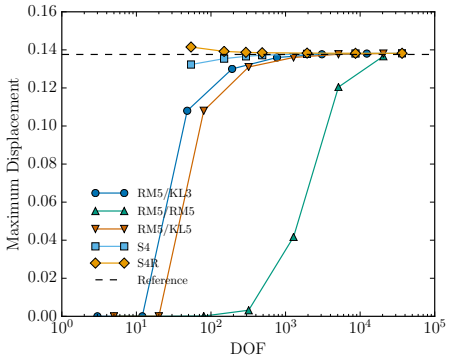

(a) $p = 2$, QP1 quadrature.

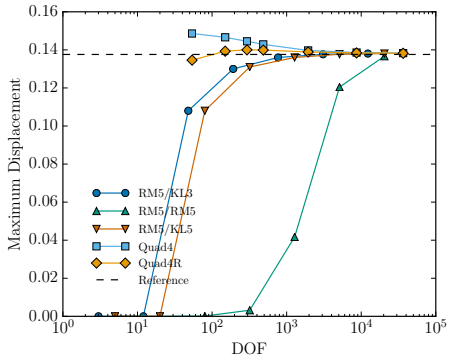

(b) $p = 2$, QP1 quadrature.

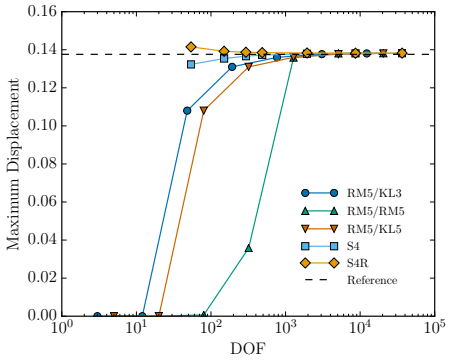

(c) $p = 2$, QP0 quadrature.

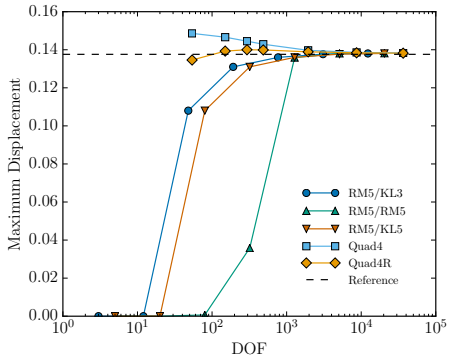

(d) $p = 2$, QP0 quadrature.

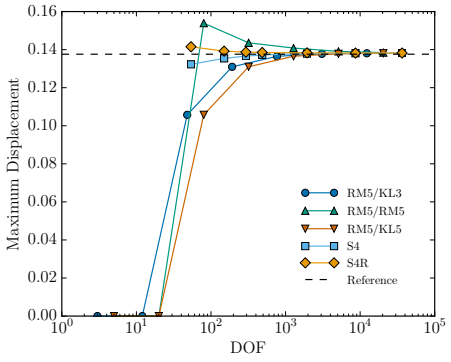

(e) $p = 2$, QNU quadrature.

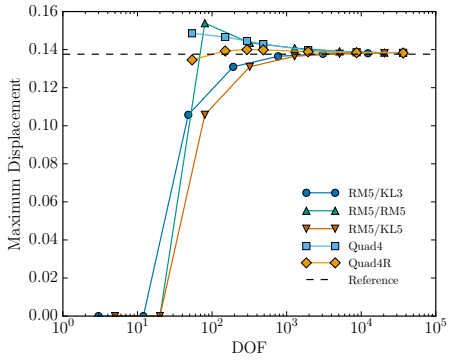

(f) $p = 2$, QNU quadrature.

Figure 6.15: Maximum deflection for a square clamped plate subject to a uniform distributed load with $L/t = 1{,}000$ for commercial FEA elements and the blended shell with different quadrature rules QP1, QP0, and QNU and polynomial degree $p = 2$.

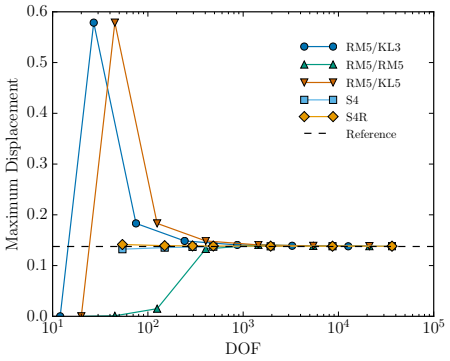

(a) $p = 3$, QP1 quadrature.

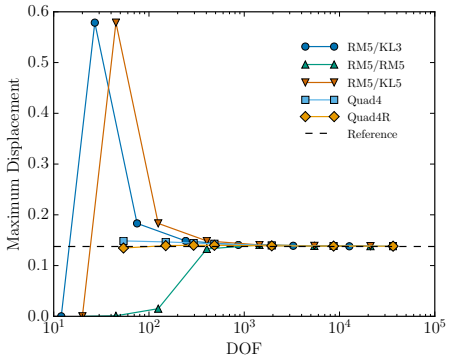

(b) $p = 3$, QP1 quadrature.

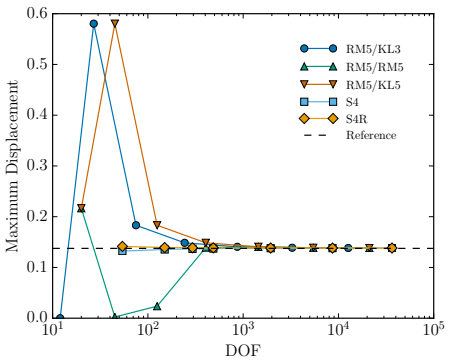

(c) $p = 3$, QP0 quadrature.

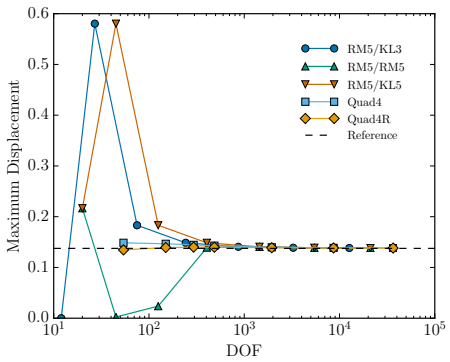

(d) $p = 3$, QP0 quadrature.

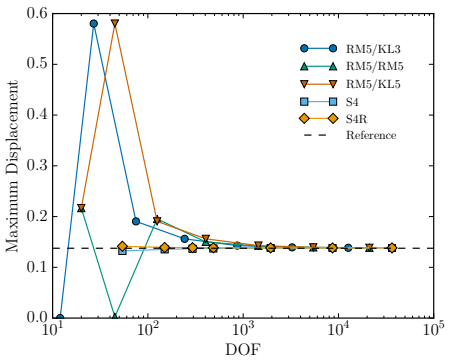

(e) $p = 3$, QNU quadrature.

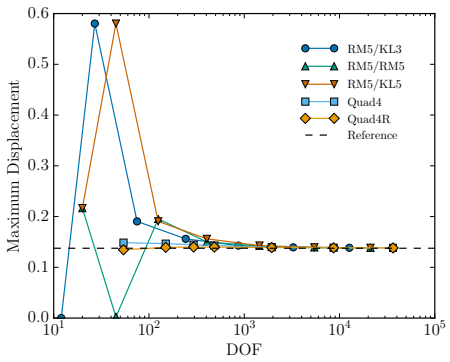

(f) $p = 3$, QNU quadrature.

Figure 6.16: Maximum deflection for a square clamped plate subject to a uniform distributed load with $L/t = 1{,}000$ for commercial FEA elements and the blended shell with different quadrature rules QP1, QP0, and QNU and polynomial degree $p = 3$.

6.1.5 Cylindrical Shell Subject to Transverse Loading in the Radial Direction

Figure 6.17 shows a schematic for a cylindrical shell subject to transverse loading in the radial direction. The beam has a radius $R = 10$ m, a width $b = 1$ m, and the thickness varies. Young's modulus and Poisson's ratio are $E = 1000$ Pa and $\nu = 0$, respectively. The curved beam is clamped at one end and subjected to a traction, $q_x = 0.1t^3$, at the other end. An analytical solution based on Bernoulli beam theory gives a value of approximately 0.942 for the radial displacement at the free end [8]. The beam is modeled with quadratic and cubic NURBS of maximal smoothness. We also employ all three quadrature schemes QP1, QP0, QNU.

Figure 6.18 illustrates the importance of using *exact* geometric quantities in the isogeometric blended shell formulation. We compare the solution computed using the exact formulations described in Sections 3.2.1 and 3.3 to one computed using the geometric approximations described in Section 3.2.1 (denoted KL3 approximate in the plots). Note that these geometric approximations are the same as those described in the first blended isogeometric shell paper [12]. This problem suffers from both shear and membrane locking. RM5/KL3 and RM5/KL5 are essentially shear locking free but still suffer from membrane locking as shown in Figures 6.18a and 6.18b. However, the reduced quadrature schemes QP0 and QNU alleviate locking, producing locking free solutions for RM5/KL3, RM5/KL5, and RM5/RM5 as shown in Figures 6.18e and 6.18f. Notice, however, that RM5/KL3 approximate remains inaccurate for all quadrature schemes. The inaccuracy is due to the geometric error in the underlying approximations which are employed in the shell formulation. These errors cannot be overcome through reduced quadrature schemes and worsen for increasing polynomial degree.

Figures 6.19 and 6.20 compare commercial FEA shell elements to the isogeometric blended shell for a slenderness ratio of $\frac{R}{t} = 100$. In this case, the membrane locking can be overcome by reduced quadrature (QP0 and QNU) or increasing polynomial degree and is very competitive with shell elements in Abaqus and Nastran. All data for this problem is tabulated in Appendix A.4.

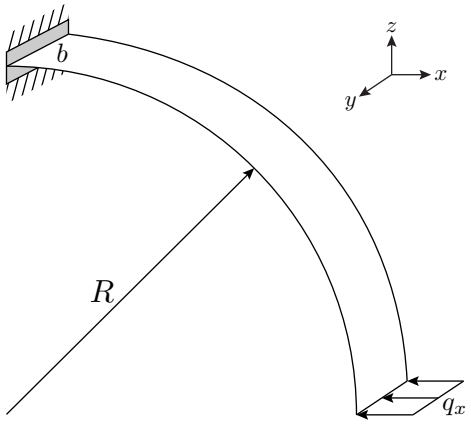

Figure 6.17: A cylindrical shell subject to tranverse loading in the radial direction.

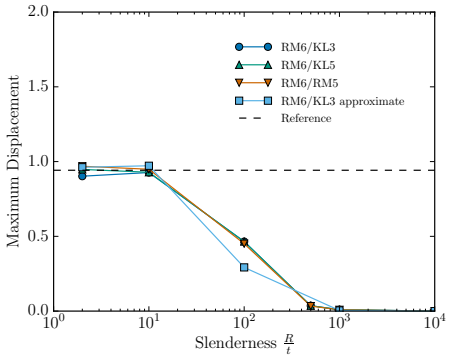

(a) $p = 2$, QP1 quadrature.

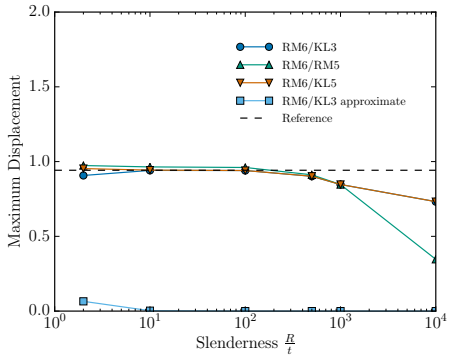

(b) $p = 3$, QP1 quadrature.

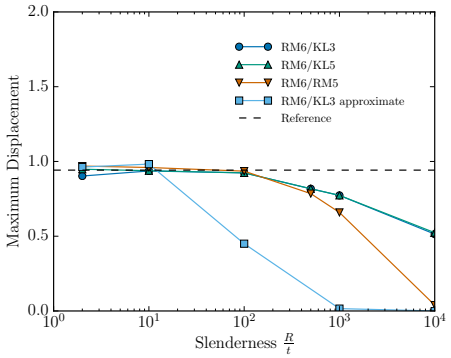

(c) $p = 2$, QP0 quadrature.

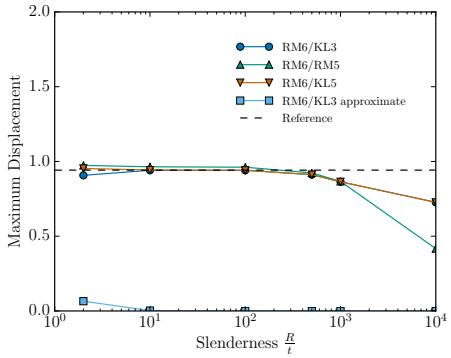

(d) $p = 3$, QP0 quadrature.

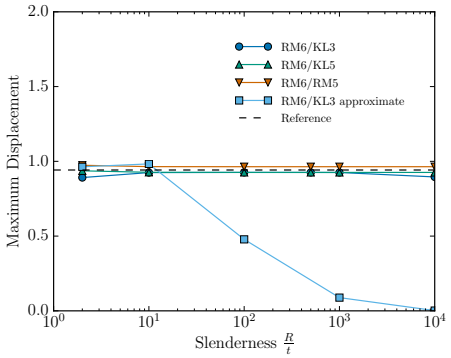

(e) $p = 2$, QNU quadrature.

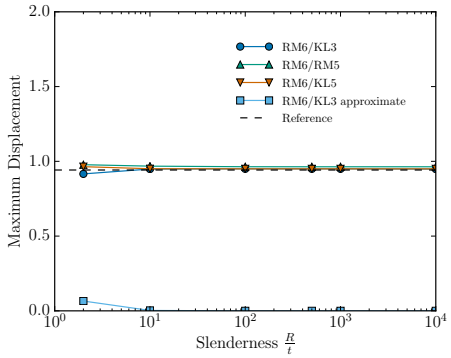

(f) $p = 3$, QNU quadrature.

Figure 6.18: Maximum radial deflection for cylindrical shell problem with 8×1 elements, for different quadrature rules QP1, QP2, QNU and polynomial degrees $p = 2, 3$.

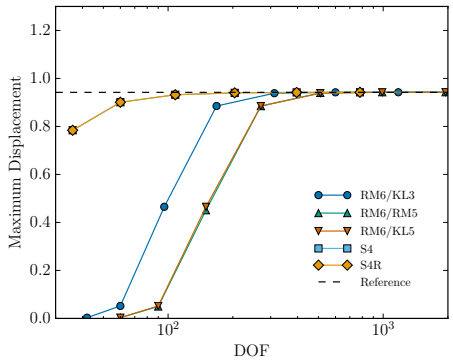

(a) $p = 2$, QP1 quadrature.

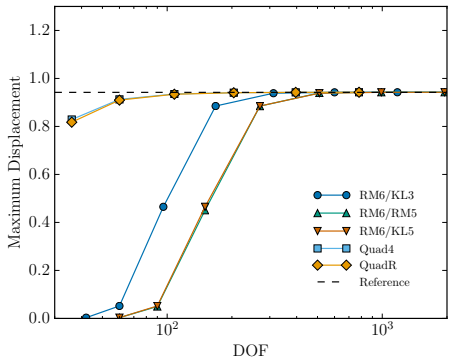

(b) $p = 2$, QP1 quadrature.

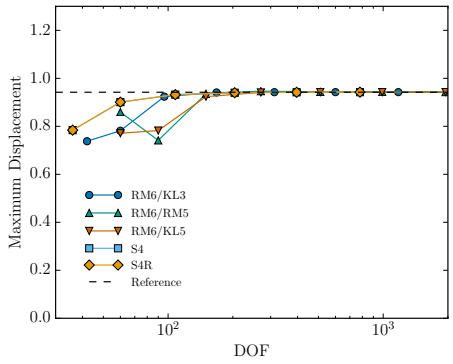

(c) $p = 2$, QP0 quadrature.

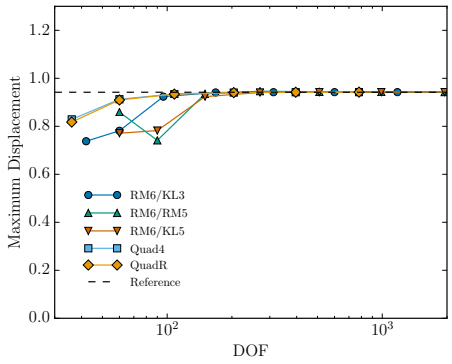

(d) $p = 2$, QP0 quadrature.

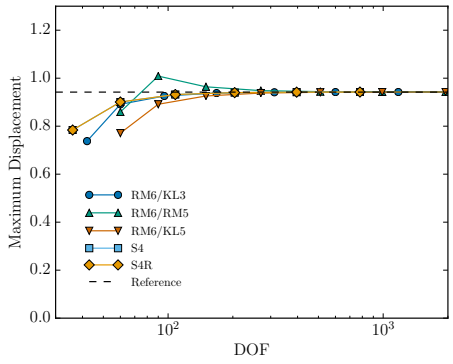

(e) $p = 2$, QNU quadrature.

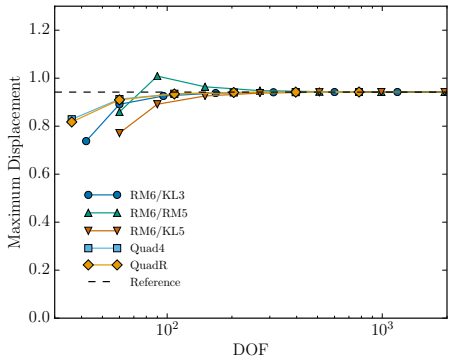

(f) $p = 2$, QNU quadrature.

Figure 6.19: Maximum radial deflection for cylindrical shell problem for different quadrature rules QP1, QP2, QNU and $\frac{R}{t} = 100$.

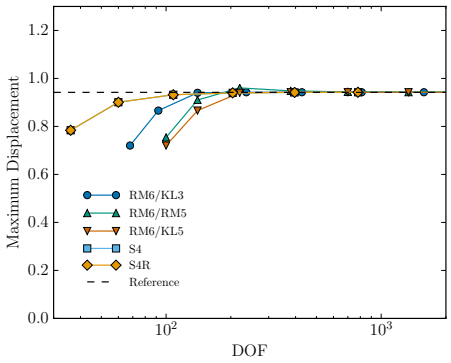

(a) $p = 3$, QP1 quadrature.

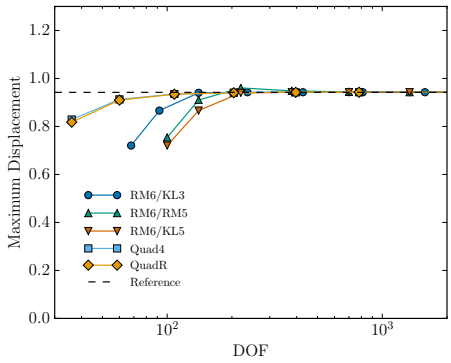

(b) $p = 3$, QP1 quadrature.

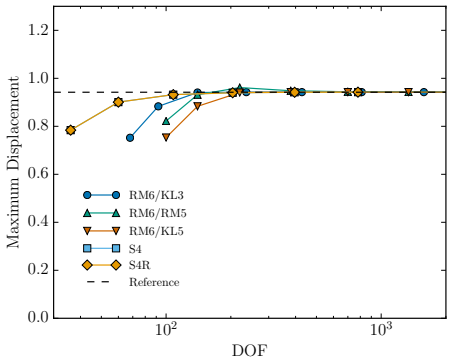

(c) $p = 3$, QP0 quadrature.

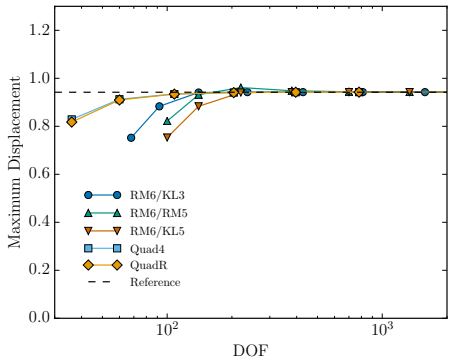

(d) $p = 3$, QP0 quadrature.

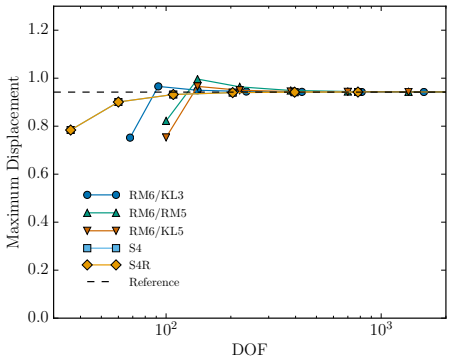

(e) $p = 3$, QNU quadrature.

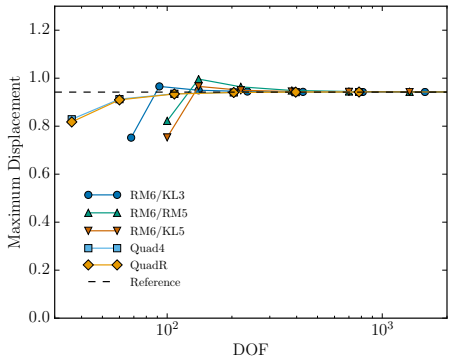

(f) $p = 3$, QNU quadrature.

Figure 6.20: Maximum radial deflection for cylindrical shell problem for different quadrature rules QP1, QP2, QNU and $\frac{R}{t} = 100$.

6.1.6 Scordelis-Lo Roof

The Scordelis-Lo roof problem is part of the shell obstacle course [18] and tests a shell element's ability to handle both membrane and bending stresses. An 80° arc of a cylinder with radius, $R = 300$, length, $L = 600$, and thickness, $t = 3.0$ is supported on each end by a rigid diaphragm. It is loaded with its own weight. The material has Young's Modulus, $E = 3.0e6$, Poisson's ratio, $\nu = 0.3$, and mass density, $\rho = 0.00053971$. The acceleration of gravity is, $g = 386$. Figure 6.21 shows the problem setup. Only one quarter of the geometry was modeled due to symmetry.

The maximum displacement occurs on the free edge at $y = \frac{L}{2}$. Multiple theoretical solutions have been reported in the literature and these solutions have varied slightly based on whether thin or thick-shell theory was used. The exact solution was reported as 3.70331 for thin shell theory and 3.59 for thick shell theory [19]. In our examples, the thick shell solution is adopted and used in the comparisons shown in Figures 6.22 and 6.23. For this example the isogeometric blended shell demonstrates superior accuracy when compared to FEA shell elements. Tabulated results for this problem can be found in Appendix A.5.

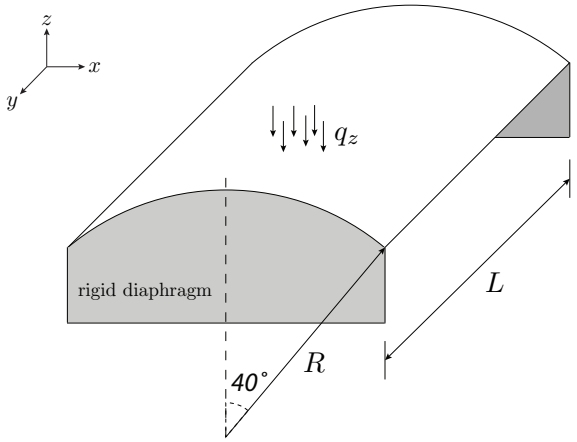

Figure 6.21: Schematic for the Scordelis-Lo roof problem.

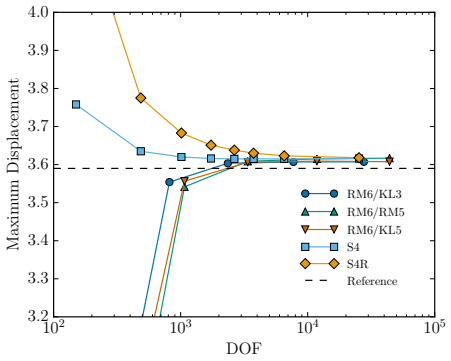

(a) $p = 2$, QP1 quadrature.

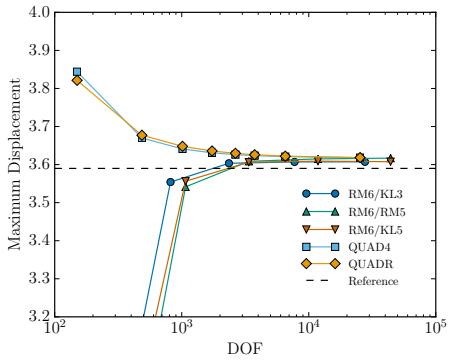

(b) $p = 2$, QP1 quadrature.

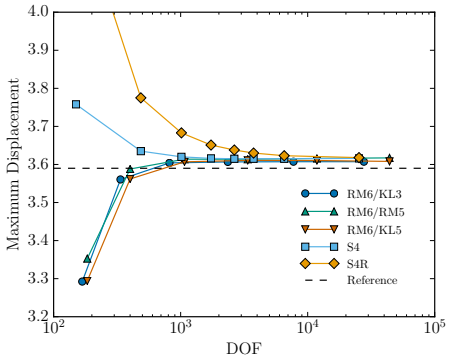

(c) $p = 2$, QP0 quadrature.

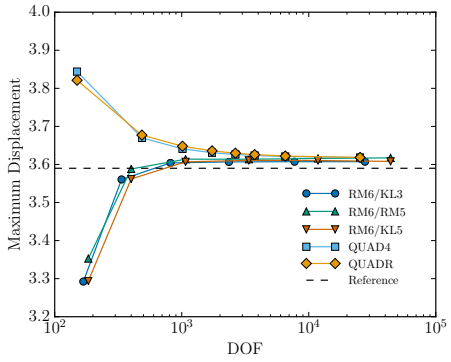

(d) $p = 2$, QP0 quadrature.

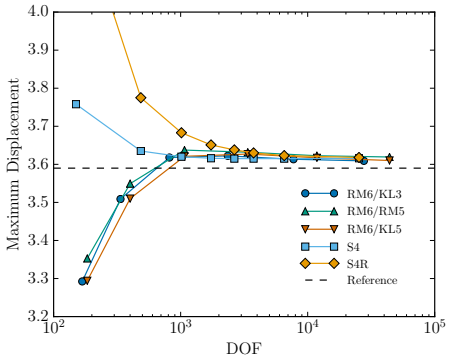

(e) $p = 2$, QNU quadrature.

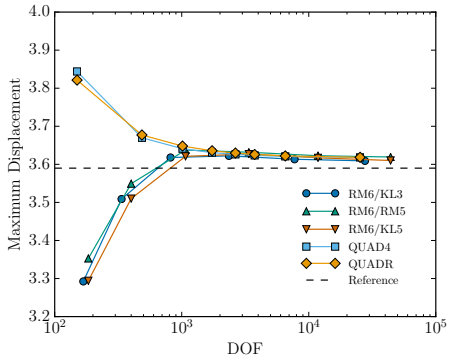

(f) $p = 2$, QNU quadrature.

Figure 6.22: Maximum deflection for the Scordelis-Lo roof problem, $p = 2$.

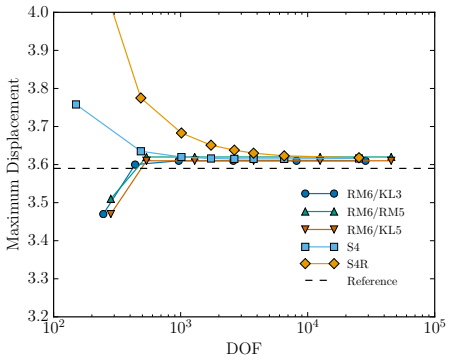

(a) $p = 3$, QP1 quadrature.

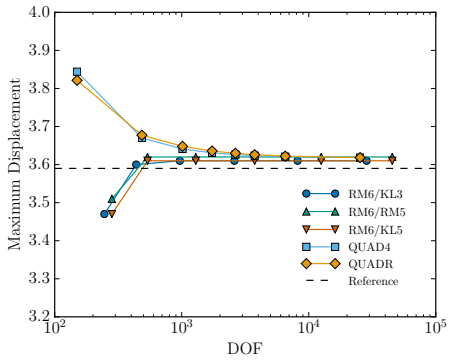

(b) $p = 3$, QP1 quadrature.

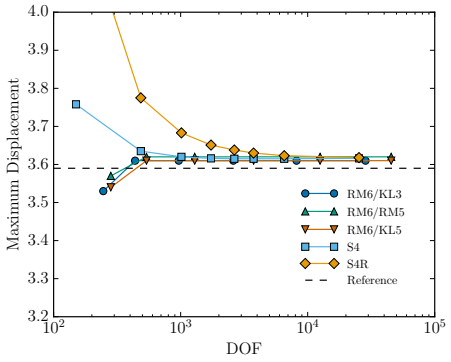

(c) $p = 3$, QP0 quadrature.

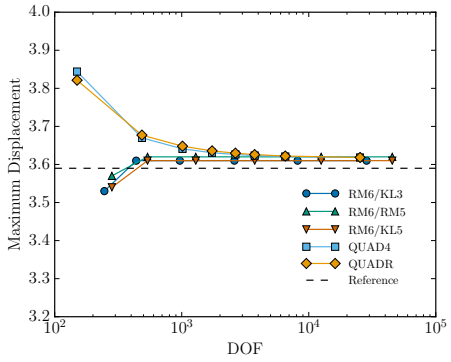

(d) $p = 3$, QP0 quadrature.

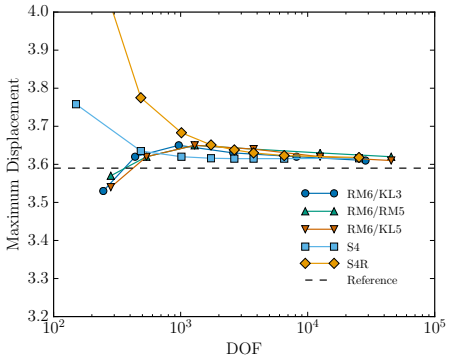

(e) $p = 3$, QNU quadrature.

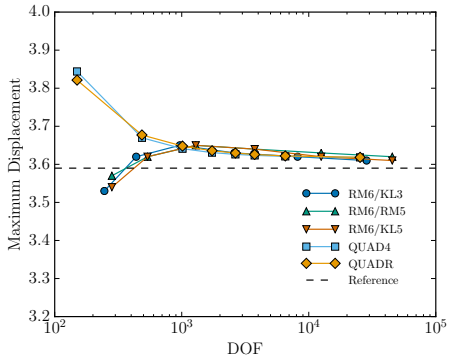

(f) $p = 3$, QNU quadrature.

Figure 6.23: Maximum deflection for the Scordelis-Lo roof problem, $p = 3$.

6.1.7 Pinched Cylinder

The pinched cylinder problem is from the shell obstacle course [18] and tests a shell element's ability to handle membrane and bending stresses. A cylinder with radius, $R = 3.0$, thickness, $t = 0.03$, and length, $L = 6$ is constrained at each end by a rigid diaphragm. The material has a Young's modulus of, $E = 3.0e10$, and Poisson's ratio, $\nu = 0.3$. The cylinder is loaded with two opposing point loads at mid-cylinder with magnitude, $P = 1.0$ as shown in Figure 6.24. One eighth of the cylinder is modeled due to symmetry. The inward radial displacement at the location of the point load is monitored and compared against a reference displacement of $u_{ref} = 1.83 * e^{-7}$, based on thin shell theory.

The behavior of the blended shell is shown in Figures 6.25 and 6.26. Similar trends to those seen in previous problems, in terms of accuracy and competitiveness with commercial FEA elements, can be observed for this problem. Tabulated results for this problem can be found in Appendix A.6.

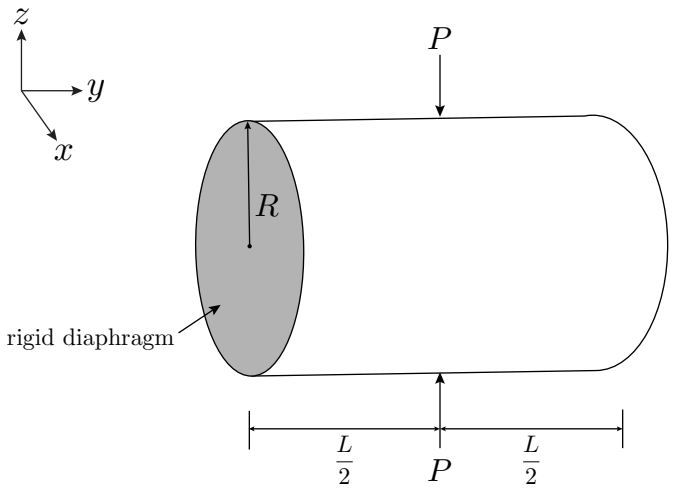

Figure 6.24: Schematic for the pinched cylinder problem.

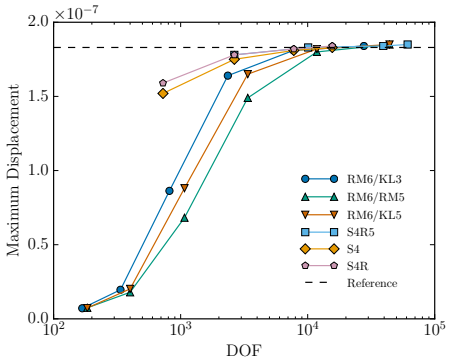

(a) $p = 2$, QP1 quadrature.

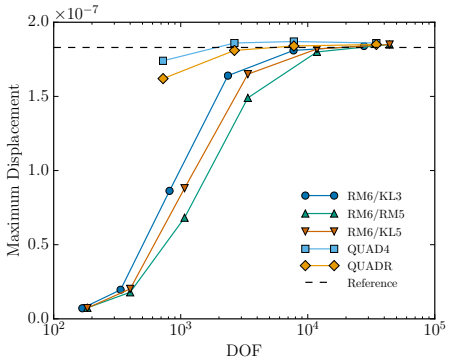

(b) $p = 2$, QP1 quadrature.

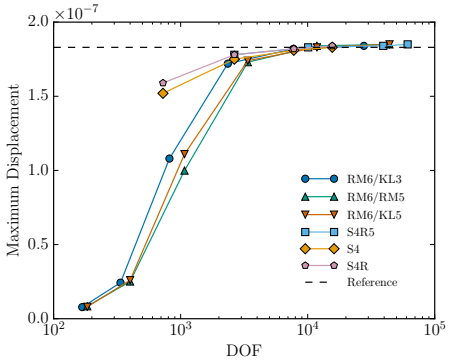

(c) $p = 2$, QP0 quadrature.

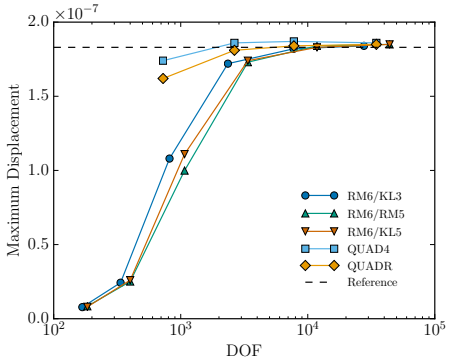

(d) $p = 2$, QP0 quadrature.

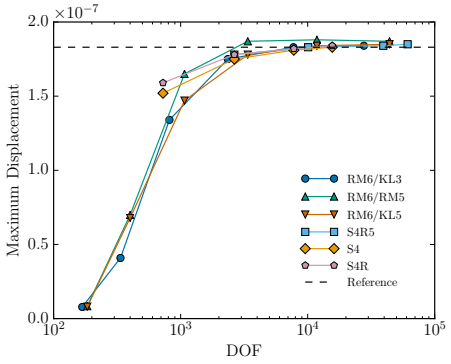

(e) $p = 2$, QNU quadrature.

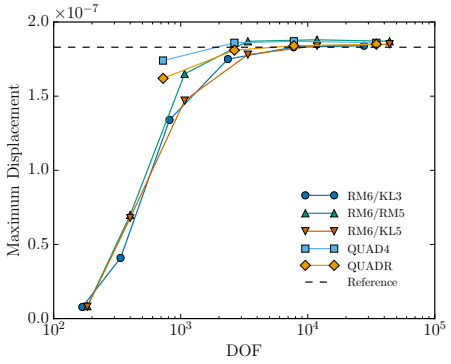

(f) $p = 2$, QNU quadrature.

Figure 6.25: Maximum deflection for the pinched cylinder problem, $p = 2$.

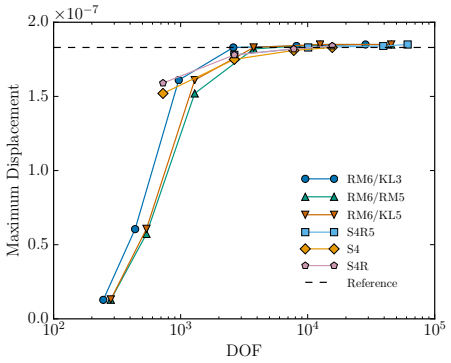

(a) $p = 3$, QP1 quadrature.

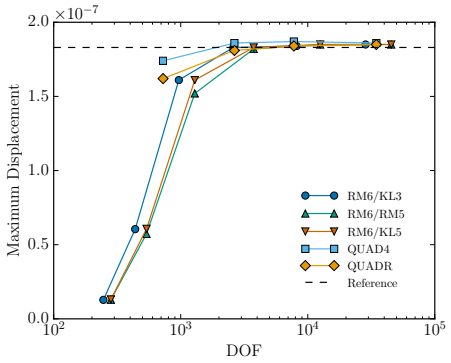

(b) $p = 3$, QP1 quadrature.

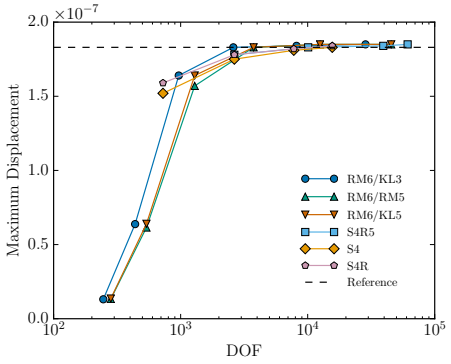

(c) $p = 3$, QP0 quadrature.

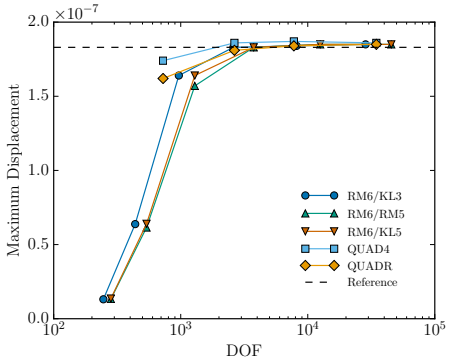

(d) $p = 3$, QP0 quadrature.

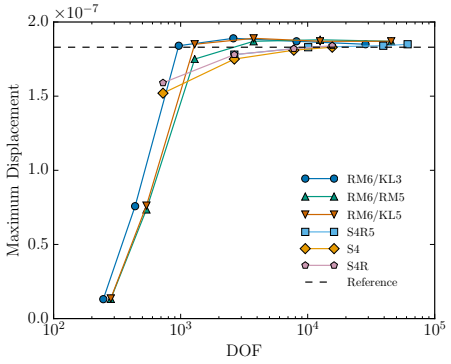

(e) $p = 3$, QNU quadrature.

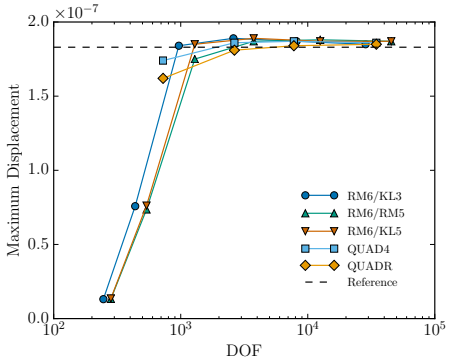

(f) $p = 3$, QNU quadrature.

Figure 6.26: Maximum deflection for the pinched cylinder problem, $p = 3$.

6.1.8 Hemispherical Shell with Hole

The hemispherical shell problem tests a shell element's ability to represent combined membrane and bending stresses [5]. The geometry is a hemisphere with radius, $R = 10$, thickness, $t = 0.04$, and an 18° hole as shown in Figure 6.27. The hemisphere is loaded with four point loads on the equator with alternating signs. Only one quarter of the hemisphere is modeled due to symmetry. The radial displacement at the location of one of the point loads is monitored and compared against a reference solution of 0.0940 [5].

The behavior of the blended shell is shown in Figures 6.28 and 6.29. Similar trends to those seen in previous problems, in terms of accuracy and competitiveness with commercial FEA elements, can be observed for this problem. Tabulated results for this problem can be found in Appendix A.7.

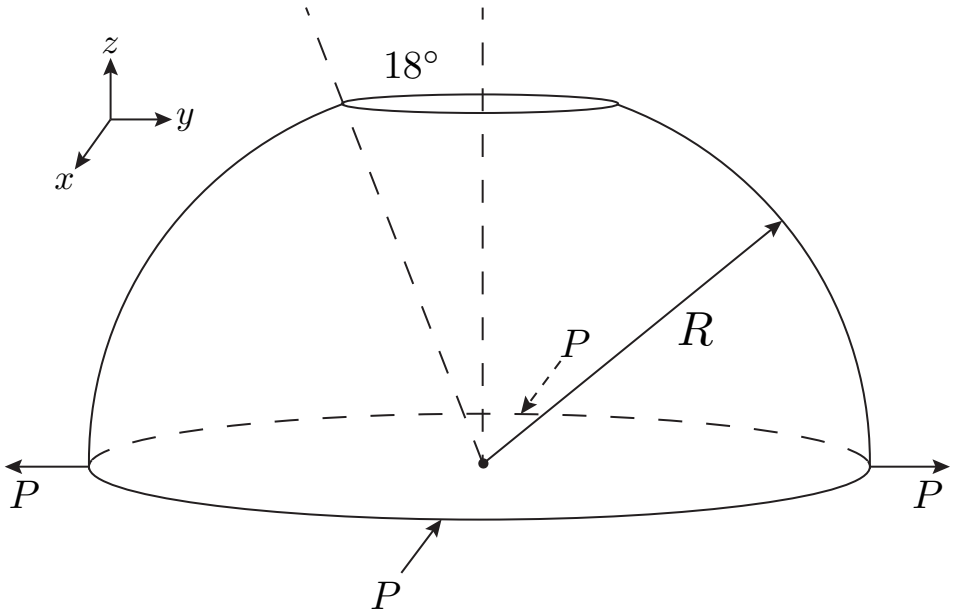

Figure 6.27: Schematic for the hemispherical shell problem [5].

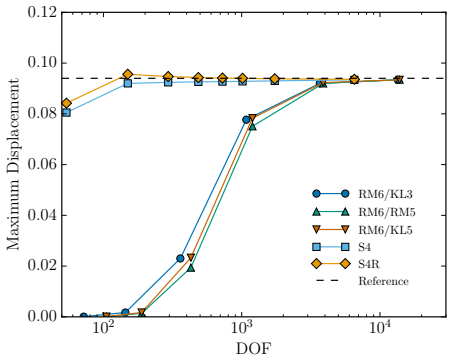

(a) $p = 2$, QP1 quadrature.

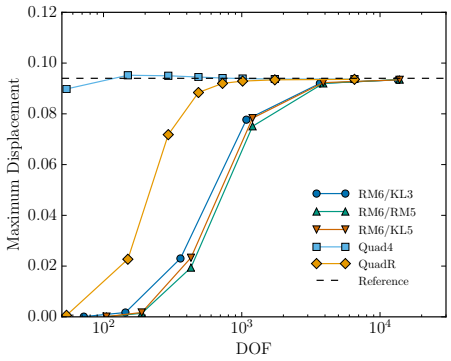

(b) $p = 2$, QP1 quadrature.

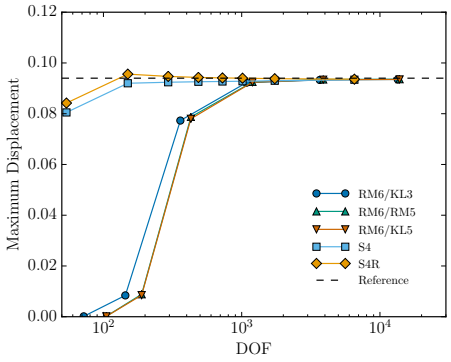

(c) $p = 2$, QP0 quadrature.

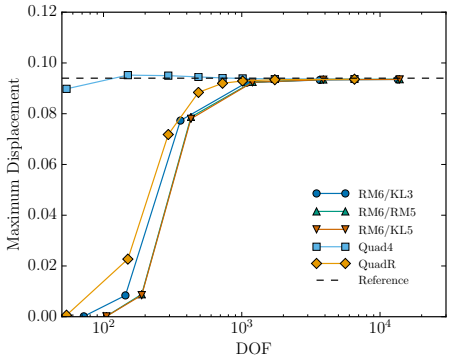

(d) $p = 2$, QP0 quadrature.

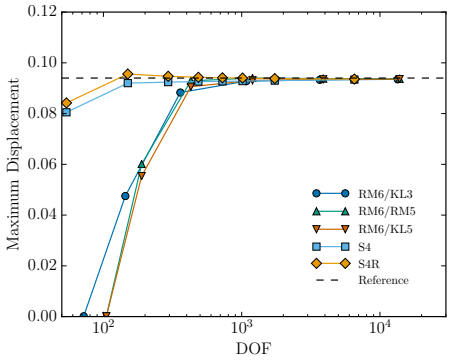

(e) $p = 2$, QNU quadrature.

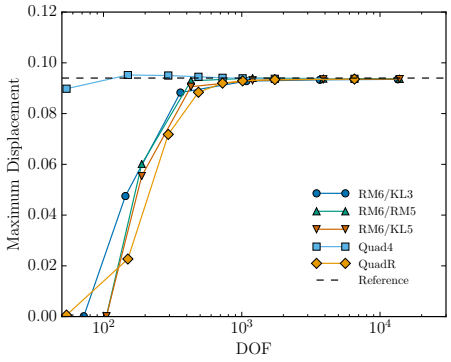

(f) $p = 2$, QNU quadrature.

Figure 6.28: Maximum deflection for the hemispherical shell with hole problem, $p = 2$.

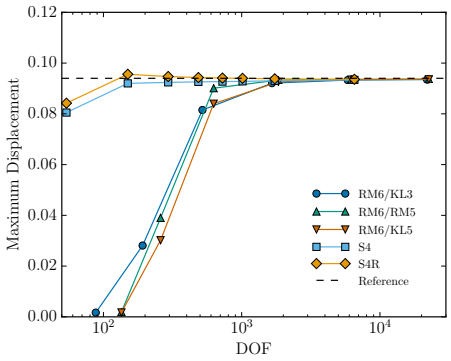

(a) $p = 3$, QP1 quadrature.

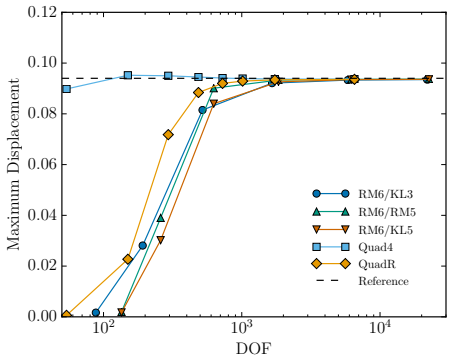

(b) $p = 3$, QP1 quadrature.

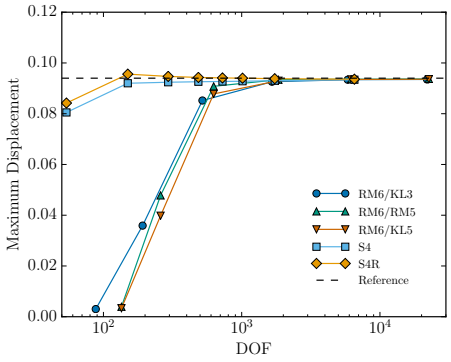

(c) $p = 3$, QP0 quadrature.

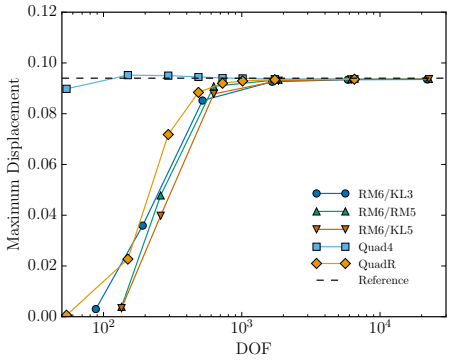

(d) $p = 3$, QP0 quadrature.

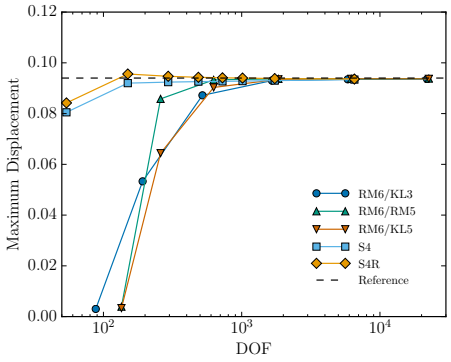

(e) $p = 3$, QNU quadrature.

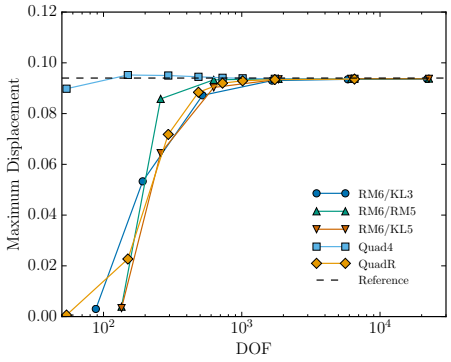

(f) $p = 3$, QNU quadrature.

Figure 6.29: Maximum deflection for the hemispherical shell with hole problem, $p = 3$.

6.1.9 Pinched Sphere

The pinched sphere problem tests a shell element's ability to handle regions of primarily bending stresses (near the poles) in addition to regions dominated by membrane stresses (near the equator). The geometry is a sphere with radius, $R = 20$, and thickness, $t = 0.04$. The sphere is loaded with two point loads on the poles with alternating signs and magnitude, $P = 10.0$. The material has a Young's modulus of, $E = 10.0e6$, and Poisson's ratio, $\nu = 0.3$. The problem setup is shown in Figure 6.30. Only one eighth of the sphere is modeled due to symmetry. The radial displacement at the location of one of the point loads is monitored, and normalized by a factor of $\frac{Et}{P}$. The reference solution is 21.2 [20].

The behavior of the blended shell is shown in Figures 6.31 and 6.32. Similar trends to those seen in previous problems, in terms of accuracy and competitiveness with commercial FEA elements, can be observed for this problem. In this case, all solutions converge to values higher then the exact solution. Tabulated results for this problem can be found in Appendix A.8.

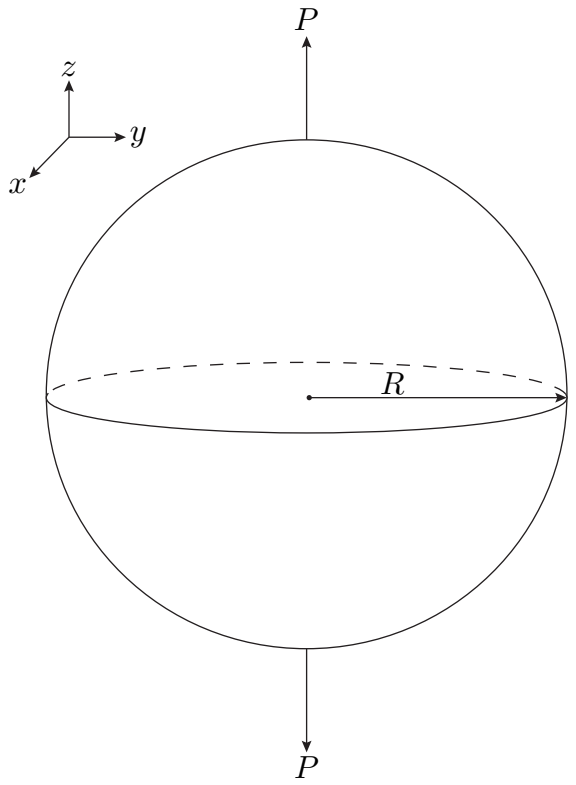

Figure 6.30: Schematic for the pinched sphere problem.

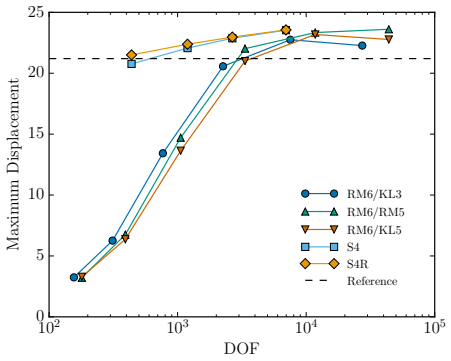

(a) $p = 2$, QP1 quadrature.

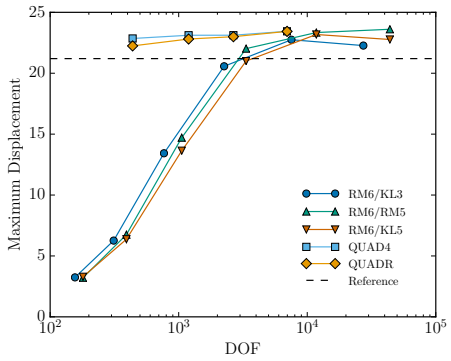

(b) $p = 2$, QP1 quadrature.

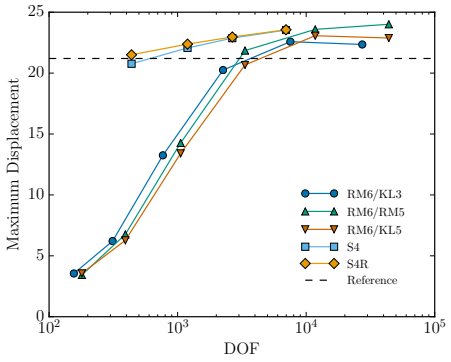

(c) $p = 2$, QP0 quadrature.

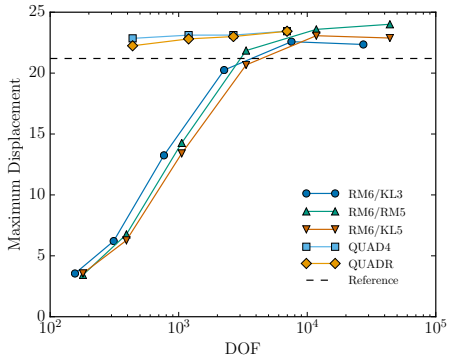

(d) $p = 2$, QP0 quadrature.

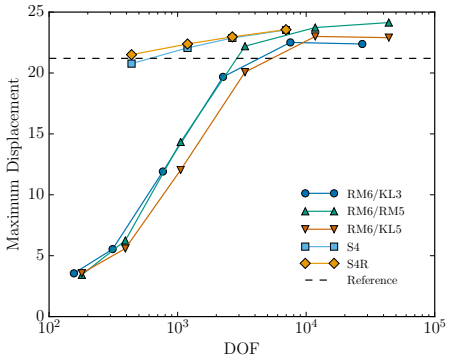

(e) $p = 2$, QNU quadrature.

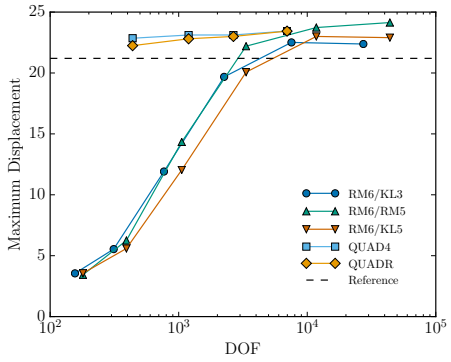

(f) $p = 2$, QNU quadrature.

Figure 6.31: Maximum deflection for the pinched sphere problem for $p = 2$.

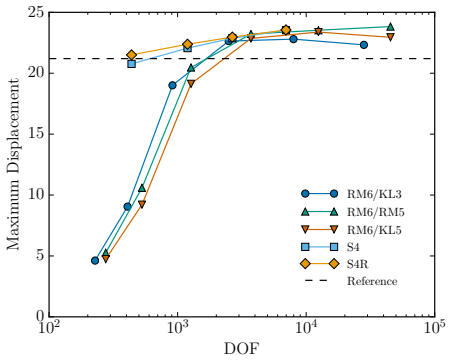

(a) $p = 3$, QP1 quadrature.

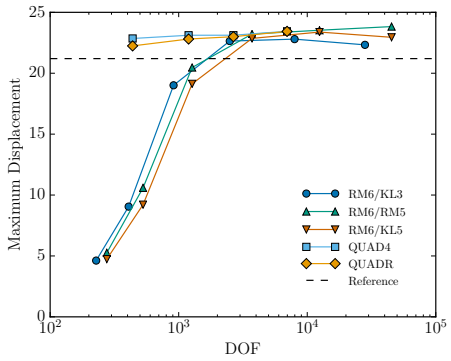

(b) $p = 3$, QP1 quadrature.

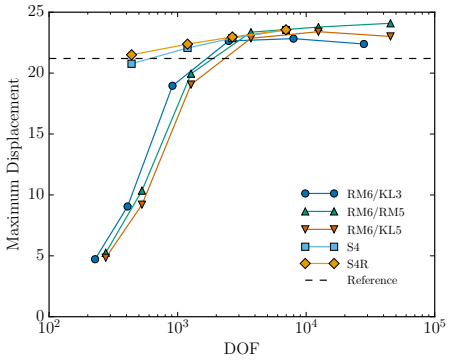

(c) $p = 3$, QP0 quadrature.

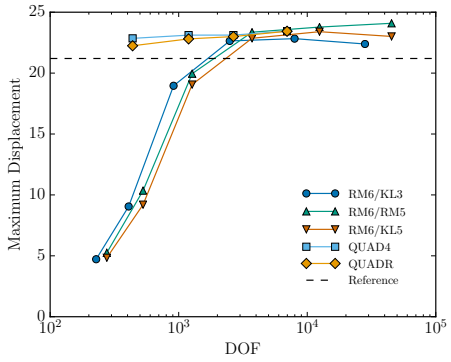

(d) $p = 3$, QP0 quadrature.

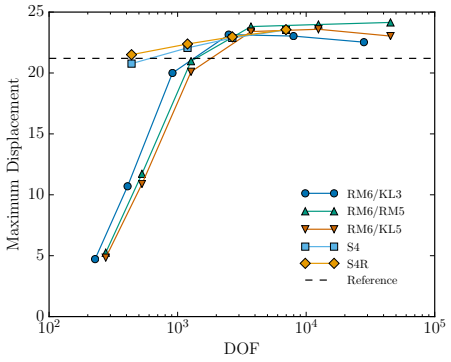

(e) $p = 3$, QNU quadrature.

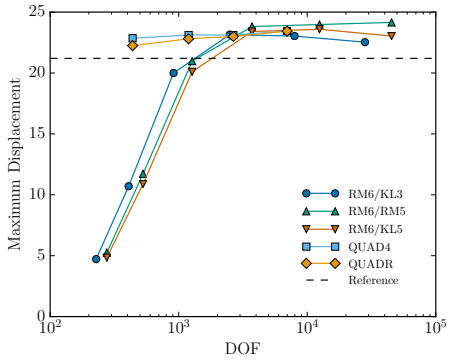

(f) $p = 3$, QNU quadrature.

Figure 6.32: Maximum deflection for the pinched sphere problem for $p = 3$.

CHAPTER 7. CONCLUSIONS

The benchmarks and numerical results discussed in Chapter 6 demonstrate numerous advantages of the geometrically exact isogeometric blended shell in comparison to: (1) commercially available shell elements from ABAQUS and NASTRAN, (2) the isogeometric blended shell proposed in [9], and (3) Reissner-Mindlin shell elements, RM5 and RM6.

Using Reissner-Mindlin shell elements on the boundaries enabled us to simulate any boundary condition. When blended with Kirchhoff-Love shell elements, KL3 or KL5, on the interior we were able to avoid shear locking. The Reissner-Mindlin elements on the boundaries did not cause any shear locking in any of the benchmarks.

Marked improvements were seen when gradient quantities were exactly lifted to the control points as compared with the approximations, as discussed in Section 3.2.1. The gradient extraction operator, discussed in Section 2.5.3, made this possible by enabling the blending of different shell descriptions. The cylindrical shell benchmark in Section 6.1.5 clearly illustrates the improved performance.

The KL5 shell element performed very well in all benchmarks, avoiding shear locking at the theoretical level, yet still capturing deformation due to transverse shear. It also produced more accurate shear stress fields, as seen in Section 6.1.4.

Overall the proposed isogeometric blended shell performed competitively with the commercial shell elements, sometimes outperforming them. This is crucial because it demonstrates that IGA is not only a viable option, but a clearly superior one. It shows that simulations can be run at the same computational cost as with commercial FEA shell elements, but with far better displacement and stress results. Furthermore, these simulations can be done without the time-consuming step of decomposing the geometry.

Another advantage of the proposed isogeometric blended shell is the generality. It performed competitively in the whole suite of benchmarks that tested all of the deformation modes.

Even the commercial FEA shell elements had benchmarks in which they performed poorly (see Section 6.1.1).

Although shear locking was avoided by using Kirchhoff-Love shell elements, membrane locking was still a major issue, as seen in Section 6.1.5. This locking was ameliorated by using different quadrature schemes and by increasing the smoothness, but it was clearly evident when full quadrature was used with degree $p = 2$. Eliminating the membrane locking could be the subject of future research.

REFERENCES

[1] Systèmes Dassault, Abaqus analysis users manual, Simulia Corp. Providence, RI, USA, 2010. vi, 33

[2] H. Hibbitt, B. Karlsson, P. Sorensen, ABAQUS theory manual, version 6.3, Pawtucket, Rhode Island, USA, 2006. vi, 33

[3] MSC Software, MSC-Nastran Linear Static Analysis User's Guide, MSC Software, 2016. vi, 33

[4] MSC Software, MSC-Nastran Reference Manual, MSC Software, 2016. vi, 33

[5] R. MacNeal, Finite elements: their design and performance., M. Dekker (1994) 444–449. viii, 61

[6] J. A. Cottrell, T. J. Hughes, Y. Bazilevs, Isogeometric analysis: toward integration of CAD and FEA, John Wiley & Sons, 2009. 1, 2

[7] T. J. Hughes, J. A. Cottrell, Y. Bazilevs, Isogeometric analysis: Cad, finite elements, nurbs, exact geometry and mesh refinement, Computer methods in applied mechanics and engineering 194 (39) (2005) 4135–4195. 2

[8] R. Echter, B. Oesterle, M. Bischoff, A hierarchic family of isogeometric shell finite elements, Computer Methods in Applied Mechanics and Engineering 254 (2013) 170 – 180. 2, 21, 50

[9] D. Benson, S. Hartmann, Y. Bazilevs, M.-C. Hsu, T. Hughes, Blended isogeometric shells, Computer Methods in Applied Mechanics and Engineering 255 (2013) 133 – 146. 3, 4, 67

[10] D. C. Thomas, M. A. Scott, J. A. Evans, K. Tew, E. J. Evans, Bézier projection: a unified approach for local projection and quadrature-free refinement and coarsening of NURBS and T-splines with particular application to isogeometric design and analysis, Computer Methods in Applied Mechanics and Engineering 284 (2015) 55–105. 12

[11] T. J. R. Hughes, The Finite Element Method: Linear Static and Dynamic Finite Element Analysis, Dover Publications, Mineola, NY, 2000. 16, 19

[12] D. Benson, S. Hartmann, Y. Bazilevs, M.-C. Hsu, T. Hughes, Blended isogeometric shells, Computer Methods in Applied Mechanics and Engineering 255 (0) (2013) 133 – 146. 20, 50

[13] W. Weaver, S. P. Timoshenko, D. H. Young, Vibration problems in engineering, Wiley, 1990. 28

[14] C. Adam, S. Bouabdallah, M. Zarroug, H. Maitournam, Improved numerical integration for locking treatment in isogeometric structural elements, part i: Beams, Computer Methods in Applied Mechanics and Engineering 279 (2014) 1–28. 31

[15] C. Adam, T. Hughes, S. Bouabdallah, M. Zarroug, H. Maitournam, Selective and reduced numerical integrations for nurbs-based isogeometric analysis, Computer Methods in Applied Mechanics and Engineering 284 (2015) 732–761. 31

[16] C. Adam, S. Bouabdallah, M. Zarroug, H. Maitournam, Improved numerical integration for locking treatment in isogeometric structural elements. part ii: Plates and shells, Computer Methods in Applied Mechanics and Engineering 284 (2015) 106–137. 31

[17] F. Calabrò, G. Sangalli, M. Tani, Fast formation of isogeometric galerkin matrices by weighted quadrature, arXiv preprint arXiv:1605.01238. 33

[18] R. H. Macneal, R. L. Harder, A proposed standard set of problems to test finite element accuracy, Finite elements in Analysis and Design 1 (1) (1985) 3–20. 33, 55, 58

[19] R. H. Gallagher, Finite elements for thin shells and curved members, John Wiley & Sons, 1976. 55

[20] W. T. Koiter, A spherical shell under point loads at its poles, Technique report in DTIC Document,1962. 64

[21] S. Ahmad, B. M. Irons, O. Zienkiewicz, Analysis of thick and thin shell structures by curved finite elements, International Journal for Numerical Methods in Engineering 2 (3) (1970) 419–451.

[22] W. Dornisch, R. Mller, S. Klinkel, An efficient and robust rotational formulation for isogeometric reissnermindlin shell elements, Computer Methods in Applied Mechanics and Engineering 303 (2016) 1–34.

[23] D. Thomas, M. Scott, J. Evans, K. Tew, E. Evans, Bézier projection: A unified approach for local projection and quadrature-free refinement and coarsening of {NURBS} and t-splines with particular application to isogeometric design and analysis, Computer Methods in Applied Mechanics and Engineering 284 (2015) 55–105, isogeometric Analysis Special Issue.

[24] T. J. Hughes, The finite element method: linear static and dynamic finite element analysis, Courier Corporation, 2000.

[25] O. C. Zienkiewicz, R. L. Taylor, The finite element method for solid and structural mechanics, Butterworth-heinemann, 2005.

[26] K.-J. Bathe, Finite element procedures, Klaus-Jurgen Bathe, 2006.

[27] A. E. H. Love, The small free vibrations and deformation of a thin elastic shell, Philosophical Transactions of the Royal Society of London 179 (1888) 491–546.

[28] E. Reissner, The effect of transverse shear deformation on the bending of elastic plates, Journal of Applied Mechanics ASME 12 (1945) 69–77.

[29] R. D. Mindlin, Influence of rotary inertia and shear on flexural motions of isotropic elastic plates, Journal of Applied Mechanics ASME 18 (1951) 31–38.

[30] K.-J. Bathe, E. N. Dvorkin, A four-node plate bending element based on mindlin/reissner plate theory and a mixed interpolation, International Journal for Numerical Methods in Engineering 21 (2) (1985) 367–383.

[31] M. L. Bucalem, K.-J. Bathe, Higher-order mitc general shell elements, International Journal for Numerical Methods in Engineering 36 (21) (1993) 3729–3754.

[32] O. Zienkiewicz, R. Taylor, J. Too, Reduced integration technique in general analysis of plates and shells, International Journal for Numerical Methods in Engineering 3 (2) (1971) 275–290.

[33] T. J. Hughes, R. L. Taylor, W. Kanoknukulchai, A simple and efficient finite element for plate bending, International Journal for Numerical Methods in Engineering 11 (10) (1977) 1529–1543.

[34] T. Belytschko, J. S.-J. Ong, W. K. Liu, J. M. Kennedy, Hourglass control in linear and nonlinear problems, Computer Methods in Applied Mechanics and Engineering 43 (3) (1984) 251–276.

[35] T. W. Sederberg, A. N. J. Zheng, A. Bakenov, T-splines and t-nurccss, ACM Transactions on Graphics 22 (3) (2003) 477–4484.

[36] T. W. Sederberg, D. L. Cardon, G. T. Finnigan, N. S. North, J. Zheng, T. Lyche, T-spline simplification and local refinement, ACM Transactions on Graphics 23 (3) (2004) 276–283.

[37] L. Piegl, W. Tiller, The NURBS book, Springer Science & Business Media, 2012.

[38] J. Kiendl, K.-U. Bletzinger, J. Linhard, R. Wchner, Isogeometric shell analysis with Kirchhoff-Love elements, Computer Methods in Applied Mechanics and Engineering 198 (4952) (2009) 3902 – 3914.

[39] J. Kiendl, M.-C. Hsu, M. C. Wu, A. Reali, Isogeometric Kirchhoff-Love shell formulations for general hyperelastic materials, Computer Methods in Applied Mechanics and Engineering 291 (2015) 280–303.

[40] A. B. Tepole, H. Kabaria, K.-U. Bletzinger, E. Kuhl, Isogeometric Kirchhoff-Love shell formulations for biological membranes, Computer Methods in Applied Mechanics and Engineering 293 (2015) 328 – 347.

[41] D. Benson, Y. Bazilevs, M.-C. Hsu, T. Hughes, A large deformation, rotation-free, isogeometric shell, Computer Methods in Applied Mechanics and Engineering 200 (1316) (2011) 1367 – 1378.

[42] A. Riffnaller-Schiefer, U. Augsdörfer, D. Fellner, Isogeometric shell analysis with nurbs compatible subdivision surfaces, Applied Mathematics and Computation 272 (2016) 139–147.

[43] T. Uhm, S. Youn, T-spline finite element method for the analysis of shell structures, International Journal for Numerical Methods in Engineering 80 (4) (2009) 507–536.

[44] D. Benson, Y. Bazilevs, M. Hsu, T. Hughes, Isogeometric shell analysis: The Reissner-Mindlin shell, Computer Methods in Applied Mechanics and Engineering 199 (58) (2010) 276 – 289.

[45] T. J. Hughes, W. K. Liu, Nonlinear finite element analysis of shells-part ii. two-dimensional shells, Computer Methods in Applied Mechanics and Engineering 27 (2) (1981) 167–181.

[46] W. Dornisch, S. Klinkel, B. Simeon, Isogeometric Reissner-Mindlin shell analysis with exactly calculated director vectors, Computer Methods in Applied Mechanics and Engineering 253 (2013) 491 – 504.

[47] Y. Guo, M. Ruess, Nitsche's method for a coupling of isogeometric thin shells and blended shell structures, Computer Methods in Applied Mechanics and Engineering 284 (2015) 881 – 905, isogeometric Analysis Special Issue.

[48] C. Adam, S. Bouabdallah, M. Zarroug, H. Maitournam, Improved numerical integration for locking treatment in isogeometric structural elements. part II: Plates and shells, Computer Methods in Applied Mechanics and Engineering 284 (2015) 106 – 137, isogeometric Analysis Special Issue.

[49] F. Koschnick, M. Bischoff, N. Camprub, K.-U. Bletzinger, The discrete strain gap method and membrane locking, Computer Methods in Applied Mechanics and Engineering 194 (2124) (2005) 2444 – 2463, computational Methods for Shells.

[50] P. Kang, S.-K. Youn, Isogeometric analysis of topologically complex shell structures, Finite Elements in Analysis and Design 99 (2015) 68 – 81.

[51] B. Oesterle, E. Ramm, M. Bischoff, A shear deformable, rotation-free isogeometric shell formulation, Computer Methods in Applied Mechanics and Engineering 307 (2016) 235 – 255.

[52] S. P. Timoshenko, S. Woinowsky-Krieger, Theory of plates and shells, McGraw-hill, 1959.

APPENDIX A. TABULATED RESULTS FOR BENCHMARK PROBLEMS

We include the tabulated results for each benchmark problem. We include both isogeometric blended shell element results as well as commercial shell elements results from both Abaqus and Nastran. Where appropriate we include both thick and thin shell solutions. For the FEA results we occasionally specify when transverse shear (TS) is included or neglected in the underlying shell formulation.

A.1 Results for the in-plane bending of a cantilever beam problem

Table A.1: Maximum displacement for the in-plane bending of a cantilever beam problem for different blended shell elements, $p = 2$.

Element	Degree	Mesh	DOF	QP1	QP0	QNU
RM5/KL3	2	2×1	27	0.0853529	0.106372	0.106372
RM5/KL3	2	4×1	45	0.101664	0.107081	0.109197
RM5/KL3	2	8×1	81	0.107089	0.107582	0.10833
RM5/KL3	2	16×1	153	0.10776	0.107834	0.108046
RM5/KL3	2	32×1	297	0.10792	0.107957	0.108014
RM5/KL3	2	64×1	585	0.107979	0.108018	0.108033
RM5/RM5	2	2×1	45	0.0853529	0.106372	0.106372
RM5/RM5	2	4×1	75	0.101664	0.107081	0.109197
RM5/RM5	2	8×1	135	0.107089	0.107582	0.10833
RM5/RM5	2	16×1	255	0.10776	0.107834	0.108046
RM5/RM5	2	32×1	495	0.10792	0.107957	0.108014
RM5/RM5	2	64×1	975	0.107979	0.108018	0.108033
RM5/KL5	2	2×1	45	0.0853529	0.106372	0.106372
RM5/KL5	2	4×1	75	0.101664	0.107081	0.109197
RM5/KL5	2	8×1	135	0.107089	0.107582	0.10833
RM5/KL5	2	16×1	255	0.10776	0.107834	0.108046
RM5/KL5	2	32×1	495	0.10792	0.107957	0.108014
RM5/KL5	2	64×1	975	0.107979	0.108018	0.108033

Table A.2: Maximum displacement for the in-plane bending of a cantilever beam problem for different blended shell elements, $p = 3$

Element	Degree	Mesh	DOF	QP1	QP0	QNU
RM5/KL3	3	2×1	48	0.10674	0.106823	0.106823
RM5/KL3	3	4×1	72	0.10736	0.107379	0.108793
RM5/KL3	3	8×1	120	0.107725	0.107734	0.108644
RM5/KL3	3	16×1	216	0.107904	0.107909	0.108412
RM5/KL3	3	32×1	408	0.107985	0.107989	0.108246
RM5/KL3	3	64×1	792	0.108014	0.108022	0.108148
RM5/RM5	3	2×1	80	0.10674	0.106823	0.106823
RM5/RM5	3	4×1	120	0.10736	0.107379	0.108793
RM5/RM5	3	8×1	200	0.107725	0.107734	0.108644
RM5/RM5	3	16×1	360	0.107904	0.107909	0.108412
RM5/RM5	3	32×1	680	0.107985	0.107989	0.108246
RM5/RM5	3	64×1	1320	0.108014	0.108022	0.108148
RM5/KL5	3	2×1	80	0.10674	0.106823	0.106823
RM5/KL5	3	4×1	120	0.10736	0.107379	0.108793
RM5/KL5	3	8×1	200	0.107725	0.107734	0.108644
RM5/KL5	3	16×1	360	0.107904	0.107909	0.108412
RM5/KL5	3	32×1	680	0.107985	0.107989	0.108246
RM5/KL5	3	64×1	1320	0.108014	0.108022	0.108148

Table A.3: Maximum displacement for the in-plane bending of a cantilever beam problem for different commercial FEA elements.

Mesh	DOF	Quad4	QuadR	S4	S4R
4×1	48	0.1064	0.1064	0.0646	0.0681
6×1	72	0.1073	0.1073	0.0770	0.0821
8×1	96	0.1077	0.1077	0.0849	0.0911
12×1	144	0.1079	0.1079	0.0938	0.1015
16×1	192	0.1080	0.1080	0.0985	0.1069

Table A.4: Maximum displacement for the out-of-plane bending of a cantilever beam problem for different blended shell elements, $p = 2$.

Element	Degree	Mesh	DOF	QP1	QP0	QNU
RM5/KL3	2	2×1	27	0.400144	0.403269	0.403269
RM5/KL3	2	4×1	45	0.421265	0.422	0.422565
RM5/KL3	2	8×1	81	0.42798	0.428319	0.428528
RM5/KL3	2	16×1	153	0.43015	0.430344	0.430414
RM5/KL3	2	32×1	297	0.430812	0.430965	0.430989
RM5/KL3	2	64×1	585	0.430905	0.431082	0.43109
RM5/RM5	2	2×1	45	0.328552	0.425263	0.425263
RM5/RM5	2	4×1	75	0.379747	0.428049	0.436548
RM5/RM5	2	8×1	135	0.424467	0.430028	0.433051
RM5/RM5	2	16×1	255	0.430357	0.430986	0.431861
RM5/RM5	2	32×1	495	0.43109	0.431399	0.431643
RM5/RM5	2	64×1	975	0.431215	0.431577	0.431631
RM5/KL5	2	2×1	45	0.400316	0.403686	0.403686
RM5/KL5	2	4×1	75	0.421386	0.422211	0.42282
RM5/KL5	2	8×1	135	0.4281	0.428529	0.428743
RM5/KL5	2	16×1	255	0.430301	0.430663	0.430756
RM5/KL5	2	32×1	495	0.431008	0.431428	0.431516
RM5/KL5	2	64×1	975	0.43119	0.43169	0.431825

A.2 Results for the out-of-plane bending of a cantilever beam problem

Table A.5: Maximum displacement for the out-of-plane bending of a cantilever beam problem for different blended shell elements, $p = 3$.

Element	Degree	Mesh	DOF	QP1	QP0	QNU
RM5/KL3	3	2×1	48	0.426526	0.426823	0.426823
RM5/KL3	3	4×1	72	0.428945	0.429011	0.433243
RM5/KL3	3	8×1	120	0.430314	0.430342	0.431807
RM5/KL3	3	16×1	216	0.430892	0.430903	0.431315
RM5/KL3	3	32×1	408	0.43104	0.431043	0.43115
RM5/KL3	3	64×1	792	0.430964	0.430965	0.430993
RM5/RM5	3	2×1	80	0.426601	0.426932	0.426932
RM5/RM5	3	4×1	120	0.429052	0.429128	0.433636
RM5/RM5	3	8×1	200	0.430446	0.430478	0.433096
RM5/RM5	3	16×1	360	0.431039	0.431052	0.432662
RM5/RM5	3	32×1	680	0.431224	0.431229	0.432071
RM5/RM5	3	64×1	1320	0.431267	0.431274	0.431668
RM5/KL5	3	2×1	80	0.42663	0.426934	0.426934
RM5/KL5	3	4×1	120	0.429061	0.42913	0.433373
RM5/KL5	3	8×1	200	0.430446	0.430479	0.431957
RM5/KL5	3	16×1	360	0.431038	0.431051	0.431458
RM5/KL5	3	32×1	680	0.431207	0.431211	0.431316
RM5/KL5	3	64×1	1320	0.431232	0.431233	0.431266

Table A.6: Maximum displacement for the out-of-plane bending of a cantilever beam problem for different commercial FEA elements.

Mesh	DOF	Quad4	QuadR	S4	S4R
4×1	48	0.4237	0.4217	0.4172	0.4248
6×1	72	0.4265	0.4254	0.4235	0.4282
8×1	96	0.4279	0.4271	0.4261	0.4294
12×1	144	0.4293	0.4287	0.4284	0.4303
16×1	192	0.4300	0.4294	0.4294	0.4306

Table A.7: Maximum displacement for the clamped plate problem for $\frac{L}{t} = 10, p = 2$.

Element	Degree	Mesh	DOF	QP1	QP0	QNU
RM5/KL3	2	2×2	72	0.0397253	0.0412743	0.0412743
RM5/KL3	2	4×4	148	0.132547	0.133351	0.129574
RM5/KL3	2	8×8	372	0.143237	0.143514	0.143806
RM5/KL3	2	16×16	1108	0.140616	0.140671	0.140905
RM5/KL3	2	32×32	3732	0.138598	0.138602	0.138685
RM5/KL3	2	64×64	13588	0.138189	0.138189	0.138213
RM5/RM5	2	2×2	80	0.0541941	0.0695444	0.0695444
RM5/RM5	2	4×4	180	0.154547	0.165162	0.180805
RM5/RM5	2	8×8	500	0.163558	0.164229	0.17107
RM5/RM5	2	16×16	1620	0.164253	0.164301	0.167195
RM5/RM5	2	32×32	5780	0.164302	0.164305	0.1652
RM5/RM5	2	64×64	21780	0.164305	0.164305	0.16455
RM5/KL5	2	2×2	80	0.0541941	0.0695444	0.0695444
RM5/KL5	2	4×4	180	0.152259	0.157515	0.156678
RM5/KL5	2	8×8	500	0.1606	0.160958	0.16236
RM5/KL5	2	16×16	1620	0.163084	0.163103	0.163471
RM5/KL5	2	32×32	5780	0.163933	0.163934	0.164011
RM5/KL5	2	64×64	21780	0.164202	0.164202	0.164219

A.3 Results for the clamped rectangular plate subject to a distributed load

Table A.8: Maximum displacement for the clamped plate problem for $\frac{L}{t} = 10, p = 3$.

Element	Degree	Mesh	DOF	QP1	QP0	QNU
RM5/KL3	3	2×2	107	0.530556	0.530083	0.530083
RM5/KL3	3	4×4	195	0.198428	0.198442	0.217874
RM5/KL3	3	8×8	443	0.155103	0.155117	0.169115
RM5/KL3	3	16×16	1227	0.143357	0.143361	0.148632
RM5/KL3	3	32×32	3947	0.139527	0.139528	0.141226
RM5/KL3	3	64×64	13995	0.138458	0.138458	0.138853
RM5/RM5	3	2×2	125	0.544672	0.561587	0.561587
RM5/RM5	3	4×4	245	0.216534	0.216144	0.197133
RM5/RM5	3	8×8	605	0.175661	0.175662	0.177799
RM5/RM5	3	16×16	1805	0.167069	0.16707	0.168942
RM5/RM5	3	32×32	6125	0.164992	0.164992	0.165956
RM5/RM5	3	64×64	22445	0.164477	0.164477	0.164927
RM5/KL5	3	2×2	125	0.563442	0.554227	0.554227
RM5/KL5	3	4×4	245	0.213402	0.213416	0.259083
RM5/KL5	3	8×8	605	0.175611	0.175612	0.201568
RM5/KL5	3	16×16	1805	0.167069	0.167069	0.172577
RM5/KL5	3	32×32	6125	0.164992	0.164992	0.166056
RM5/KL5	3	64×64	22445	0.164477	0.164477	0.164712

Table A.9: Maximum displacement for the clamped plate problem for $\frac{L}{t} = 100, p = 2$.

Element	Degree	Mesh	DOF	QP1	QP0	QNU
RM5/KL3	2	2×2	72	0.000406158	0.000422158	0.000422158
RM5/KL3	2	4×4	148	0.108129	0.108439	0.106006
RM5/KL3	2	8×8	372	0.130674	0.130696	0.131135
RM5/KL3	2	16×16	1108	0.136349	0.136353	0.136598
RM5/KL3	2	32×32	3732	0.137743	0.137745	0.137828
RM5/KL3	2	64×64	13588	0.138076	0.138077	0.138101
RM5/RM5	2	2×2	80	0.000648533	0.000980525	0.000980525
RM5/RM5	2	4×4	180	0.0135136	0.0462474	0.154172
RM5/RM5	2	8×8	500	0.0984809	0.137783	0.143859
RM5/RM5	2	16×16	1620	0.134769	0.138396	0.1411
RM5/RM5	2	32×32	5780	0.138185	0.138448	0.139347
RM5/RM5	2	64×64	21780	0.138433	0.13845	0.138708
RM5/KL5	2	2×2	80	0.000648533	0.000980525	0.000980525
RM5/KL5	2	4×4	180	0.108633	0.109623	0.107414
RM5/KL5	2	8×8	500	0.131084	0.131497	0.132724
RM5/KL5	2	16×16	1620	0.136691	0.13684	0.137403
RM5/KL5	2	32×32	5780	0.138027	0.138051	0.138167
RM5/KL5	2	64×64	21780	0.138342	0.138344	0.13837

Table A.10: Maximum displacement for the clamped plate problem for $\frac{L}{t} = 100, p = 3$.

Element	Degree	Mesh	DOF	QP1	QP0	QNU
RM5/KL3	3	2×2	107	0.578044	0.579696	0.579696
RM5/KL3	3	4×4	195	0.183263	0.183279	0.190787
RM5/KL3	3	8×8	443	0.14862	0.14862	0.156299
RM5/KL3	3	16×16	1227	0.140739	0.140739	0.142946
RM5/KL3	3	32×32	3947	0.13882	0.13882	0.139378
RM5/KL3	3	64×64	13995	0.138339	0.138339	0.138481
RM5/RM5	3	2×2	125	0.0870593	0.166056	0.166056
RM5/RM5	3	4×4	245	0.181453	0.188348	0.19239
RM5/RM5	3	8×8	605	0.148938	0.14893	0.150358
RM5/RM5	3	16×16	1805	0.140976	0.140978	0.142329
RM5/RM5	3	32×32	6125	0.139078	0.139078	0.139872
RM5/RM5	3	64×64	22445	0.138607	0.138607	0.13901
RM5/KL5	3	2×2	125	0.57792	0.578573	0.578573
RM5/KL5	3	4×4	245	0.183429	0.183448	0.19167
RM5/KL5	3	8×8	605	0.148829	0.148829	0.157485
RM5/KL5	3	16×16	1805	0.140979	0.140979	0.143983
RM5/KL5	3	32×32	6125	0.139078	0.139078	0.139905
RM5/KL5	3	64×64	22445	0.138607	0.138607	0.138792

Table A.11: Maximum displacement for the clamped plate problem for $\frac{L}{t} = 1,000, p = 2$.

Element	Degree	Mesh	DOF	QP1	QP0	QNU
RM5/KL3	2	2×2	72	4.06E-06	4.22E-06	4.22E-06
RM5/KL3	2	4×4	148	1.08E-01	1.08E-01	0.105735
RM5/KL3	2	8×8	372	1.30E-01	1.31E-01	0.130957
RM5/KL3	2	16×16	1108	1.36E-01	1.36E-01	0.136498
RM5/KL3	2	32×32	3732	0.137692	0.137693	0.137776
RM5/KL3	2	64×64	13588	0.138053	0.138053	0.138077
RM5/RM5	2	2×2	80	6.50E-06	9.85E-06	9.85E-06
RM5/RM5	2	4×4	180	1.49E-04	0.000675559	0.153904
RM5/RM5	2	8×8	500	3.20E-03	0.0357875	0.143572
RM5/RM5	2	16×16	1620	4.17E-02	0.135888	0.140822
RM5/RM5	2	32×32	5780	0.120443	0.138103	0.139071
RM5/RM5	2	64×64	21780	0.136667	0.138174	0.138433
RM5/KL5	2	2×2	80	6.50E-06	9.85E-06	9.85E-06
RM5/KL5	2	4×4	180	1.08E-01	1.08E-01	0.105749
RM5/KL5	2	8×8	500	1.31E-01	1.31E-01	0.130978
RM5/KL5	2	16×16	1620	1.36E-01	1.36E-01	0.136523
RM5/KL5	2	32×32	5780	0.137696	0.137698	0.1378
RM5/KL5	2	64×64	21780	0.138056	0.138057	0.13809

Table A.12: Maximum displacement for the clamped plate problem for $\frac{L}{t} = 1,000, p = 3$.

Element	Degree	Mesh	DOF	QP1	QP0	QNU
RM5/KL3	3	2×2	107	0.578664	0.580351	0.580351
RM5/KL3	3	4×4	195	0.183114	0.183131	0.190491
RM5/KL3	3	8×8	443	0.148545	0.148545	0.156098
RM5/KL3	3	16×16	1227	0.1407	0.1407	0.142853
RM5/KL3	3	32×32	3947	1.39E-01	0.138801	0.139338
RM5/KL3	3	64×64	13995	1.38E-01	0.13833	0.138462
RM5/RM5	3	2×2	125	0.00102938	0.00235151	0.00235151
RM5/RM5	3	4×4	245	0.0150572	0.0237003	0.195381
RM5/RM5	3	8×8	605	0.132796	0.139056	0.150056
RM5/RM5	3	16×16	1805	0.140583	0.140596	0.141825
RM5/RM5	3	32×32	6125	0.138796	0.138799	0.139283
RM5/RM5	3	64×64	22445	0.138332	0.138332	0.138527
RM5/KL5	3	2×2	125	0.578662	0.580339	0.580339
RM5/KL5	3	4×4	245	0.183115	0.183132	0.1905
RM5/KL5	3	8×8	605	0.148547	0.148547	0.156111
RM5/KL5	3	16×16	1805	0.140703	0.140703	0.142867
RM5/KL5	3	32×32	6125	0.138803	0.138803	0.139351
RM5/KL5	3	64×64	22445	0.138332	0.138332	0.138473

Table A.13: Maximum displacement for the clamped plate problem for $\frac{L}{t} = 10,000, p = 2$.

Element	Degree	Mesh	DOF	QP1	QP0	QNU
RM5/KL3	2	2×2	72	4.06E-08	4.22E-08	4.22E-08
RM5/KL3	2	4×4	148	1.08E-01	1.08E-01	0.105732
RM5/KL3	2	8×8	372	1.30E-01	1.31E-01	0.130955
RM5/KL3	2	16×16	1108	1.36E-01	1.36E-01	0.136497
RM5/KL3	2	32×32	3732	0.137692	0.137692	0.137775
RM5/KL3	2	64×64	13588	0.138053	0.138053	0.138077
RM5/RM5	2	2×2	80	6.50E-08	9.85E-08	9.85E-08
RM5/RM5	2	4×4	180	1.49E-06	6.79E-06	0.153902
RM5/RM5	2	8×8	500	3.27E-05	0.000473325	0.143569
RM5/RM5	2	16×16	1620	5.93E-04	0.0256329	0.14082
RM5/RM5	2	32×32	5780	0.009272	0.133304	0.139068
RM5/RM5	2	64×64	21780	0.074124	0.138075	0.13843
RM5/KL5	2	2×2	80	6.50E-08	9.85E-08	9.85E-08
RM5/KL5	2	4×4	180	1.08E-01	1.08E-01	0.105732
RM5/KL5	2	8×8	500	1.30E-01	1.31E-01	0.130955
RM5/KL5	2	16×16	1620	1.36E-01	1.36E-01	0.136497
RM5/KL5	2	32×32	5780	0.137692	0.137692	0.137776
RM5/KL5	2	64×64	21780	0.138053	0.138053	0.138077

Table A.14: Maximum displacement for the clamped plate problem for $\frac{L}{t} = 10,000, p = 3$.

Element	Degree	Mesh	DOF	QP1	QP0	QNU
RM5/KL3	3	2×2	107	0.57867	0.580357	0.580357
RM5/KL3	3	4×4	195	0.183112	0.183129	0.190488
RM5/KL3	3	8×8	443	0.148544	0.148544	0.156096
RM5/KL3	3	16×16	1227	0.1407	0.1407	0.142852
RM5/KL3	3	32×32	3947	1.39E-01	0.138801	0.139337
RM5/KL3	3	64×64	13995	1.38E-01	0.13833	0.138461
RM5/RM5	3	2×2	125	1.03E-05	2.36E-05	2.36E-05
RM5/RM5	3	4×4	245	0.000162351	0.000267821	0.195416
RM5/RM5	3	8×8	605	0.0079066	0.0110308	0.150053
RM5/RM5	3	16×16	1805	0.116086	0.123716	0.141817
RM5/RM5	3	32×32	6125	0.138642	0.138646	0.139265
RM5/RM5	3	64×64	22445	0.138319	0.138322	0.13849
RM5/KL5	3	2×2	125	0.57867	0.580357	0.580357
RM5/KL5	3	4×4	245	0.183112	0.183129	0.190489
RM5/KL5	3	8×8	605	0.148544	0.148544	0.156096
RM5/KL5	3	16×16	1805	0.1407	0.1407	0.142852
RM5/KL5	3	32×32	6125	0.138801	0.138801	0.139337
RM5/KL5	3	64×64	22445	0.13833	0.13833	0.138461

Table A.15: Maximum displacement for the clamped plate problem for NASTRAN Quad4, QuadR.

L/t	Mesh	DOF	Quad4 w/o TS	Quad4	QuadR w/o TS	QuadR
10	4×4	150	0.1486	0.1960	0.1387	0.1779
10	6×6	294	0.1466	0.1811	0.1422	0.1725
10	8×8	486	0.1445	0.1742	0.1420	0.1692
10	10×10	726	0.1429	0.1707	0.1413	0.1675
10	20×20	2646	0.1397	0.1659	0.1393	0.1651
10	40×40	10086	0.1386	0.1647	0.1385	0.1645
10	80×80	39366	0.1383	0.1644	0.1383	0.1644
100	4×4	150	0.1486	0.1505	0.1387	0.1341
100	6×6	294	0.1466	0.1487	0.1422	0.1399
100	8×8	486	0.1445	0.1461	0.1420	0.1410
100	10×10	726	0.1429	0.1442	0.1413	0.1409
100	20×20	2646	0.1397	0.1402	0.1393	0.1393
100	40×40	10086	0.1386	0.1389	0.1385	0.1387
100	80×80	39366	0.1383	0.1386	0.1383	0.1385
1000	4×4	150	0.1486	0.1486	0.1387	0.1346
1000	6×6	294	0.1466	0.1466	0.1422	0.1393
1000	8×8	486	0.1445	0.1445	0.1420	0.1400
1000	10×10	726	0.1429	0.1429	0.1413	0.1399
1000	20×20	2646	0.1397	0.1397	0.1393	0.1389
1000	40×40	10086	0.1386	0.1386	0.1385	0.1384
1000	80×80	39366	0.1383	0.1383	0.1383	0.1382
10000	4×4	150	0.1486	0.1486	0.1387	0.1346
10000	6×6	294	0.1466	0.1466	0.1422	0.1393
10000	8×8	486	0.1445	0.1445	0.1420	0.1400
10000	10×10	726	0.1429	0.1429	0.1413	0.1399
10000	20×20	2646	0.1397	0.1397	0.1393	0.1389
10000	40×40	10086	0.1386	0.1386	0.1385	0.1384
10000	80×80	39366	0.1383	0.1383	0.1383	0.1382

Table A.16: Maximum displacement for the clamped plate problem for ABAQUS S4, S4R.

L/t	Mesh	DOF	S4 w/o TS	S4	S4R w/o TS	S4R
10	4×4	150	0.1325	0.1575	0.1417	0.1658
10	6×6	294	0.1356	0.1619	0.1395	0.1654
10	8×8	486	0.1369	0.1629	0.139	0.1649
10	10×10	726	0.1374	0.1634	0.1388	0.1647
10	20×20	2646	0.1382	0.1641	0.1385	0.1644
10	40×40	10086	0.1384	0.1643	0.1385	0.1643
10	80×80	39366	0.1384	0.1643	0.1385	0.1643
100	4×4	150	0.1323	0.1325	0.1414	0.1417
100	6×6	294	0.1354	0.1356	0.1392	0.1395
100	8×8	486	0.1366	0.1369	0.1387	0.1390
100	10×10	726	0.1372	0.1374	0.1385	0.1388
100	20×20	2646	0.1379	0.1382	0.1383	0.1385
100	40×40	10086	0.1381	0.1384	0.1382	0.1385
100	80×80	39366	0.1382	0.1384	0.1382	0.1385
1000	4×4	150	0.1323	0.1323	0.1414	0.1415
1000	6×6	294	0.1354	0.1354	0.1392	0.1392
1000	8×8	486	0.1366	0.1366	0.1387	0.1387
1000	10×10	726	0.1371	0.1372	0.1385	0.1385
1000	20×20	2646	0.1379	0.1379	0.1383	0.1383
1000	40×40	10086	0.1381	0.1381	0.1382	0.1382
1000	80×80	39366	0.1382	0.1382	0.1382	0.1382
10000	4×4	150	0.1323	0.1323	0.1414	0.1414
10000	6×6	294	0.1354	0.1354	0.1392	0.1392
10000	8×8	486	0.1366	0.1366	0.1387	0.1387
10000	10×10	726	0.1371	0.1371	0.1385	0.1385
10000	20×20	2646	0.1379	0.1379	0.1383	0.1383
10000	40×40	10086	0.1381	0.1381	0.1382	0.1382
10000	80×80	39366	0.1382	0.1382	0.1382	0.1382

Table A.17: Maximum radial displacement for the cylindrical shell problem for $\frac{L}{t} = 10$ and $p = 2$.

Element	Degree	Mesh	DOF	QP1	QP0	QNU
RM5/KL3	2	2×1	42	0.225159	0.793012	0.793012
RM5/KL3	2	4×1	60	0.785359	0.913523	0.890282
RM5/KL3	2	8×1	96	0.926749	0.936237	0.924779
RM5/KL3	2	16×1	168	0.939284	0.939883	0.936596
RM5/KL3	2	32×1	312	0.94073	0.940767	0.9399
RM5/KL3	2	64×1	600	0.940987	0.94099	0.940767
RM5/KL3	2	128×1	1176	0.941045	0.941045	0.940989
RM5/KL3	2	256×1	2328	0.941059	0.941059	0.941045
RM5/KL3	2	512×1	4632	0.941063	0.941063	0.941059
RM5/RM5	2	2×1	60	0.239022	0.913872	0.913872
RM5/RM5	2	4×1	90	0.829483	0.984962	1.01348
RM5/RM5	2	8×1	150	0.948672	0.959554	0.964562
RM5/RM5	2	16×1	270	0.946675	0.947339	0.948625
RM5/RM5	2	32×1	510	0.944026	0.944067	0.944397
RM5/RM5	2	64×1	990	0.943227	0.94323	0.943314
RM5/RM5	2	128×1	1950	0.943018	0.943018	0.943039
RM5/RM5	2	256×1	3870	0.942965	0.942965	0.942971
RM5/RM5	2	512×1	7710	0.942952	0.942952	0.942953
RM5/KL5	2	2×1	60	0.227361	0.796101	0.796101
RM5/KL5	2	4×1	90	0.786811	0.915311	0.892065
RM5/KL5	2	8×1	150	0.928566	0.938087	0.926629
RM5/KL5	2	16×1	270	0.941158	0.941759	0.938468
RM5/KL5	2	32×1	510	0.942612	0.942649	0.94178
RM5/KL5	2	64×1	990	0.94287	0.942873	0.94265
RM5/KL5	2	128×1	1950	0.942929	0.942929	0.942872
RM5/KL5	2	256×1	3870	0.942943	0.942943	0.942929
RM5/KL5	2	512×1	7710	0.942904	0.943013	0.942949

A.4 Results for the cylindrical shell

Table A.18: Maximum radial displacement for the cylindrical shell problem for $\frac{L}{t} = 10$ and $p = 3$.

Element	Degree	Mesh	DOF	QP1	QP0	QNU
RM5/KL3	3	2×1	68	0.880924	0.894634	0.894634
RM5/KL3	3	4×1	92	0.938437	0.938863	0.967695
RM5/KL3	3	8×1	140	0.941004	0.941011	0.948472
RM5/KL3	3	16×1	236	0.941062	0.941062	0.943058
RM5/KL3	3	32×1	428	0.941064	0.941064	0.941589
RM5/KL3	3	64×1	812	0.941066	0.941068	0.941199
RM5/KL3	3	128×1	1580	0.941064	0.941064	0.941101
RM5/KL3	3	256×1	3116	0.941064	0.941064	0.941074
RM5/KL3	3	512×1	6188	0.941064	0.941064	0.941067
RM5/RM5	3	2×1	100	1.02016	1.03548	1.03548
RM5/RM5	3	4×1	140	1.01246	1.01324	1.01765
RM5/RM5	3	8×1	220	0.964393	0.964403	0.967796
RM5/RM5	3	16×1	380	0.948677	0.948677	0.95068
RM5/RM5	3	32×1	700	0.944424	0.944424	0.945474
RM5/RM5	3	64×1	1340	0.943322	0.943322	0.943856
RM5/RM5	3	128×1	2620	0.943042	0.943042	0.943311
RM5/RM5	3	256×1	5180	0.942971	0.942971	0.943106
RM5/RM5	3	512×1	10300	0.942953	0.942953	0.943021
RM5/KL5	3	2×1	100	0.884585	0.898638	0.898638
RM5/KL5	3	4×1	140	0.940367	0.940799	0.970018
RM5/KL5	3	8×1	220	0.942888	0.942895	0.950496
RM5/KL5	3	16×1	380	0.942945	0.942945	0.944987
RM5/KL5	3	32×1	700	0.942962	0.942947	0.943506
RM5/KL5	3	64×1	1340	0.94311	0.943076	0.943201
RM5/KL5	3	128×1	2620	0.942947	0.942947	0.942988
RM5/KL5	3	256×1	5180	0.942948	0.942985	0.962903
RM5/KL5	3	512×1	10300	0.942822	0.519298	1.01125

Table A.19: Maximum radial displacement for the cylindrical shell problem for $\frac{L}{t} = 100$ and $p = 2$.

Element	Degree	Mesh	DOF	QP1	QP0	QNU
RM5/KL3	2	2×1	42	0.00303845	0.73782	0.73782
RM5/KL3	2	4×1	60	0.0519076	0.781418	0.891118
RM5/KL3	2	8×1	96	0.465018	0.923616	0.925822
RM5/KL3	2	16×1	168	0.885042	0.941031	0.93794
RM5/KL3	2	32×1	312	0.93845	0.942163	0.941296
RM5/KL3	2	64×1	600	0.942156	0.942389	0.942166
RM5/KL3	2	128×1	1176	0.94243	0.942445	0.942389
RM5/KL3	2	256×1	2328	0.942458	0.942459	0.942445
RM5/KL3	2	512×1	4632	0.942463	0.942463	0.942459
RM5/RM5	2	2×1	60	0.00310376	0.859315	0.859315
RM5/RM5	2	4×1	90	0.0496456	0.741359	1.00876
RM5/RM5	2	8×1	150	0.450769	0.935216	0.964036
RM5/RM5	2	16×1	270	0.884661	0.946413	0.948172
RM5/RM5	2	32×1	510	0.939491	0.943597	0.943936
RM5/RM5	2	64×1	990	0.942508	0.942766	0.94285
RM5/RM5	2	128×1	1950	0.942538	0.942554	0.942575
RM5/RM5	2	256×1	3870	0.942499	0.9425	0.942506
RM5/RM5	2	512×1	7710	0.942487	0.942487	0.942488
RM5/KL5	2	2×1	60	0.00307756	0.771117	0.771117
RM5/KL5	2	4×1	90	0.0519738	0.782246	0.891391
RM5/KL5	2	8×1	150	0.465055	0.923642	0.925879
RM5/KL5	2	16×1	270	0.88506	0.94105	0.937981
RM5/KL5	2	32×1	510	0.938469	0.942181	0.941316
RM5/KL5	2	64×1	990	0.942175	0.942408	0.942185
RM5/KL5	2	128×1	1950	0.942449	0.942464	0.942408
RM5/KL5	2	256×1	3870	0.942476	0.942478	0.942464
RM5/KL5	2	512×1	7710	0.942482	0.957747	0.944448

Table A.20: Maximum radial displacement for the cylindrical shell problem for $\frac{L}{t} = 100$ and $p = 3$.

Element	Degree	Mesh	DOF	QP1	QP0	QNU
RM5/KL3	3	2×1	68	0.720376	0.752267	0.752267
RM5/KL3	3	4×1	92	0.866042	0.883212	0.965761
RM5/KL3	3	8×1	140	0.940142	0.94079	0.949711
RM5/KL3	3	16×1	236	0.942427	0.942438	0.944428
RM5/KL3	3	32×1	428	0.942463	0.942463	0.942974
RM5/KL3	3	64×1	812	0.942465	0.942466	0.942592
RM5/KL3	3	128×1	1580	0.942464	0.942464	0.942497
RM5/KL3	3	256×1	3116	0.942464	0.942464	0.942472
RM5/KL3	3	512×1	6188	0.942464	0.942464	0.942466
RM5/RM5	3	2×1	100	0.754246	0.82203	0.82203
RM5/RM5	3	4×1	140	0.910032	0.931565	0.996332
RM5/RM5	3	8×1	220	0.960558	0.961514	0.963904
RM5/RM5	3	16×1	380	0.948177	0.948191	0.948773
RM5/RM5	3	32×1	700	0.943962	0.943962	0.9446
RM5/RM5	3	64×1	1340	0.942858	0.942858	0.943317
RM5/RM5	3	128×1	2620	0.942577	0.942577	0.942835
RM5/RM5	3	256×1	5180	0.942506	0.942506	0.94264
RM5/RM5	3	512×1	10300	0.942488	0.942488	0.942556
RM5/KL5	3	2×1	100	0.720472	0.753252	0.753252
RM5/KL5	3	4×1	140	0.866098	0.883274	0.965798
RM5/KL5	3	8×1	220	0.940161	0.940809	0.949731
RM5/KL5	3	16×1	380	0.942446	0.942456	0.944448
RM5/KL5	3	32×1	700	0.942489	0.942482	0.942994
RM5/KL5	3	64×1	1340	0.942485	0.942533	0.942634
RM5/KL5	3	128×1	2620	0.942482	0.942483	0.942516
RM5/KL5	3	256×1	5180	0.941906	0.801469	0.871817
RM5/KL5	3	512×1	10300	2.14761	20.8036	1.14343

Table A.21: Maximum radial displacement for the cylindrical shell problem for $\frac{L}{t} = 1,000$ and $p = 2$.

Element	Degree	Mesh	DOF	QP1	QP0	QNU
RM5/KL3	2	2×1	42	3.05E-05	1.39E-01	1.39E-01
RM5/KL3	2	4×1	60	5.50E-04	6.07E-01	8.65E-01
RM5/KL3	2	8×1	96	9.29E-03	7.73E-01	9.25E-01
RM5/KL3	2	16×1	168	1.31E-01	9.20E-01	9.38E-01
RM5/KL3	2	32×1	312	6.77E-01	9.42E-01	9.41E-01
RM5/KL3	2	64×1	600	9.20E-01	9.42E-01	9.42E-01
RM5/KL3	2	128×1	1176	0.941006	9.42E-01	9.42E-01
RM5/KL3	2	256×1	2328	0.942382	9.42E-01	9.42E-01
RM5/KL3	2	512×1	4632	0.942474	9.42E-01	9.42E-01
RM5/RM5	2	2×1	60	3.11E-05	8.59E-01	8.59E-01
RM5/RM5	2	4×1	90	5.24E-04	6.72E-02	1.01E+00
RM5/RM5	2	8×1	150	8.59E-03	6.59E-01	9.64E-01
RM5/RM5	2	16×1	270	1.22E-01	9.14E-01	9.48E-01
RM5/RM5	2	32×1	510	6.61E-01	9.43E-01	9.44E-01
RM5/RM5	2	64×1	990	9.18E-01	9.43E-01	9.43E-01
RM5/RM5	2	128×1	1950	9.41E-01	9.43E-01	9.43E-01
RM5/RM5	2	256×1	3870	9.42E-01	9.42E-01	9.43E-01
RM5/RM5	2	512×1	7710	9.42E-01	9.42E-01	9.42E-01
RM5/KL5	2	2×1	60	3.09E-05	7.71E-01	7.71E-01
RM5/KL5	2	4×1	90	5.51E-04	6.37E-01	8.91E-01
RM5/KL5	2	8×1	150	9.29E-03	7.73E-01	9.26E-01
RM5/KL5	2	16×1	270	1.31E-01	9.20E-01	9.38E-01
RM5/KL5	2	32×1	510	6.77E-01	9.42E-01	9.41E-01
RM5/KL5	2	64×1	990	9.20E-01	9.42E-01	9.42E-01
RM5/KL5	2	128×1	1950	9.41E-01	9.42E-01	9.42E-01
RM5/KL5	2	256×1	3870	9.42E-01	9.42E-01	9.42E-01
RM5/KL5	2	512×1	7710	9.42E-01	9.43E-01	9.42E-01

Table A.22: Maximum radial displacement for the cylindrical shell problem for $\frac{L}{t} = 1,000$ and $p = 3$.

Element	Degree	Mesh	DOF	QP1	QP0	QNU
RM5/KL3	3	2×1	68	0.146749	0.598412	0.598412
RM5/KL3	3	4×1	92	0.71725	0.721199	0.961793
RM5/KL3	3	8×1	140	0.846753	0.864026	0.949658
RM5/KL3	3	16×1	236	0.939176	0.940156	0.94443
RM5/KL3	3	32×1	428	0.942427	0.942441	0.942991
RM5/KL3	3	64×1	812	0.942482	0.942479	0.942615
RM5/KL3	3	128×1	1580	0.942478	0.942478	0.942511
RM5/KL3	3	256×1	3116	0.942477	0.942478	0.942486
RM5/KL3	3	512×1	6188	0.942478	0.942479	0.942481
RM5/RM5	3	2×1	100	0.0539724	0.125083	0.125083
RM5/RM5	3	4×1	140	0.428783	0.493852	0.980543
RM5/RM5	3	8×1	220	0.846367	0.86676	0.963579
RM5/RM5	3	16×1	380	0.943645	0.944956	0.948261
RM5/RM5	3	32×1	700	0.943887	0.943909	0.944047
RM5/RM5	3	64×1	1340	0.942859	0.942871	0.942936
RM5/RM5	3	128×1	2620	0.942572	0.942572	0.942643
RM5/RM5	3	256×1	5180	0.942502	0.942502	0.942572
RM5/RM5	3	512×1	10300	0.942483	0.942483	0.942542
RM5/KL5	3	2×1	100	0.146795	0.632785	0.632785
RM5/KL5	3	4×1	140	0.717254	0.721264	0.964464
RM5/KL5	3	8×1	220	0.846754	0.864028	0.949668
RM5/KL5	3	16×1	380	0.939181	0.940164	0.944444
RM5/KL5	3	32×1	700	0.942427	0.942449	0.943167
RM5/KL5	3	64×1	1340	0.942491	0.942485	0.942821
RM5/KL5	3	128×1	2620	0.942478	0.942478	0.942511
RM5/KL5	3	256×1	5180	0.942725	0.711158	0.942489
RM5/KL5	3	512×1	10300	0.940971	0.936717	0.955089

Table A.23: Maximum radial displacement for the cylindrical shell problem for $\frac{L}{t} = 10,000$ and $p = 2$.

Element	Degree	Mesh	DOF	QP1	QP0	QNU
RM5/KL3	2	2×1	42	0	0.00169	0.00169
RM5/KL3	2	4×1	60	0.00001	0.02964	0.56406
RM5/KL3	2	8×1	96	0.00009	0.51404	0.89565
RM5/KL3	2	16×1	168	0.00153	0.76409	0.93751
RM5/KL3	2	32×1	312	0.02399	0.91159	0.94128
RM5/KL3	2	64×1	600	0.27607	0.9418	0.94218
RM5/KL3	2	128×1	1176	0.81683	0.94248	0.9424
RM5/KL3	2	256×1	2328	0.93346	0.94247	0.94245
RM5/KL3	2	512×1	4632	0.94208	0.94276	0.94257
RM5/RM5	2	2×1	60	0	0.8586	0.8586
RM5/RM5	2	4×1	90	0.00001	0.00073	1.00869
RM5/RM5	2	8×1	150	0.00009	0.03932	0.96404
RM5/RM5	2	16×1	270	0.0014	0.58904	0.94817
RM5/RM5	2	32×1	510	0.02206	0.89808	0.94393
RM5/RM5	2	64×1	990	0.26017	0.94164	0.94285
RM5/RM5	2	128×1	1950	0.80689	0.94254	0.94258
RM5/RM5	2	256×1	3870	0.93253	0.94254	0.94253
RM5/RM5	2	512×1	7710	0.94211	0.94278	0.94257
RM5/KL5	2	2×1	60	0	0.77079	0.77079
RM5/KL5	2	4×1	90	0.00001	0.03827	0.89138
RM5/KL5	2	8×1	150	0.00009	0.52363	3.20304
RM5/KL5	2	16×1	270	0.00153	0.76422	0.93787
RM5/KL5	2	32×1	510	0.02399	0.91159	0.94127
RM5/KL5	2	64×1	990	0.27607	0.9418	0.94218
RM5/KL5	2	128×1	1950	0.81684	0.94245	0.94242
RM5/KL5	2	256×1	3870	0.93347	0.94167	0.94354
RM5/KL5	2	512×1	7710	0.94137	0.94116	1.53406

Table A.24: Maximum radial displacement for the cylindrical shell problem for $\frac{L}{t} = 10,000$ and $p = 3$.

Element	Degree	Mesh	DOF	QP1	QP0	QNU
RM5/KL3	3	2×1	68	0.0018241	0.0299509	0.0299509
RM5/KL3	3	4×1	92	0.129832	0.144528	0.738002
RM5/KL3	3	8×1	140	0.732106	0.726584	0.948353
RM5/KL3	3	16×1	236	0.828009	0.844341	0.944481
RM5/KL3	3	32×1	428	0.937478	0.939145	0.943242
RM5/KL3	3	64×1	812	0.943238	0.942422	0.942523
RM5/KL3	3	128×1	1580	0.942482	0.942482	0.942506
RM5/KL3	3	256×1	3116	0.942499	0.94252	0.942473
RM5/KL3	3	512×1	6188	0.942626	0.942716	0.942643
RM5/RM5	3	2×1	100	0.000575448	0.00146227	0.00146227
RM5/RM5	3	4×1	140	0.0091087	0.0126177	0.980242
RM5/RM5	3	8×1	220	0.346302	0.416947	0.963585
RM5/RM5	3	16×1	380	0.810296	0.830804	0.948246
RM5/RM5	3	32×1	700	0.937853	0.939356	0.944354
RM5/RM5	3	64×1	1340	0.943863	0.944103	0.942997
RM5/RM5	3	128×1	2620	0.942598	0.942606	0.942573
RM5/RM5	3	256×1	5180	0.942558	0.94252	0.942504
RM5/RM5	3	512×1	10300	0.942639	0.942679	0.942335
RM5/KL5	3	2×1	100	0.00182481	0.0410149	0.0410149
RM5/KL5	3	4×1	140	0.129837	0.144743	0.88315
RM5/KL5	3	8×1	220	0.732095	0.726608	0.949551
RM5/KL5	3	16×1	380	0.838221	0.844338	0.944523
RM5/KL5	3	32×1	700	0.938386	0.938941	0.961458
RM5/KL5	3	64×1	1340	0.942975	0.941754	0.944656
RM5/KL5	3	128×1	2620	0.94248	0.942504	0.942478
RM5/KL5	3	256×1	5180	0.94249	0.942585	0.942708
RM5/KL5	3	512×1	10300	0.942544	0.911414	1.46567

Table A.25: Maximum radial displacement for the cylindrical shell problem for NASTRAN Quad4, QuadR.

R/t	Mesh	DOF	Quad4 w/o TS	Quad4	QuadR w/o TS	QuadR
10	2×1	36	0.8295	0.8314	0.8295	0.8202
10	4×1	60	0.9135	0.9153	0.9135	0.9124
10	8×1	108	0.9357	0.9376	0.9357	0.9369
10	16×1	204	0.9414	0.9433	0.9414	0.9431
10	32×1	396	0.9428	0.9447	0.9428	0.9446
10	64×1	780	0.9431	0.9450	0.9432	0.9450
100	2×1	36	0.8288	0.8288	0.8288	0.8176
100	4×1	60	0.9127	0.9127	0.9127	0.9097
100	8×1	108	0.9349	0.9350	0.9349	0.9342
100	16×1	204	0.9406	0.9406	0.9406	0.9404
100	32×1	396	0.9420	0.9420	0.9420	0.9420
100	64×1	780	0.9424	0.9424	0.9424	0.9424
1000	2×1	36	0.8288	0.8288	0.8288	0.8176
1000	4×1	60	0.9127	0.9127	0.9127	0.9097
1000	8×1	108	0.9349	0.9349	0.9349	0.9342
1000	16×1	204	0.9406	0.9406	0.9406	0.9404
1000	32×1	396	0.9420	0.9420	0.9420	0.9420
1000	64×1	780	0.9424	0.9424	0.9424	0.9423
10000	2×1	36	0.8288	0.8288	0.8288	0.8176
10000	4×1	60	0.9127	0.9127	0.9127	0.9097
10000	8×1	108	0.9349	0.9349	0.9349	0.9342
10000	16×1	204	0.9406	0.9406	0.9406	0.9404
10000	32×1	396	0.9420	0.9420	0.9420	0.9420
10000	64×1	780	0.9423	0.9424	0.9424	0.9423

Table A.26: Maximum radial displacement for the cylindrical shell problem for ABAQUS S4, S4R.

R/t	Mesh	DOF	S4 w/o TS	S4	S4R w/o TS	S4R
10	2×1	36	0.7847	0.7865	0.7847	0.7865
10	4×1	60	0.9016	0.9034	0.9016	0.9034
10	8×1	108	0.9327	0.9346	0.9327	0.9346
10	16×1	204	0.9407	0.9425	0.9407	0.9425
10	32×1	396	0.9426	0.9445	0.9426	0.9445
10	64×1	780	0.9431	0.9450	0.9431	0.9450
100	2×1	36	0.7839	0.7840	0.7839	0.7840
100	4×1	60	0.9008	0.9008	0.9008	0.9008
100	8×1	108	0.9319	0.9320	0.9319	0.9320
100	16×1	204	0.9398	0.9399	0.9398	0.9399
100	32×1	396	0.9418	0.9418	0.9418	0.9418
100	64×1	780	0.9423	0.9423	0.9423	0.9423
1000	2×1	36	0.7839	0.7839	0.7839	0.7839
1000	4×1	60	0.9008	0.9008	0.9008	0.9008
1000	8×1	108	0.9319	0.9319	0.9319	0.9319
1000	16×1	204	0.9398	0.9398	0.9398	0.9398
1000	32×1	396	0.9418	0.9418	0.9418	0.9418
1000	64×1	780	0.9423	0.9423	0.9422	0.9423
10000	2×1	36	0.7839	0.7839	0.7839	0.7839
10000	4×1	60	0.9008	0.9008	0.9008	0.9008
10000	8×1	108	0.9319	0.9319	0.9319	0.9319
10000	16×1	204	0.9398	0.9398	0.9398	0.9398
10000	32×1	396	0.9418	0.9418	0.9418	0.9418
10000	64×1	780	0.9423	0.9423	0.9423	0.9423

Table A.27: Maximum displacement for the Scordelis-Lo problem for different blended shell elements, $p = 2$.

Elements	Degree	Mesh	DOF	QP1	QP0	QNU
RM6/KL3	2	2×2	168	0.878	3.292	3.292
RM6/KL3	2	4×4	336	2.910	3.561	3.509
RM6/KL3	2	8×8	816	3.554	3.604	3.618
RM6/KL3	2	16×16	2352	3.603	3.607	3.622
RM6/KL3	2	32×32	7728	3.607	3.607	3.613
RM6/KL3	2	64×64	27696	3.607	3.607	3.609
RM6/RM5	2	2×2	184	0.859	3.353	3.353
RM6/RM5	2	4×4	400	2.785	3.588	3.549
RM6/RM5	2	8×8	1072	3.541	3.614	3.637
RM6/RM5	2	16×16	3376	3.609	3.614	3.632
RM6/RM5	2	32×32	11824	3.615	3.616	3.623
RM6/RM5	2	64×64	44080	3.617	3.617	3.619
RM6/KL5	2	2×2	184	0.879	3.294	3.294
RM6/KL5	2	4×4	400	2.911	3.562	3.510
RM6/KL5	2	8×8	1072	3.556	3.607	3.621
RM6/KL5	2	16×16	3376	3.606	3.611	3.627
RM6/KL5	2	32×32	11824	3.609	3.610	3.617
RM6/KL5	2	64×64	44080	3.608	3.608	3.610

A.5 Results for the Scordelis-Lo roof problem

Table A.28: Maximum displacement for the Scordelis-Lo problem for different blended shell elements, $p = 3$.

Elements	Degree	Mesh	DOF	QP1	QP0	QNU
RM6/KL3	3	2×2	246	3.471	3.534	3.534
RM6/KL3	3	4×4	438	3.604	3.605	3.620
RM6/KL3	3	8×8	966	3.608	3.608	3.645
RM6/KL3	3	16×16	2598	3.608	3.608	3.630
RM6/KL3	3	32×32	8166	3.607	3.607	3.616
RM6/KL3	3	64×64	28518	3.607	3.607	3.610
RM6/RM5	3	2×2	282	3.508	3.569	3.569
RM6/RM5	3	4×4	538	3.619	3.621	3.625
RM6/RM5	3	8×8	1290	3.616	3.616	3.654
RM6/RM5	3	16×16	3754	3.615	3.615	3.642
RM6/RM5	3	32×32	12522	3.617	3.617	3.629
RM6/RM5	3	64×64	45418	3.618	3.618	3.622
RM6/KL5	3	2×2	282	3.472	3.535	3.535
RM6/KL5	3	4×4	538	3.605	3.607	3.622
RM6/KL5	3	8×8	1290	3.611	3.611	3.650
RM6/KL5	3	16×16	3754	3.613	3.613	3.637
RM6/KL5	3	32×32	12522	3.612	3.612	3.623
RM6/KL5	3	64×64	45418	3.609	3.609	3.614

Table A.29: Maximum displacement for the Scordelis-Lo problem for NASTRAN Quad4, QuadR.

Mesh	Load	DOF	Quad4 w/o TS	Quad4	QuadR w/o TS	QuadR
4×4	39219	150	3.8390	3.8440	3.8283	3.8213
8×8	39256	486	3.6628	3.6698	3.6767	3.6771
12×12	39263	1014	3.6338	3.6411	3.6447	3.6480
16×16	39266	1734	3.6232	3.6308	3.6311	3.6357
20×20	39267	2646	3.6183	3.6262	3.6241	3.6297
24×24	39268	3750	3.6153	3.6235	3.6197	3.6259
32×32	39268	6534	3.6123	3.6209	3.6150	3.6221
64×64	39269	25350	3.6089	3.6183	3.6097	3.6184

Table A.30: Maximum displacement for the Scordelis-Lo problem for ABAQUS S4, S4R.

Mesh	Load	DOF	S4 w/o TS	S4	S4R w/o TS	S4R
4×4	39219	150	3.638	3.7580	4.138	4.2970
8×8	39256	486	3.5040	3.6350	3.633	3.7750
12×12	39263	1014	3.4970	3.6200	3.555	3.6830
16×16	39266	1734	3.5040	3.6160	3.537	3.6510
20×20	39267	2646	3.5160	3.6150	3.5370	3.6380
24×24	39268	3750	3.5270	3.6150	3.5420	3.6300
32×32	39268	6534	3.5470	3.6150	3.5550	3.6230
64×64	39269	25350	3.5850	3.6160	3.5870	3.6180

Table A.31: Maximum displacement for the pinched cylinder problem for different blended shell elements, $p = 2$.

Element	Degree	Mesh	DOF	QP1	QP0	QNU
RM6/KL3	2	2×2	168	-7.140E-09	-7.820E-09	-7.820E-09
RM6/KL3	2	4×4	336	-1.960E-08	-2.430E-08	-4.090E-08
RM6/KL3	2	8×8	816	-8.630E-08	-1.080E-07	-1.340E-07
RM6/KL3	2	16×16	2352	-1.640E-07	-1.720E-07	-1.750E-07
RM6/KL3	2	32×32	7728	-1.811E-07	-1.820E-07	-1.826E-07
RM6/KL3	2	64×64	27696	-1.837E-07	-1.839E-07	-1.842E-07
RM6/RM5	2	2×2	184	-7.450E-09	-8.400E-09	-8.400E-09
RM6/RM5	2	4×4	400	-1.790E-08	-2.510E-08	-6.990E-08
RM6/RM5	2	8×8	1072	-6.820E-08	-9.990E-08	-1.650E-07
RM6/RM5	2	16×16	3376	-1.490E-07	-1.730E-07	-1.870E-07
RM6/RM5	2	32×32	11824	-1.804E-07	-1.840E-07	-1.882E-07
RM6/RM5	2	64×64	44080	-1.848E-07	-1.852E-07	-1.869E-07
RM6/KL5	2	2×2	184	-7.300E-09	-8.030E-09	-8.030E-09
RM6/KL5	2	4×4	400	-2.020E-08	-2.600E-08	-6.790E-08
RM6/KL5	2	8×8	1072	-8.810E-08	-1.110E-07	-1.470E-07
RM6/KL5	2	16×16	3376	-1.650E-07	-1.740E-07	-1.780E-07
RM6/KL5	2	32×32	11824	-1.816E-07	-1.828E-07	-1.841E-07
RM6/KL5	2	64×64	44080	-1.845E-07	-1.847E-07	-1.852E-07

A.6 Results for the pinched cylinder problem

Table A.32: Maximum displacement for the pinched cylinder problem for different blended shell elements, $p = 3$.

Element	Degree	Mesh	DOF	QP1	QP0	QNU
RM6/KL3	3	2×2	246	-1.280E-08	-1.310E-08	-1.310E-08
RM6/KL3	3	4×4	438	-6.050E-08	-6.380E-08	-7.580E-08
RM6/KL3	3	8×8	966	-1.610E-07	-1.640E-07	-1.840E-07
RM6/KL3	3	16×16	2598	-1.830E-07	-1.830E-07	-1.890E-07
RM6/KL3	3	32×32	8166	-1.843E-07	-1.844E-07	-1.867E-07
RM6/KL3	3	64×64	28518	-1.846E-07	-1.846E-07	-1.855E-07
RM6/RM5	3	2×2	282	-1.290E-08	-1.330E-08	-1.330E-08
RM6/RM5	3	4×4	538	-5.730E-08	-6.150E-08	-7.360E-08
RM6/RM5	3	8×8	1290	-1.520E-07	-1.570E-07	-1.750E-07
RM6/RM5	3	16×16	3754	-1.820E-07	-1.830E-07	-1.870E-07
RM6/RM5	3	32×32	12522	-1.849E-07	-1.850E-07	-1.878E-07
RM6/RM5	3	64×64	45418	-1.855E-07	-1.855E-07	-1.871E-07
RM6/KL5	3	2×2	282	-1.310E-08	-1.360E-08	-1.360E-08
RM6/KL5	3	4×4	538	-6.070E-08	-6.400E-08	-7.620E-08
RM6/KL5	3	8×8	1290	-1.610E-07	-1.640E-07	-1.850E-07
RM6/KL5	3	16×16	3754	-1.830E-07	-1.830E-07	-1.890E-07
RM6/KL5	3	32×32	12522	-1.849E-07	-1.849E-07	-1.875E-07
RM6/KL5	3	64×64	45418	-1.854E-07	-1.854E-07	-1.865E-07

Table A.33: Maximum displacement for the pinched cylinder problem for NASTRAN Quad4, QuadR.

Mesh	DOF	Quad4 w/o TS	Quad4	QuadR w/o TS	QuadR
10×10	726	1.6906E-05	1.7380E-05	1.6234E-05	1.6196E-05
20×20	2646	1.8158E-05	1.8624E-05	1.7858E-05	1.8067E-05
35×35	7776	1.8321E-05	1.8679E-05	1.8195E-05	1.8427E-05
75×75	34656	1.8315E-05	1.8581E-05	1.8280E-05	1.8505E-05
100×100	61206	1.8305E-05	1.8563E-05	1.8284E-05	1.8516E-05
200×200	242406	1.8287E-05	1.8558E-05	1.8281E-05	1.8544E-05
400×400	964806	1.8280E-05	1.8581E-05	1.8278E-05	1.8577E-05
800×800	3849606	1.8277E-05	1.8615E-05	1.8277E-05	1.8614E-05
1600×1600	15379206	1.8276E-05	1.8652E-05	1.8276E-05	1.8652E-05
3200×3200	61478406	1.8265E-05	1.8690E-05	1.8265E-05	1.8690E-05

Table A.34: Maximum displacement for the pinched cylinder problem for ABAQUS S4, S4R.

Mesh	DOF	S4	S4R
10×10	726	1.5185E-05	1.5913E-05
20×20	2646	1.7503E-05	1.7786E-05
35×35	7776	1.8131E-05	1.8248E-05
50×50	15606	1.8313E-05	1.8378E-05
75×75	34656	1.8389E-05	1.8422E-05
100×100	61206	1.8473E-05	1.8493E-05
200×200	242406	1.8544E-05	1.8550E-05
400×400	964806	1.8591E-05	1.8593E-05
800×800	3849606	1.8632E-05	1.8632E-05
1600×1600	15379206	1.8670E-05	1.8671E-05
3200×3200	61478406	1.8709E-05	1.8709E-05

Table A.35: Maximum displacement for the hemispherical shell with hole problem for different blended shell elements, $p = 2$.

Element	Degree	Mesh	DOF	QP1	QP0	QNU
RM6/KL3	2	2×2	72	8.24E-05	1.43E-04	1.43E-04
RM6/KL3	2	4×4	144	1.71E-03	8.40E-03	4.75E-02
RM6/KL3	2	8×8	360	2.30E-02	7.73E-02	8.83E-02
RM6/KL3	2	16×16	1080	7.77E-02	9.22E-02	9.28E-02
RM6/KL3	2	32×32	3672	9.20E-02	9.33E-02	9.33E-02
RM6/KL3	2	64×64	13464	9.34E-02	9.35E-02	9.35E-02
RM6/RM5	2	2×2	105	8.66E-05	1.93E-04	1.93E-04
RM6/RM5	2	4×4	189	1.40E-03	8.85E-03	6.01E-02
RM6/RM5	2	8×8	429	1.94E-02	7.87E-02	9.29E-02
RM6/RM5	2	16×16	1197	7.51E-02	9.25E-02	9.40E-02
RM6/RM5	2	32×32	3885	9.20E-02	9.35E-02	9.38E-02
RM6/RM5	2	64×64	13869	9.35E-02	9.36E-02	9.37E-02
RM6/KL5	2	2×2	105	8.32E-05	1.44E-04	1.44E-04
RM6/KL5	2	4×4	189	1.72E-03	8.51E-03	5.54E-02
RM6/KL5	2	8×8	429	2.33E-02	7.80E-02	9.06E-02
RM6/KL5	2	16×16	1197	7.83E-02	9.24E-02	9.31E-02
RM6/KL5	2	32×32	3885	9.23E-02	9.34E-02	9.35E-02
RM6/KL5	2	64×64	13869	9.34E-02	9.35E-02	9.36E-02

A.7 Results for the hemispherical shell with a hole problem

Table A.36: Maximum displacement for the hemispherical shell with hole problem for different blended shell elements, $p = 3$.

Element	Degree	Mesh	DOF	QP1	QP0	QNU
RM6/KL3	3	2×2	88	1.66E-03	3.02E-03	3.02E-03
RM6/KL3	3	4×4	192	2.81E-02	3.59E-02	5.33E-02
RM6/KL3	3	8×8	520	8.15E-02	8.52E-02	8.72E-02
RM6/KL3	3	16×16	1656	9.21E-02	9.26E-02	9.30E-02
RM6/KL3	3	32×32	5848	9.33E-02	9.34E-02	9.35E-02
RM6/KL3	3	64×64	21912	9.35E-02	9.35E-02	9.36E-02
RM6/RM5	3	2×2	135	1.94E-03	3.92E-03	3.92E-03
RM6/RM5	3	4×4	259	3.90E-02	4.78E-02	8.58E-02
RM6/RM5	3	8×8	627	9.01E-02	9.08E-02	9.33E-02
RM6/RM5	3	16×16	1843	9.33E-02	9.34E-02	9.37E-02
RM6/RM5	3	32×32	6195	9.36E-02	9.36E-02	9.37E-02
RM6/RM5	3	64×64	22579	9.37E-02	9.37E-02	9.38E-02
RM6/KL5	3	2×2	135	1.73E-03	3.35E-03	3.35E-03
RM6/KL5	3	4×4	259	3.02E-02	3.98E-02	6.44E-02
RM6/KL5	3	8×8	627	8.40E-02	8.78E-02	9.03E-02
RM6/KL5	3	16×16	1843	9.26E-02	9.30E-02	9.35E-02
RM6/KL5	3	32×32	6195	9.35E-02	9.35E-02	9.37E-02
RM6/KL5	3	64×64	22579	9.36E-02	9.36E-02	9.37E-02

Table A.37: Maximum displacement for the hemispherical shell with hole problem for NASTRAN Quad4, QuadR.

Mesh	DOF	Quad4 w/o TS	Quad4	QuadR w/o TS	QuadR
2×2	54	0.0898	0.0898	0.0006	0.0006
4×4	150	0.0952	0.0952	0.0227	0.0227
6×6	294	0.0950	0.0950	0.0721	0.0718
8×8	486	0.0944	0.0945	0.0887	0.0884
10×10	726	0.0941	0.0941	0.0922	0.0920
12×12	1014	0.0938	0.0939	0.0932	0.0929
16×16	1734	0.0937	0.0937	0.0935	0.0934
32×32	6534	0.0936	0.0937	0.0936	0.0936

Table A.38: Maximum displacement for the hemispherical shell with hole problem for ABAQUS S4, S4R.

Mesh	DOF	S4 w/o TS	S4	S4R w/o TS	S4R
2×2	54	0.0805	0.0805	0.0842	0.0842
4×4	150	0.0920	0.0920	0.0956	0.0956
6×6	294	0.0924	0.0924	0.0947	0.0947
8×8	486	0.0926	0.0926	0.0943	0.0943
10×10	726	0.0927	0.0927	0.0941	0.0941
12×12	1014	0.0928	0.0928	0.0940	0.0940
16×16	1734	0.0930	0.0930	0.0938	0.0938
32×32	6534	0.0934	0.0934	0.0936	0.0936

Table A.39: Maximum normalized displacement for the pinched sphere problem for different blended shell elements (normalized by $\frac{Et}{P}$).

Element	Degree	Mesh	DOF	QP1	QP0	QNU
RM6/KL3	2	2×2	156	3.24	3.55	3.55
RM6/KL3	2	4×4	312	6.26	6.21	5.54
RM6/KL3	2	8×8	768	13.43	13.25	11.91
RM6/KL3	2	16×16	2256	20.57	20.25	19.68
RM6/KL3	2	32×32	7536	22.75	22.58	22.51
RM6/KL3	2	64×64	27312	22.27	22.35	22.38
RM6/RM5	2	2×2	180	3.21	3.43	3.43
RM6/RM5	2	4×4	392	6.75	6.76	6.25
RM6/RM5	2	8×8	1056	14.71	14.27	14.34
RM6/RM5	2	16×16	3344	22.02	21.85	22.2
RM6/RM5	2	32×32	11760	23.34	23.59	23.73
RM6/RM5	2	64×64	43952	23.61	24.01	24.14
RM6/KL5	2	2×2	180	3.29	3.56	3.56
RM6/KL5	2	4×4	392	6.37	6.27	5.59
RM6/KL5	2	8×8	1056	13.64	13.41	12.04
RM6/KL5	2	16×16	3344	21	20.67	20.07
RM6/KL5	2	32×32	11760	23.18	23.07	23
RM6/KL5	2	64×64	43952	22.77	22.88	22.9

A.8 Results for the pinched sphere problem

A.9 Results for the L-bracket problem

Table A.40: Maximum normalized displacement for the pinched sphere problem for different blended shell elements (normalized by $\frac{Et}{P}$).

Element	Degree	Mesh	DOF	QP1	QP0	QNU
RM6/KL3	3	2×2	228	4.62	4.72	4.72
RM6/KL3	3	4×4	408	9.05	9.05	10.7
RM6/KL3	3	8×8	912	19.01	18.96	20
RM6/KL3	3	16×16	2496	22.64	22.64	23.15
RM6/KL3	3	32×32	7968	22.8	22.83	23.03
RM6/KL3	3	64×64	28128	22.33	22.39	22.53
RM6/RM5	3	2×2	276	5.26	5.25	5.25
RM6/RM5	3	4×4	528	10.59	10.35	11.72
RM6/RM5	3	8×8	1272	20.47	19.95	20.97
RM6/RM5	3	16×16	3720	23.22	23.36	23.81
RM6/RM5	3	32×32	12456	23.53	23.78	23.98
RM6/RM5	3	64×64	45288	23.83	24.09	24.15
RM6/KL5	3	2×2	276	4.74	4.84	4.84
RM6/KL5	3	4×4	528	9.21	9.2	10.89
RM6/KL5	3	8×8	1272	19.13	19.06	20.1
RM6/KL5	3	16×16	3720	22.86	22.86	23.4
RM6/KL5	3	32×32	12456	23.38	23.4	23.59
RM6/KL5	3	64×64	45288	22.95	23.01	23.03

Table A.41: Maximum normalized displacement for the pinched sphere problem for NASTRAN Quad4, QuadR (normalized by $\frac{Et}{P}$).

Elements	DOF	Quad4 w/o TS	Quad4	QuadR w/o TS	QuadR
58	438	20.769628	22.852684	20.682064	22.243764
175	1194	21.239888	23.118268	21.21116	22.808556
406	2664	21.267936	23.120728	21.255668	23.000136
1097	6966	21.211128	23.44242	21.221772	23.435428

Table A.42: Maximum normalized displacement for the pinched sphere problem for ABAQUS S4, S4R (normalized by $\frac{Et}{P}$).

Elements	DOF	S4 w/o TS	S4	S4R w/o TS	S4R
58	438	17.4416	20.7688	17.9092	21.5036
175	1194	19.3668	22.0632	19.6264	22.38
406	2664	20.582	22.872	20.6676	22.9668
1097	6966	21.0224	23.5356	21.0432	23.5568

Table A.43: Maximum displacement for the L-bracket problem for different blended shell elements.

Elements	Degree	Mesh	DOF	QP1	QP0	QNU
RM6/KL3	2	2×2	114	3.75E-01	3.75E-01	3.75E-01
RM6/KL3	2	4×4	246	4.13E-01	4.13E-01	4.16E-01
RM6/KL3	2	8×8	654	4.39E-01	4.39E-01	4.39E-01
RM6/KL3	2	16×16	2046	4.48E-01	4.48E-01	4.48E-01
RM6/KL3	2	32×32	7134	4.50E-01	4.50E-01	4.51E-01
RM6/KL3	2	64×64	26526	4.52E-01	4.52E-01	4.52E-01
RM6/KL3	2	128×128	102174	4.52E-01	4.52E-01	4.52E-01
RM6/RM5	2	2×2	150	2.51E-01	4.25E-01	4.25E-01
RM6/RM5	2	4×4	346	2.61E-01	4.10E-01	4.41E-01
RM6/RM5	2	8×8	978	3.32E-01	4.10E-01	4.51E-01
RM6/RM5	2	16×16	3202	4.08E-01	4.41E-01	4.52E-01
RM6/RM5	2	32×32	11490	4.41E-01	4.51E-01	4.53E-01
RM6/RM5	2	64×64	43426	4.51E-01	4.53E-01	4.53E-01
RM6/RM5	2	128×128	168738	4.53E-01	4.53E-01	4.53E-01
RM6/KL5	2	2×2	150	3.75E-01	3.76E-01	3.76E-01
RM6/KL5	2	4×4	346	4.13E-01	4.13E-01	4.16E-01
RM6/KL5	2	8×8	978	4.39E-01	4.39E-01	4.40E-01
RM6/KL5	2	16×16	3202	4.48E-01	4.48E-01	4.49E-01
RM6/KL5	2	32×32	11490	4.51E-01	4.52E-01	4.52E-01
RM6/KL5	2	64×64	43426	4.53E-01	4.53E-01	4.53E-01
RM6/KL5	2	128×128	168738	4.53E-01	4.53E-01	4.53E-01